Utilizing Fiber-Reinforced Polymers to Retrofit Steel Bridge Girders Damaged by Fatigue Loading.

By

Eric Bonet

Submitted to the graduate degree program in Civil Engineering and the Graduate Faculty of the Universtiy of Kansas in partial fulfillment of the requirements for the degree of Masters of Science.

_____	_____
Co- Chairperson Dr. Caroline Bennett	Co- Chairperson Dr. Adolfo Matamoros
	_____
	Dr. Ron Barrett - Gonzalez
	_____
	Dr. Stanley Rolfe
	_____
	Robert Lyon

Date Defended May 27, 2014

Lawrence Kansas

Keywords: Bridge, Girder, Steel, Retrofit, Composite, FRP, Kevlar, Fatigue, Fracture, Stiffen Connection

The Thesis Committee for Eric Bonet

certifies that this is the approved version of the following thesis:

Utilizing Fiber-Reinforced Polymers to Retrofit Steel Bridge Girders Damaged by Fatigue Loading.

Co- Chairperson Dr. Caroline Bennett

Co- Chairperson Dr. Adolfo Matamoros

Dr. Ron Barrett - Gonzalez

Dr. Stanley Rolfe

Robert Lyon

Date approved: June 5, 2014

Executive Summary

Tens of thousands of steel bridges constructed prior to the mid-1980s are susceptible to distortion-induced fatigue, which caused nearly 90% of cracking observed in steel bridge girders (Connor, R. and Fisher, J. 2006). Distortion-induced fatigue is caused by secondary stresses induced in cross-frames or diaphragms as differential deflection occurs between bridge girders. Girders are interconnected at discrete locations with cross bracing; as one girder deflects due to traffic loads, the cross bracing induces a force on the adjacent girder, causing high stresses at connections which can eventually lead to the formation of fatigue cracks. Retrofits which can be easily installed without disrupting bridge traffic are needed in order to retard the growth of these fatigue cracks and prevent bridge failure.

This research utilized computer models as well as experimental testing to develop and test multiple retrofit techniques to prevent the growth of fatigue cracks. A retrofit measure referred to herein as the "composite block retrofit" was developed and successfully tested in a laboratory setting utilizing a 2.82-meter (9.25-ft.) model of a steel girder. This retrofit uses a block of carbon fiber reinforced polymer (CFRP) material applied at a cracked location to distribute stresses away from the crack. This retrofit measure was successful in preventing crack growth under severe fatigue loading.

The magnitude of stress reduction calculated with the computer models was compared with the magnitude of stress reduction recorded from a strain gage attached to the girder subassembly. The computer analyses indicated a 96% stress reduction and the strain gage on the girder subassembly recorded a 92% stress reduction. Thus, this process extended the fatigue life of the retrofitted girder considerably, possibly as much as 4 million cycles or more. This comparison showed that if properly used, computer models could provide an accurate representation of the magnitude of stress reduction that may be expected during physical test trials.

Acknowledgements

This research would not have been possible without the help and tireless support of lab tech David Woody. He constantly took time out of his busy schedule to teach me how to use all of the tools in the lab and all of the tricks he has learned from a lifetime of work experience. David Woody was the man behind the scenes who transformed the ideas in my head to physical realities.

I am greatly indebted to Professor Dr. Ronald Barrett for his professional guidance, constant encouragement to continue researching novel ideas unheard of in the field of civil engineering, and providing me with the resources to do so.

I am eternally grateful to Professors Dr. Caroline Bennett, Dr. Adolfo Matamoros and Dr. Stan Rolfe for entrusting me with the "keys" to the Fracture and Fatigue lab in M2SEC and providing me with the professional guidance and means to undertake and complete this research.

I am thankful for the help and outstanding suggestions of Professor Dr. Matt O'Reilly.

The experimental research was made possible by the assistance of laboratory personnel Matt Maksimowicz and Eric Nicholson. Further, I would like to thank my fellow graduate students: Alisha Elmore, Amanda Hartman, Danqing Yu, Jack Przywara, James Zhou, Jessica Galvis, Katie McElrath, and Say Hak Bun. The assistance of the undergraduate research assistants Brad Prewitt, Riley Piles and Zach Olson was greatly appreciated. I would like to specially thank undergraduate research assistant Nick Crain for his hard work ethic and patience.

Professor Bob Lyon played a key role in this research project with his 30+ years of bridge engineering expertise. I have also had the pleasure of being Professor Lyon's student for four years and the knowledge he has passed onto me is invaluable. I cannot thank him enough and look forward to working with him as I begin my professional career.

I would also like to thank my family and friends for their support.

Table of Contents

List of Figures, Tables and Equations

Retrofitting Steel Bridge Girders

Appendix A: Finite Element Modeling techniques used in analytical models.

Appendix B: Experimental Setup

Appendix C: Lower Composite Block Retrofit Installation

Appendix D: ASTM D3039 – 08 Stand test method for Tensile Properties of Polymer Matrix Composite Materials.

Appendix E: ASTM D5961-13 Standard Test Method for Bearing Response of Polymer Matrix Composite Laminates.

Appendix F: Upper Composite Block Retrofit Installation

Appendix G: Kevlar Stitching Retrofit Installation

Appendix H: Rotation on Fascia Side of Girder

Appendix I: Relative Stresses on Fascia Side of Girder Subassembly

Appendix J: Steel Wool Tension Specimens

Appendix K: Aramid (Kevlar) Yarn Testing and Material Properties

Appendix L: Corrosion Testing

Appendix M: Procedure for installing composite block retrofit in the field

Utilizing Fiber-Reinforced Polymers to Retrofit Steel Bridge Girders Damaged by Fatigue Loading.

Introduction and Background

The Federal Aid Highway Act of 1956 created a new age for transportation across the United States, namely the interstate highway system. To connect all of the highway systems thousands of multigirder steel bridges were constructed because they provided an effective solution to span short distances (Jajich and Schultz 2003). Unknown at the time, thousands of these bridges were constructed with a design detail which was highly prone to developing distortion-induced fatigue cracks.

In order to prevent lateral-torsional bucking during bridge construction, bridge girders are joined by attaching lateral bracing (cross-frames or diaphragms) to the girders using transverse connection plates (Tedesco, et al. 1995). In the 1930s brittle fractures in European Bridges were observed at the tension flange along the transverse connection plate to flange weld (Roddis K. and Zhao, Y. 2001). To prevent future failures of this type, engineers decided to avoid introducing imperfections and discontinuities at regions of high tensile stresses by eliminating the connection plate to tension flange weld. Although this detailing practice was well-intended, it is estimated to be responsible for over 90% of all fatigue cracking seen in steel bridge girders (Connor, R. and Fisher, J. 2006).

Distortion-induced fatigue is caused by secondary stresses induced in cross-frames or diaphragms as differential deflection occurs between bridge girders. Steel girders are usually interconnected at discrete locations with cross bracing; as one girder deflects due to traffic loads, the cross bracing induces a concentrated force on the adjacent girder causing high stresses on a localized region of the girder web. Because the top flange is laterally restrained by the concrete deck and the bottom flange is free to rotate (Figure 1), distortion occurs in the flexible region of the web between the restrained flange and connection stiffener. This region of the web is commonly referred to as the "web-gap region" (Dexter, R and Ocel, J. 2013).

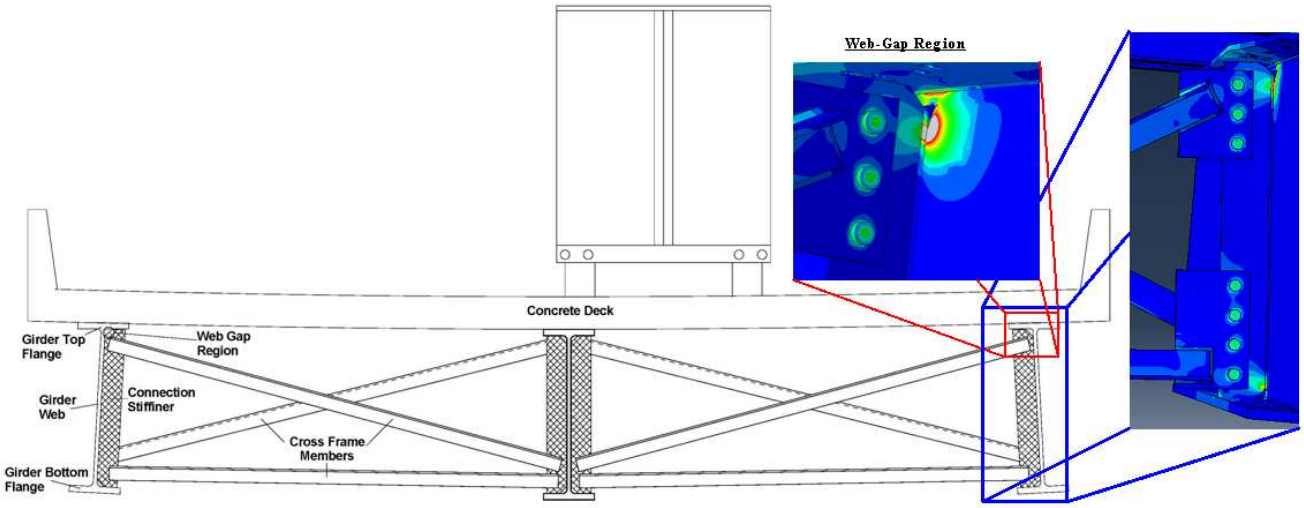

Figure 1: Out of Plane Distortion in Steel Bridge Girder

The majority of bridges currently in use were designed prior to 1985. For example, a study performed by the State of Minnesota determined that 85% of steel bridges were built prior to 1986 (Altay, A. K. et al. 2003). Due to cracking observed in web-gap regions, from 1985 onward the AASHTO Bridge Design Specification has required positive attachment between connection plates and both girder flanges (AASHTO, 2010). This connection is most commonly implemented by welding, which was the exact detail that was of concern in the bridge failures of the 1930s. However, as a result of modern steel fabrication processes, there are reduced concerns of welding connection plates to flanges (Dexter, R and Ocel, J. 2013). By providing this positive attachment, the majority of bridges designed after 1985 do not experience distortion-induced fatigue problems.

A workshop held in August 2002 with experts on bridge fatigue and fracture resulted in the creation of the "Manual for Repair and Retrofit of Fatigue Cracks in Steel Bridges (Dexter, R and Ocel, J. 2013)." Over half of this manual is related to distortion-induced-fatigue. The manual states that to properly repair web-gap fatigue cracks, the source of the out-of-plane distortion must be eliminated. Most of the retrofit measures described in this manual to reduce out-of-plane distortion can be categorized as: web-gap softening and web-gap stiffening. Web-gap softening techniques include: hole drilling, diaphragm or crossframe removal, diaphragm repositioning, or bolt loosening. Web-gap softening techniques are successful in reducing the out of plane stresses; but have the disadvantage that out-of-plane bending can still occur.

Web-gap stiffening retrofits provide positive attachment from the connection plate to the girder flange. Depending on the retrofit type this positive attachment can either eliminate or greatly reduce the relative displacement between the connection plate and girder flange, thereby lowering the distortion-induced stresses. The web-gap stiffening retrofits provided in the manual are created by attaching a steel angle from the connection plate to the girder flange. The manual offers a variety of techniques for creating this connection, and addresses the pros and cons of each technique. The techniques listed in the manual include: welding the angle to the tension flange (which is not recommended since adding a weld to the flange can create a location for fatigue cracks to develop [(Keating et al., 1996]); bolting the angle to the flange (which requires removal of a portion of the concrete deck); a hybrid connection including both welding and bolting the angle to the flange; utilizing adhesives to connect the angle to the flange; and nailing the angle to the flange (Dexter, R and Ocel, J. 2013). These reinforcing methods are not always successful since cracks may reinitiate close to the reinforced area and often reinforcements achieved using steel plates can introduce additional stresses due to welding or bolting (Colombi 2014).

Fiber-reinforced polymers (FRPs) have received much attention since the 1990s for their use in rehabilitation of civil infrastructure. In the majority of civil engineering applications, FRPs have been utilized in conjunction with reinforced concrete structures. There are now numerous examples of the efficacy of FRP composites to rehabilitate concrete bridges including: the flexural and shear strengthening of girders, the strengthening of decks and slabs, and the strengthening and/or seismic retrofitting of columns (Karbhari, 2014). In fact, in Washington, D.C. a 120-year-old bridge was retrofitted such that the entire deck was replaced with a 127-mm (5-in.) thick FRP deck in order to reduce the dead load from the decking by a factor of five. (Kavanaugh 2014).

While FRP materials have proven to be highly successful when used in conjunction with reinforced concrete, a significant portion of aging and deteriorating infrastructure is constructed out of steel. Steel bridges are susceptible to corrosion, fatigue cracks, and stresses higher than originally designed for due to increased traffic volumes. Only recently have FRP materials been adopted to reinforce steel structures to combat these issues (Hollaway and Cedei, 2002; Shaat *et al.*, 2004; Zhao and Zhang, 2007; Teng *et al.*, 2012).

A common method which utilizes FRP materials to retrofit metal structures is performed by bonding FRP wraps (Wu *et al.* 2012) or strips (Jones *et al.* 2003; Liu *et al.* 2009; Taljsten *et al.* 2009) to a structure's metal surface. Numerous theoretical and experimental analyses have been conducted on the use of FRP adhesively bonded to steel beams as a retrofit to extend fatigue life. As reported by Tavakkolizadeh and Saadatmanesh (2003), beams in aged steel bridges can have their fatigue life extended more than three-fold through FRP reinforcement. However, test results have shown that debonding is the main failure mode for beams retrofitted with bonded FRPs (Cadei *et al.*, 2004.; Curley et al., 2000.; Cheuk et al. 2002.). This failure mode is primarily the result of stress concentrations in the adhesive layer where the FRP terminates on the beam (Deng et al., 2004). Other drawbacks pertaining to the long-term behavior of the adhesive joint between FRP and metals include the fact that the adhesive layer may be sensitive to high temperature, water and moisture exposure (Zhao 2011).

This paper describes a novel retrofit technique utilizing FRP materials to eliminate the growth of fatigue cracks in steel bridge girders subjected to distortion-induced fatigue by providing positive attachment from the connection plate to the girder flange without relying on an adhesive bond layer. To accomplish this, computer models and physical models of 2.82-meter (9.25-ft.) long girder subassemblies were conducted. Linear analyses of high-resolution Finite Element (FE) models of the 2.82-meter (9.25-ft.) girder subassemblies were performed utilizing the commercially-available Finite Element Analysis (FEA) software ABAQUS v6.10.

Objective

The main objective of this study was to create an effective retrofit measure, which can be easily installed in the field to a variety of different connection geometries, to repair the web-gap region of steel bridge girders with distortion-induced fatigue cracks. An extensive literature review showed that FRP materials are highly fatigue resistant and can be cast on site to fit any connection geometry (GangaRao, H. and Vijay, P. 2010). It was proposed that, for an FRP retrofit to be most effective, loads should be transferred to the FRP retrofit through mechanical connection, rather than the retrofit relying on an adhesive bond layer between the steel and FRPs. This study included Finite Element Analyses (FEA) to investigate various retrofit geometries utilizing FRPs and a mechanical device to create a positive connection. The performance of this retrofit was investigated experimentally by positively attaching the girder flange to the connection stiffener with the use of an FRP system, as was suggested for all of the web-gap stiffening retrofits provided in the "Manual for Repair and Retrofit of Fatigue Cracks in Steel Bridges" (Dexter, R and Ocel, J. 2013).

Computer Simulations

Methods

Finite Element Models (FEMs) were created to resemble as closely as possible the girder-cross frame subassemblies that would be tested. A detailed finite element model of the 2.82-meter (9.25-ft.) subassembly was developed using ABAQUS v.6.10. The models were constructed using three-dimensional solid elements with linear-elastic material properties. Each model contained approximately 2.3 million elements and 77 million degrees of freedom. Cracks were modeled explicitly by removing a 0.8-mm (0.03-in.) strip of elements. Appendix A provides a detailed description of the construction of these analytical models.

The goal of the modeling effort was to develop a retrofit measure which would provide the greatest magnitude of stress reduction in the web-gap region, where fatigue cracks have already developed. The goal of the retrofit was to prevent the growth of fatigue cracks in the web-gap region. By selecting the initial retrofit through computer simulations, the most promising configuration could be tested on a physical girder.

Results

The concept behind the retrofit that was developed was to install low modulus FRP blocks at the web-gap region, where cracking has occurred. These blocks would stiffen the web-gap region and prevent crack growth from occurring. A large fiber-volume ratio in an FRP composite block can be difficult to achieve, and the cost of fibers typically govern the cost of the FRP. A lower fiber-volume ratio typically creates a lower modulus FRP, while a large fiber-volume ratio typically creates a higher modulus FRP. For this reason low modulus FRP blocks were utilized. FEM models were constructed with a mechanical device which connected the FRP blocks to the stiffener, the web, and the flange. The analytical models with a composite block retrofit which provided positive attachment between the girder flange and connection stiffener provided the greatest stress reduction in the web-gap region. The composite blocks would prevent rotation between the connection stiffener and girder flange in the web-gap region by redistributing load to the remainder of the structure. These analytical results agreed with the retrofit selections devised at the fatigue and fracture workshop held in 2002.

After numerous models were created and analyzed a mechanical connector designated the Bonet Stud was developed. In the FEM models all composite-to-steel interactions were defined as a hard-contact with a coefficient of friction between the surfaces of 0.3. The Bonet Stud embedded in an FRP block was shown to successfully reduce the stress demand, at a 38-mm (1½-in.) “horseshoe-shaped crack” around the toe of the connection stiffener to web weld, in analytical models by over 95%. The composite block retrofit geometry is shown in Figure 2 and is further detailed in Appendix C. The specific geometry of the Bonet Stud was found to be effective because a large surface of the Bonet Stud is in bearing against the girder flange preventing excessive bending from occurring. The large surface area on the top of the Bonet Stud also provides a location for the composite to bear against. Figure 3 shows the composite block retrofit used in the analytical models and Figure 4 shows a stress path taken from the analytical models for both the retrofitted and unretrofitted specimens. The

stress path is taken at a distance of half the web thickness 4.8mm (0.19 in.) away from the edge of the crack. This path was used to quantify the magnitude of stress reduction from the unretrofitted to retrofitted state.

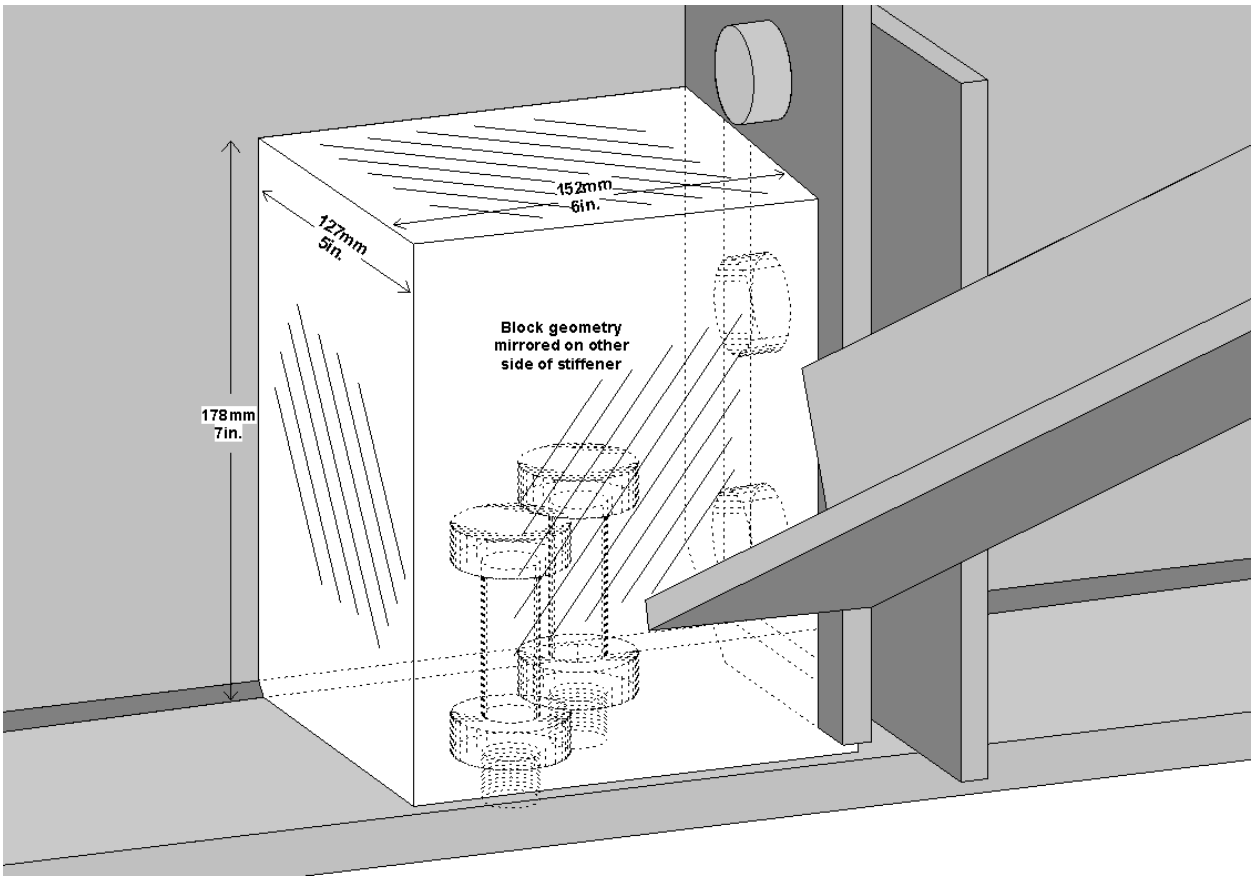

Figure 2: Dimension of composite block retrofit

Figure 5 presents a comparison of maximum principal stresses from the path in the unretrofitted and retrofitted models. The retrofit geometry in each retrofitted model is exactly the same, the differences in the models are the composite material properties used; the modulus of elasticity for each retrofitted model was varied. Increasing the modulus of elasticity of the composite block did not have a significant effect on the magnitude of stress reduction.

In the field the composite block retrofit would be installed by drilling and tapping holes into the top flange of the girder and subsequently installing Bonet Studs after first applying Locktite compound (or equivalent) to prevent loosening of the Bonet Studs from the girder. A temporary mold would then be installed around the web-gap region. FRP would be pumped into the mold and allowed to cure. The cure time would be a function of the matrix system used and the temperature at the bridge site. After the composite has cured the mold could then be removed, Appendix M outlines this procedure in further detail. Drilling and tapping the top flange of a girder, to avoid having to remove a portion of the concrete bridge deck, is not a new idea. On the Poplar Street Bridge Complex in East St. Louis, Missouri and on the Neville Island bridges which carries 1-79 near Pittsburgh, Pennsylvania, distortion-induced fatigue cracks were retrofitted by attaching steel angles from the connection stiffener to the top flange of the girder (Koob et al. 1985). To accomplish this, holes were drilled and

tapped into the top flange of the girder and high-strength threaded studs were installed into the holes. Steel angles were then attached to the high strength studs (Koob et al. 1985).

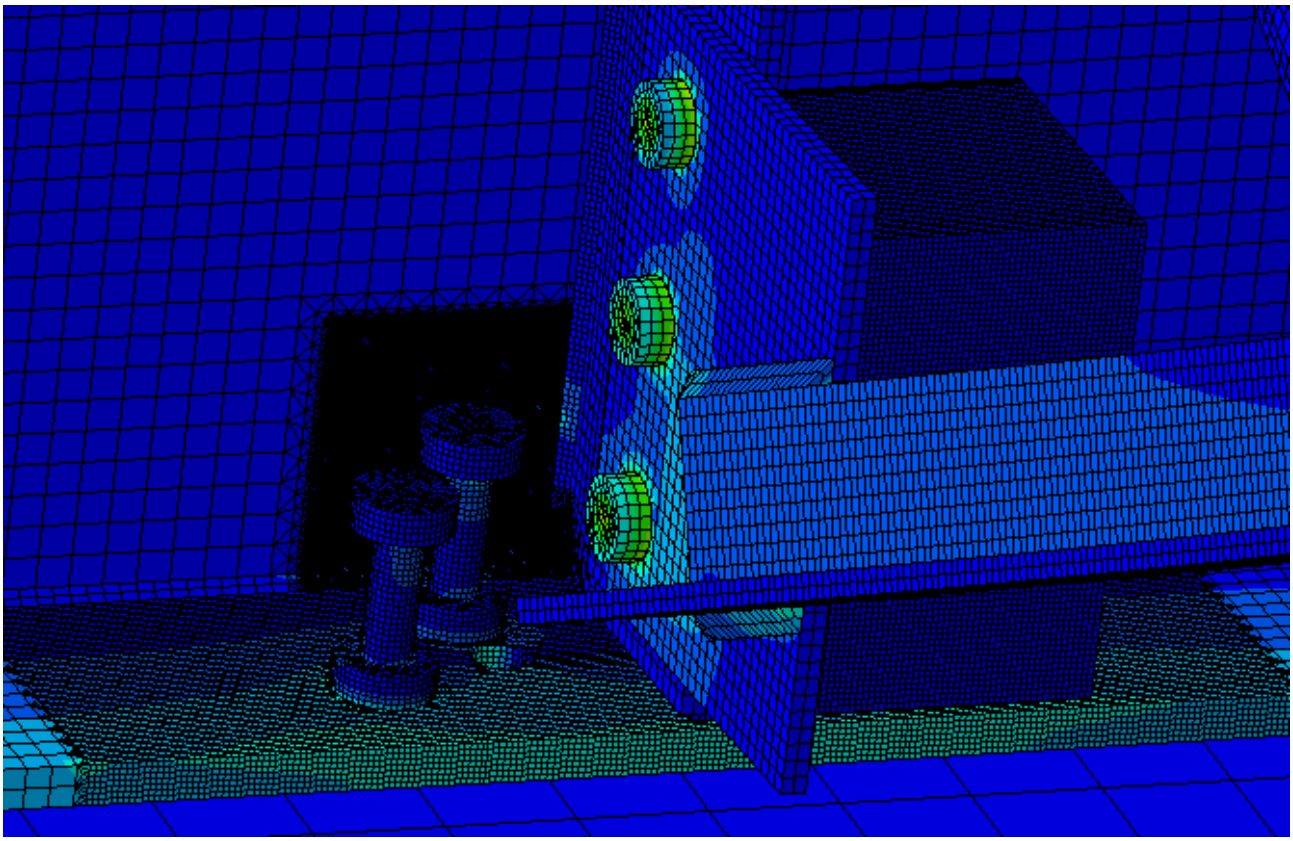

Figure 3: Web-gap region with composite block and stud locations (left composite block was removed from view)

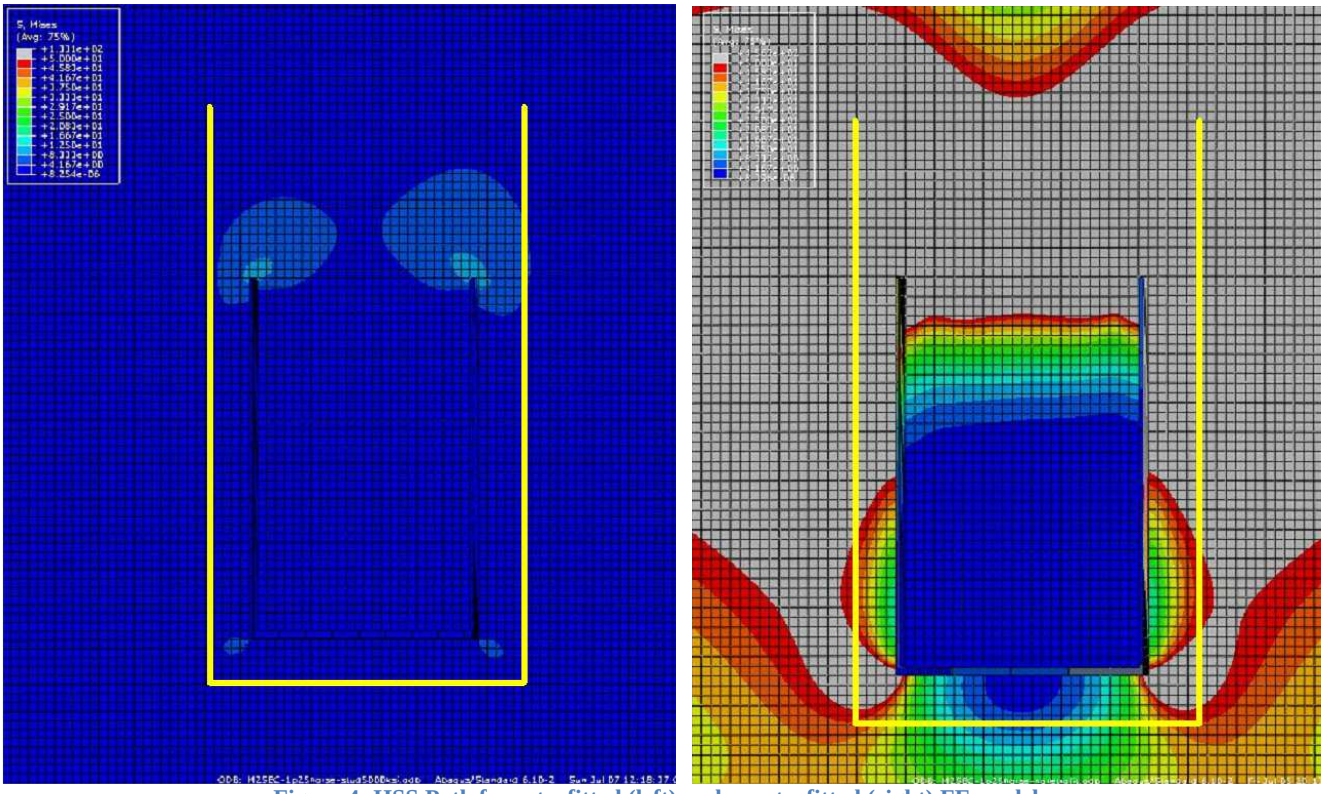

Figure 4: HSS Path for retrofitted (left) and unretrofitted (right) FE models

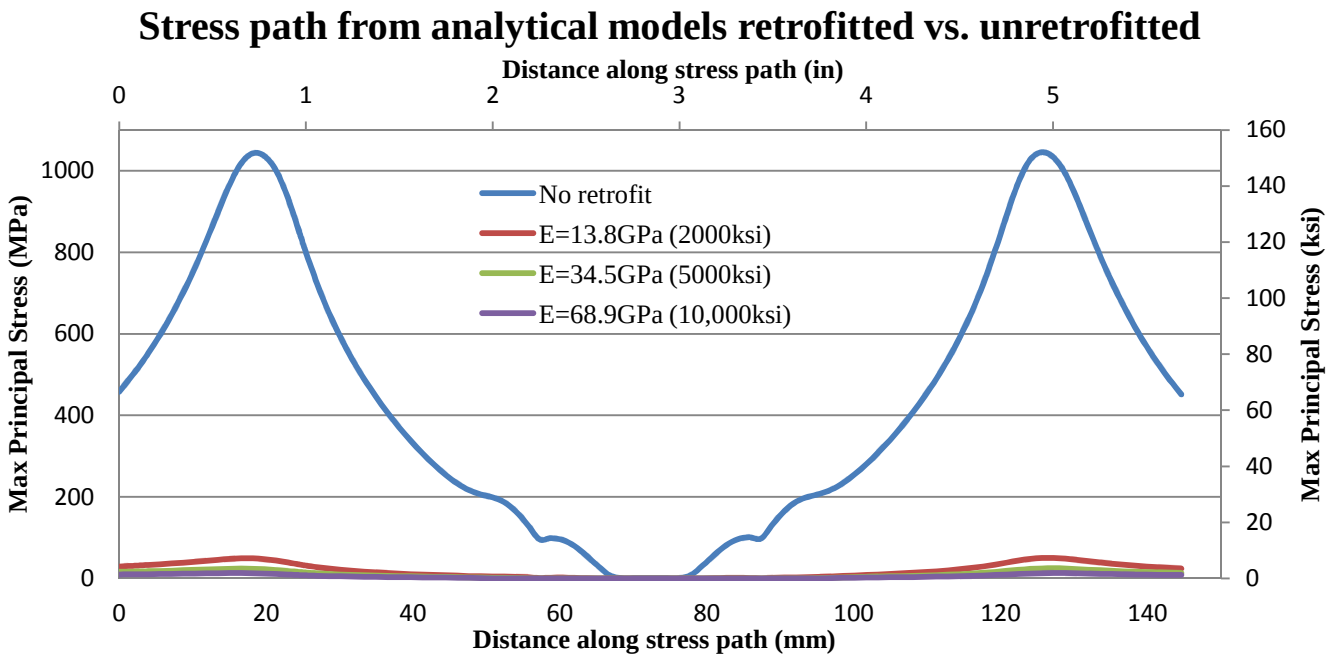

Figure 5: Retrofitted specimen using the composite block retrofit with varying modulus of elasticity vs. unretrofitted specimen

Experimental Program

The goal of the experimental study was to test the composite block retrofit under fatigue loading, to determine if the retrofit is effective at preventing the formation and growth of fatigue cracks caused by distortion-induced fatigue, and to determine if the finite element simulations were accurate at estimating the magnitude of stress reduction experienced in the web-gap region from an unretrofitted to retrofitted state. In web-gap regions of bridges, the top flange is restrained from lateral motion while the bottom flange is free to move out-of-plane. The top flange experiences some degree of bending and rotation as the entire bridge deflects due to passing traffic. It is difficult to replicate the same boundary conditions that exist in a bridge when preforming component tests. In previous 2.82-meter (9.25-ft.) girder models tested at the University of Kansas the specimens were fully fixed to the strong floor preventing any rotation of the flange. It was decided that a more rigorous test for the composite block retrofit would be one that would allow rotation in the bottom flange because, by allowing the bottom flange to rotate, the block could debond from the girder at a faster rate. For that reason the 2.82-meter (9.25-ft.) girder subassembly was only restrained at its ends as shown in Figure 6. Figure 7 shows an elevation view of the crossframe and the girder subassembly. Further details about the construction of the subassembly as well as the instrumentation of the specimen can be found in Appendix B.

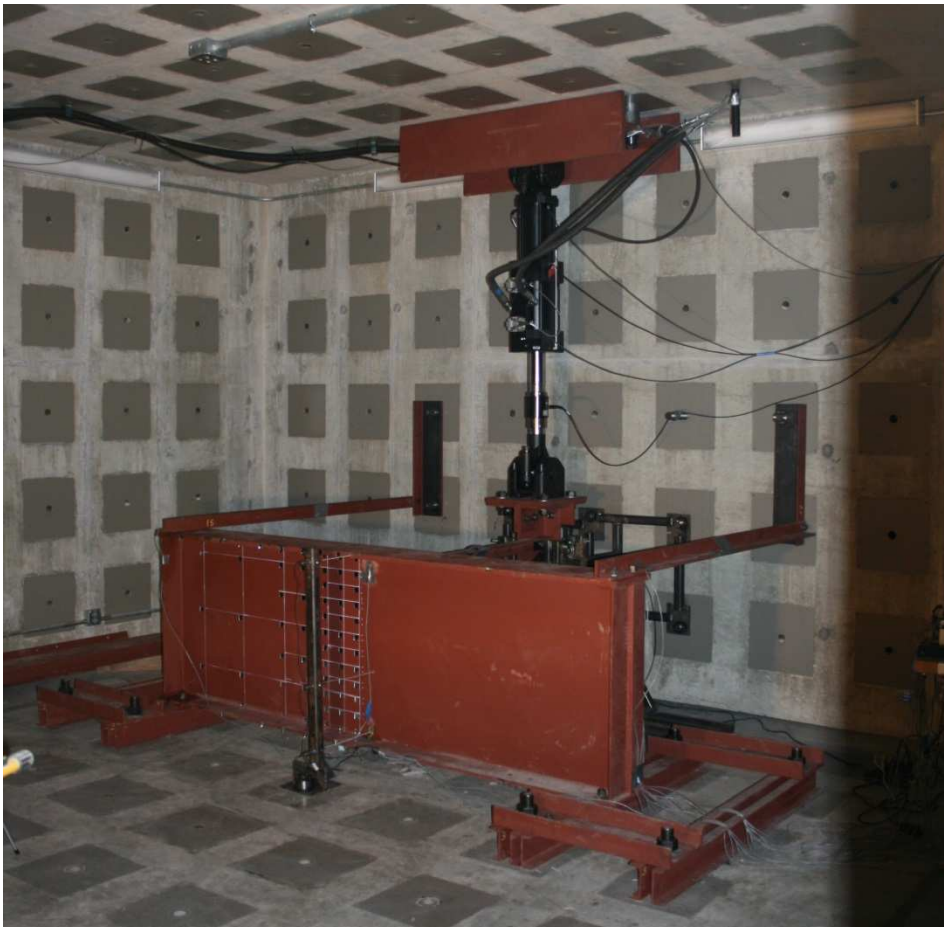

Figure 6: Experimental Setup in Fracture and Fatigue Lab at M2SEC

Figure 7: Elevation view of girder subassembly in Fracture and Fatigue Lab at M2SEC

The loading protocol of the girder subassembly included multiple trials. The first trial, designated G1.1, began by applying cyclic loading, ranging from 2.2 kN (0.5 kips) to 24.5 kN (5.5 kips) at a rate of 2 cycles per second to an uncracked and unretrofitted girder subassembly. The main objective of Trial G1.1 was to allow cracks to initiate and propagate. After 35,000 loading cycles, a through-thickness horseshoe-shaped fatigue crack was observed along the connection plate-to-web weld, in the web-gap region as shown in Figure 8. The crack was inspected every thousand cycles using UV light and dye penetrant. After the crack had reached a length of 48 mm ($1\frac{7}{8}$ in.) Trial G1.1 was ended and the composite block retrofit was applied to the bottom web-gap region of the girder subassembly, as shown in Figure 9. The retrofit was applied by drilling holes through the flange, grinding paint off of the specimen in the region where the block would be installed, bolting the Bonet Studs to the flange, constructing a plywood mold around the web-gap region, and then putting the FRP mixture into the mold and letting it cure. The FRP mix had a 15% carbon fiber to epoxy ratio by volume. Appendix C describes in detail the retrofit installation process.

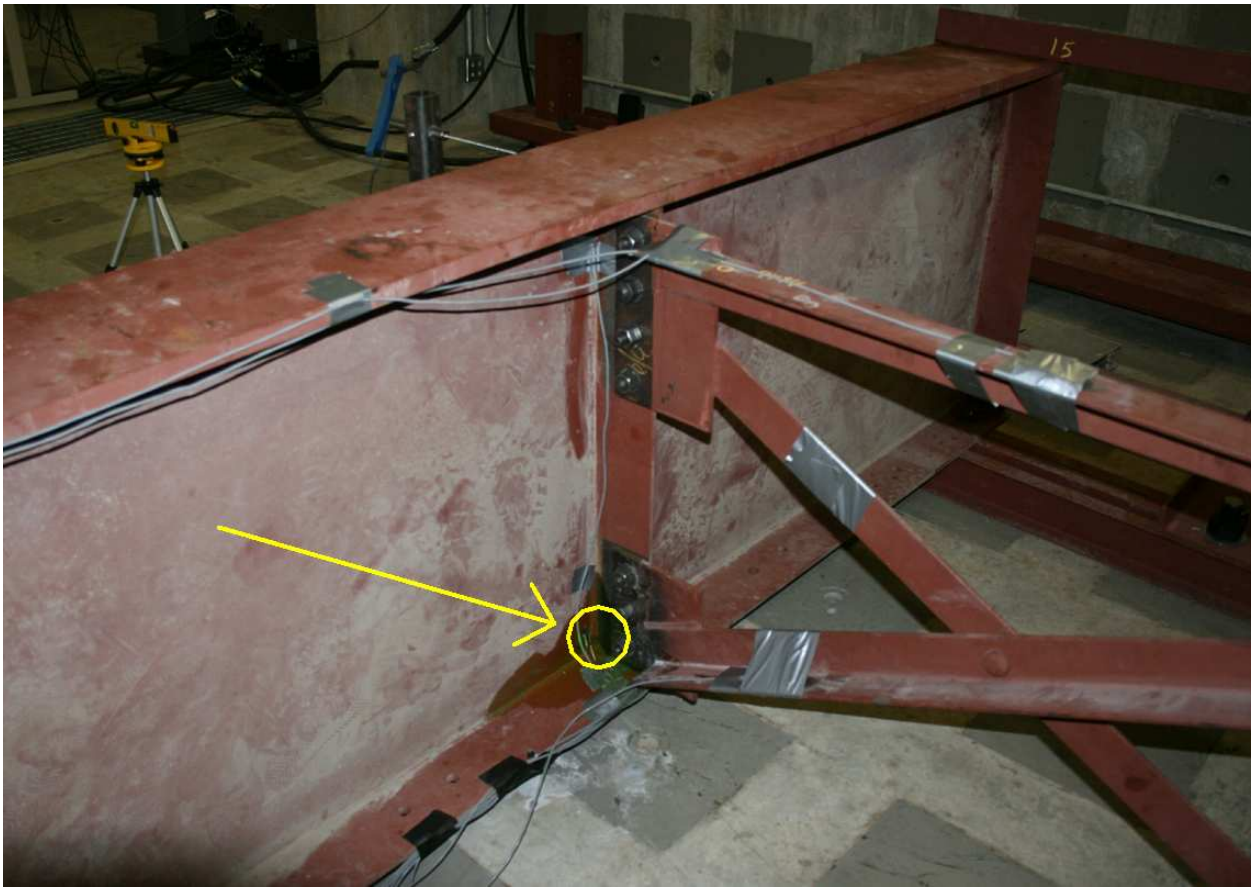

Figure 8: Cross frame to connection stiffener detail, crack location circled in yellow

Utilizing the same composite mix design as was used in the composite block retrofit, five carbon-fiber-reinforced polymer (CFRP) tensile specimens were fabricated and tested in accordance with ASTM D3039-08 to obtain the tensile strength, modulus of elasticity and Poisson's ratio. Five bearing specimens were also fabricated and tested in accordance with ASTM D5961-13. Appendices D and E provide the ASTM reports for each respective test. The average modulus of elasticity calculated from the tension specimens was 4751MPa (689ksi), and the average tensile strength was 30 MPa (4.3ksi). The bearing tests showed that the bearing strength of the

material was 69 MPa (10ksi). Compared with steel, the strength and elastic properties of the CFRP specimens were low, but FRPs are known for their high fatigue endurance (GangaRao, H. and Vijay, P. 2010), the computer simulations had shown that the modulus of elasticity of the composite block was not relevant (Figure 5), and given the large-volume technique being applied, testing began.

Figure 9: Composite block retrofit installed in the lower web-gap region

After the CFRP composite blocks were installed, the girder subassembly was subjected to 1.2 million cycles (Trial G1.2). This number of cycles was chosen because in the S-N diagram of the AASHTO-LRFD Bridge Design Specifications (AASHTO 2010) for a Category A fatigue detail it corresponds to a stress range of 193 MPa (28 ksi). The 193-MPa (28-ksi) stress range was measured experimentally at the bottom web-gap of an uncracked girder subassembly without any retrofit measures during trial G1.1. Based on field measurements recently recorded at the web-gap region of a bridge in Wichita, Kansas under the action of a 267-kN (60-kip) truck, it is estimated that the stress range applied to the girder subassembly corresponded approximately to 5 times the stress range that would be induced by the fatigue design truck load specified in the AASHTO Bridge Design Specifications. The fascia side of the web-gap region was unobstructed by the retrofit measure, which allowed the length of the through-thickness horseshoe-shaped crack to be closely monitored throughout the entire trial. At the end of Trial G1.2 the 48-mm ($1\frac{7}{8}$ in.) horseshoe-shaped crack did not undergo any measurable growth, and the retrofit showed no signs of failure or debonding from the girder.

For Trial G1.3 the actuator force range was increased by 50% to a range of 3.3-kN (0.75-kips)(P_{min}) - 36.7-kN (8.25-kips)(P_{max}), at a loading rate of 2Hz. The displacement range of the actuator for this load range was approximately 12m m (0.48 in.) compared with 8.4 mm (0.33 in.) during Trial G1.2. The girder subassembly

underwent 950,000 cycles at the increased force range (2.15 million total cycles) before an 89-mm (3.5-in.) crack was spotted along the flange-to-web weld in the top web-gap region of the subassembly, which was not retrofitted. Loading continued with the same configuration and loading protocol until a total of 1.2 million cycles was reached (2.4 million total cycles). When testing concluded, the crack in the top web-gap region was 165-mm (6.5-in.) long and through-thickness cracks were observed along the connection plate-to-web weld in the top web-gap region.

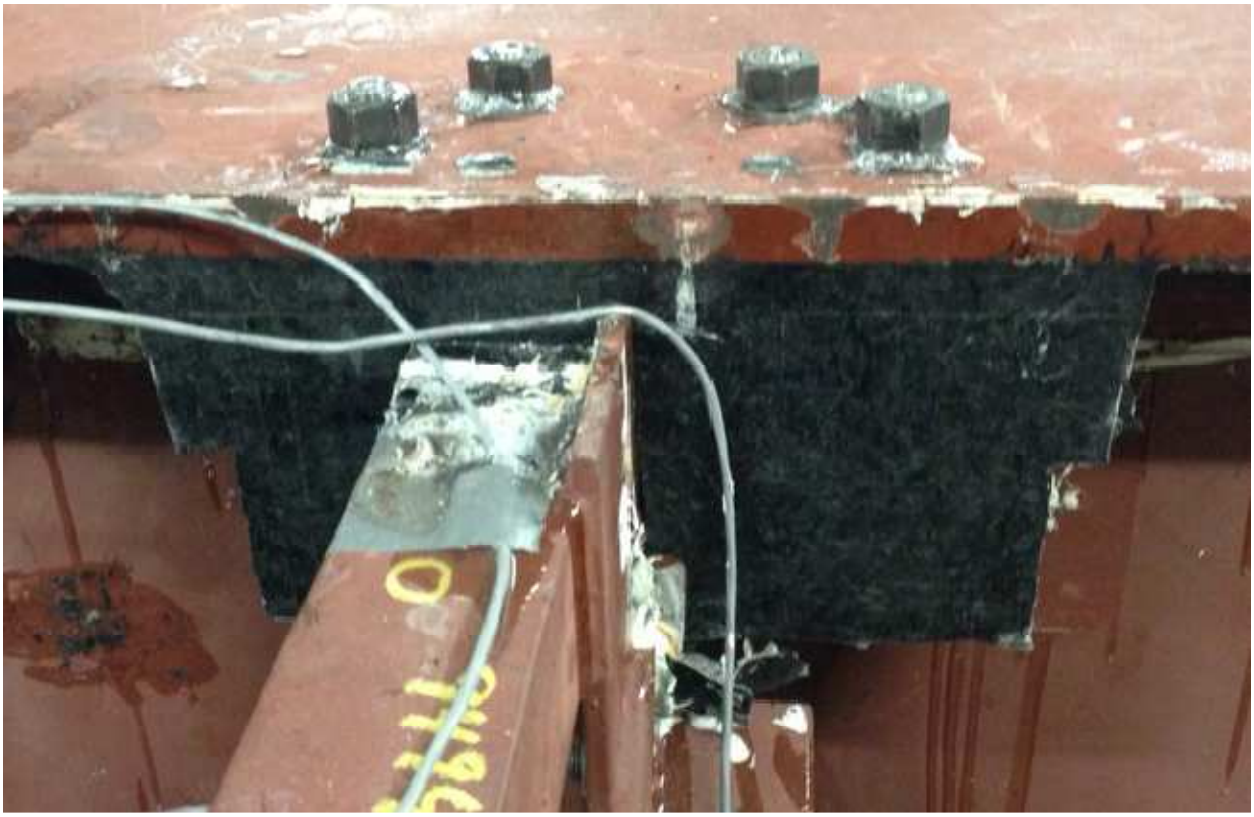

Figure 10: Upper web-gap region with composite block retrofit

In Trial G1.4, CFRP blocks were cast in the top web-gap region of the girder as shown in Figure 10. The block geometry mirrored the geometry used in the lower web-gap region (the upper web-gap installation process can be found in Appendix F). The composite blocks installed in the upper web-gap region more closely resembled how a composite block would be installed on a bridge in the field because, on a bridge in the field, the composite block needs to overcome the force of gravity during its casting and curing process. To achieve this, a mold was constructed around the upper web-gap region with a 127x102-mm (5x4-in.) tunnel on the side of the mold. CFRP was put into the mold through the side tunnel. After the mold was full of CFRP a 127x102-mm (5x4-in.) piece of plywood was forced into the side tunnel of the mold by a 51x102-mm (2x4-in.) compacting the CFRP while it cured. After the CFRP cured the mold was removed.

After the retrofit measure was successfully installed, testing continued at the increased load range of 3.3 kN (0.75 kips) - 36.7 kN (8.25 kips). After 44,838 cycles, a 165-mm (6½-in.) mode I fatigue crack was found on

the tab plate connecting the cross-frame to the connection plate in the bottom web-gap region, as shown in Figure 11 and Figure 12.

The crack on the tab plate was ground down with an angle grinder on both sides to allow an arc-weld to fully penetrate the crack. A certified welder, arc-welded the cracked portion of the tab plate back together. Testing resumed and 80,000 cycles later (2,525,000 total cycles) the weld on the tab plate fractured. The weld was gouged out and the tab plate was rewelded. Testing resumed. Just 20,000 cycles later (2,545,000 total cycles) the second weld on the tab plate fractured; it was then rewelded for the third time. Testing resumed and 35,000 cycles later (2,580,000 total cycles) the weld on the tab plate fractured again. Following these results it was obvious welding the crack on the tab plate was a temporary solution.

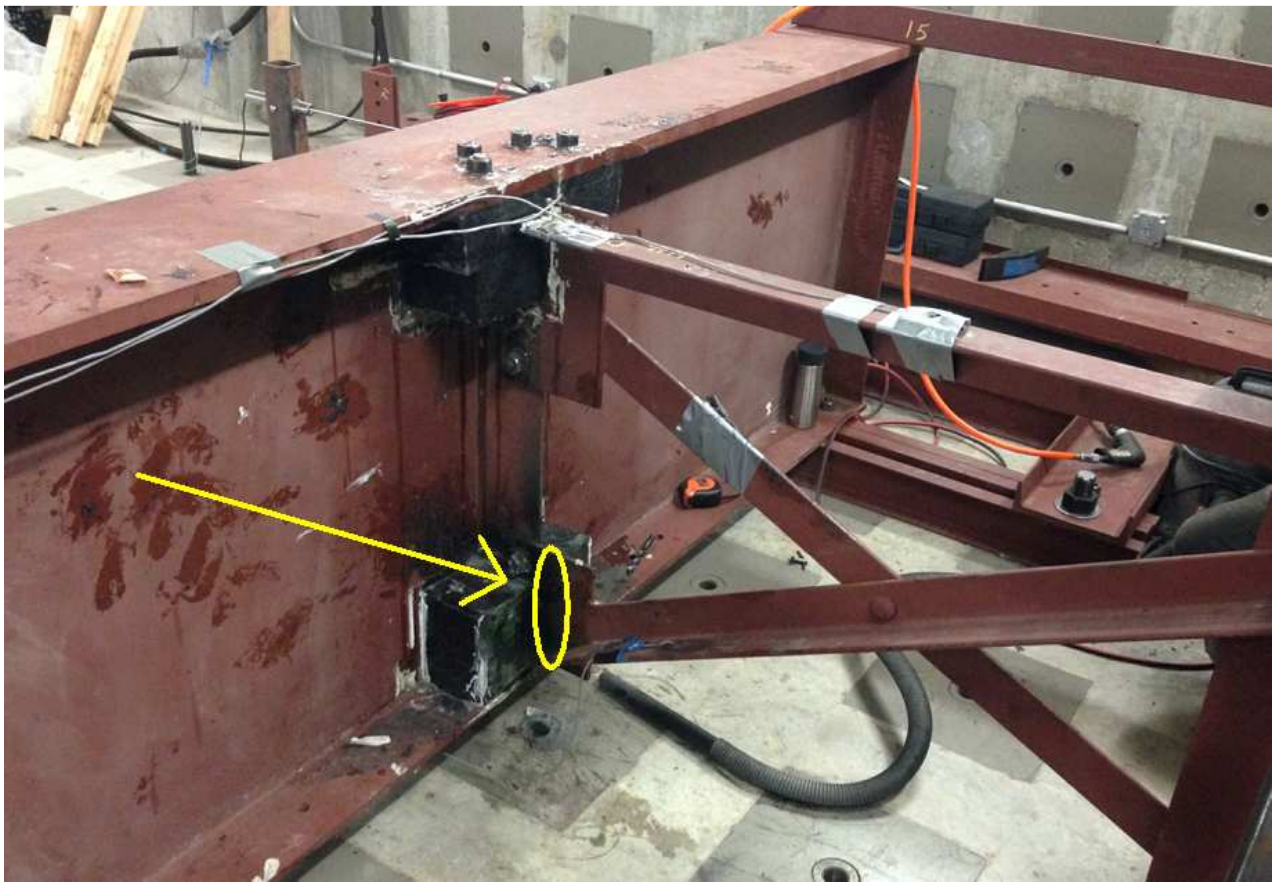

Figure 11: Location of tab plate crack, circled in yellow

The weld on the Tab plate continually experienced Mode 1 fracture, since the primary direction of stresses through the tab plate was perpendicular to the weld direction. For testing to successfully continue, another path would be needed to transfer stresses from the girder to the cross frame members. Since a large portion of the tab plate was embedded in the composite block and the crack was located closely to the block there was not enough remaining surface area on the tab plate to utilize a standard bolted steel plate retrofit.

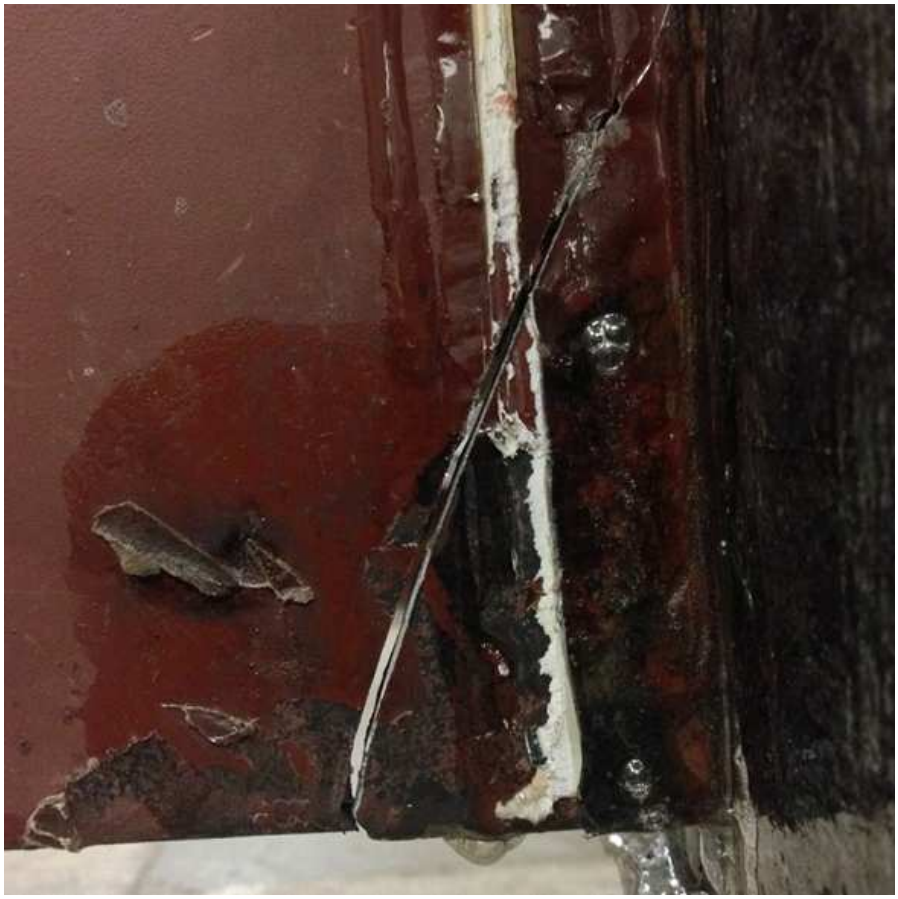

Figure 12: Crack on tab plate

As a result other nonconventional retrofit options were evaluated for the purpose of completing the web-gap test trial. Because materials used in the aerospace industry are highly resistant to fracture, literature was reviewed to parse retrofits which prevented Mode I fractures. Delamination cracking is one of the most dangerous modes of failure in laminated composites. Stitching is used to prevent delamination of composite laminates by diverting the primary stress direction from the weak areas to the stitches themselves, and has been found to be a reliable method of reducing delamination tendencies (Birman and Byrd, 2006). According to research conducted by Dexter and Funk (1986), Mode I fracture toughness of Kevlar stitched laminates increases by a factor of 30 when compared with non-stitched laminates. There is a large body of research on various aspects of stitched laminates, which can be found in the papers by Chen et al. (2003), Gui and Li (2001), Jegley et al. (2001), Lau et al. (2004), Yavuz et al. (2005), and Yeh et al. (2004).

In this research the crack on the tab plate was experiencing Mode I fracture, so it was determined that a stitching repair similar to the ones used to prevent delamination in laminated composites, but on a much larger scale, might successfully prevent the tab plate from reopening and allow the test trial to be completed. Since Kevlar has been proven effective in the field of aerospace engineering for stitching retrofits, and is widely available for commercial use, Kevlar stitching was utilized to repair the tab plate.

In order to apply the Kevlar stitching retrofit, the fractured weld was first gouged out and rewelded. The girder subassembly was prepped for the stitching retrofit by drilling two 16-mm (5/8 -in.) holes through the composite block and web in the lower web-gap region on both sides of the stiffener. Five holes were drilled

through the lower cross frame angle section and 10-mm (3/8-in.) diameter medium strength steel screws were installed in the holes on the angle section. Kevlar strands coated in epoxy were then used to stitch the tab plate together. Appendix G further explains the preparation and application of the stitching retrofit. Figure 13, Figure 14 and Figure 15 show the Kevlar stitching retrofit applied to the specimen.

After the stitching retrofit was applied, test trial G1.4 resumed. The girder subassembly was then successfully loaded to 1.2 million cycles (3.75million total cycles) at the force range of 3.3kN (0.75 kips) - 36.7kN (8.25 kips) with no visible crack growth, thus concluding Trial G1.4.

The only fracture that occurred during test trial G1.4 occurred at 2.73 million total cycles at a bolt hole location below the MTS actuator at the cross frame-to-WT connection. This bolt hole fracture location was on the opposite end of the same angle section to which the stitching retrofit was applied, as shown in Figure 16. Two new holes were drilled through the angle section and the WT, then new 19-mm (¾-in.) A325 bolts were installed. For the remainder of testing (another 1.42 million cycles) the angle section did not fracture.

Figure 13: Kevlar stitching retrofit, north stiffener side

Figure 14: Kevlar stitching retrofit, south stiffener side

Figure 15: Kevlar stitching retrofit, fascia side

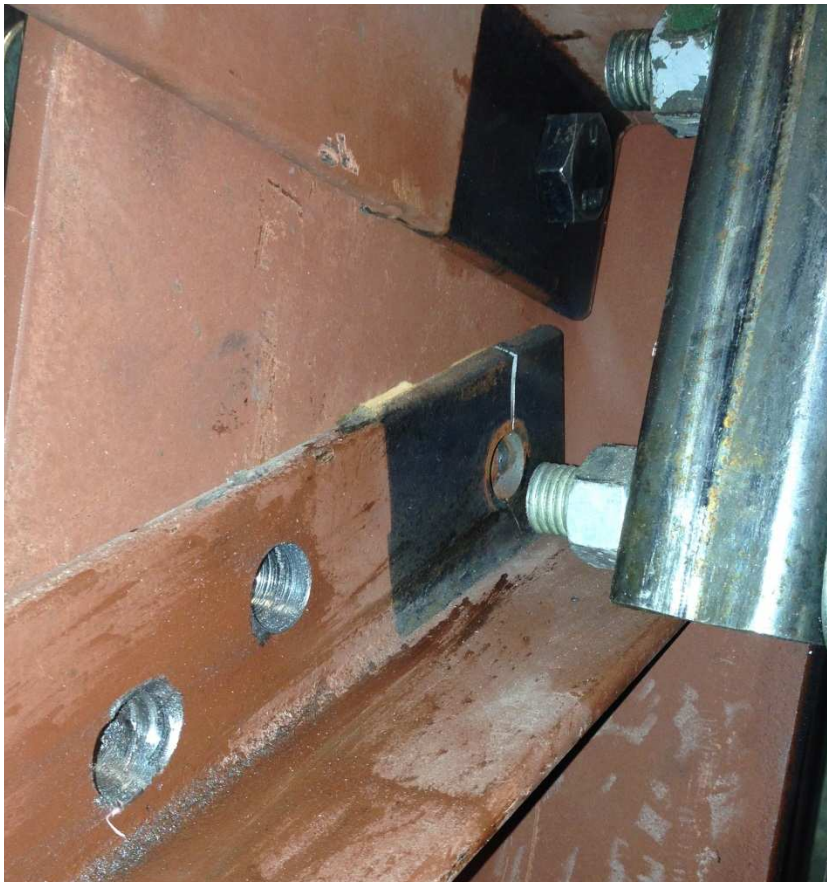

Figure 16: Crossframe angle fracture at bolt hole

For Trial G1.5 the actuator force range was further increased to a force range of 4.4 kN (1.0 kips) - 48.9 kN (11 kips), at a loading rate of 2 cycles per second. The displacement range of the actuator for this load range was approximately 15 mm (0.58 in.). After 377,000 cycles (4,127,000 total cycles), the welded repair on the tab plate refractured. Testing continued with the fractured weld, the force in the cross frame being fully carried by the Kevlar stitching. When the girder subassembly reached 400,000 cycles (4,150,000 total cycles), the crack on the tab plate propagated all the way to the top bolt hole as shown in Figure 17. After the specimen underwent almost 25,000 additional cycles the closest bolt wrapped in Kevlar on the vertical leg of the cross frame L angle fractured in shear, as shown in Figure 18. Less than 1,000 cycles later, all three of the bolts wrapped in Kevlar on the vertical leg of the L angle fractured in shear as shown in Figure 19. After those bolts fractured the actuator was displacing 19 mm (¾ in.) each load cycle, and for that reason the actuator frequency was lowered from 2Hz to 1Hz. Less than 100 cycles after the three bolts wrapped in Kevlar fractured in shear the tab plate fully fractured above the last bolt hole as shown in Figure 20.

The Kevlar stitching was still fully intact but due to the fracture of over half of the bolts connecting the stitching to the cross frame angle, testing could not be continued. These bolts proved to be the weak link, if the Kevlar was stitched directly to holes drilled into the crossframe, this weak link, would have been eliminated. Also, the extremely high force range that the girder subassembly was undergoing at the time of failure was well beyond what this connection would be expected to endure in the field.

Figure 17: Tab plate fracture with Kevlar stitching

Figure 18: First bolt wrapped in Kevlar fractures at 4,024,848 total cycles

Figure 19: All three bolts wrapped in Kevlar fracture at 4,025,683 total cycles

Figure 20: Tab plate fully fractured

Removal of the composite block

After testing concluded, the composite block retrofit needed to be removed from the lower web-gap region of the girder subassembly to inspect the stiffener side of the web-gap region for crack growth. The composite block was removed with steel chisels, drills and a reciprocating saw. Figure 21 shows the final Bonet Stud in the lower web-gap region of the composite block, on the north side of the girder subassembly. After the studs were removed from the composite block the remainder of the CFRP material was easily detached. With the block successfully removed, the lower web-gap region the crack was visually inspected. Due to the fracture of the tab plate the girder subassembly was unable to be cycled under load to inspect the crack. However, there was no visible crack growth; in fact, epoxy from the CFRP had made its way into the crack during casting of the composite block in the lower web-gap region. This epoxy was still inside the crack after over 4 million cyclic load cycles.

The upper web-gap region was detached from the girder subassembly by plasma cutting the section of the girder where the composite block was installed. The detached upper web-gap region was then used for corrosion testing as described in Appendix L. After the corrosion testing was concluded a 355mm (14-in.) chop saw with a steel worker chop saw blade was utilized to take a section cut of the block. Figure 22 shows how the block was cut and a section cut of the composite block in the upper web-gap region. From visually inspecting the section cut of the composite block in the upper web-gap region it appeared that the block had not debonded from the girder web or flange and that the crack in the upper web-gap region did not appear to have experienced growth.

Figure 21: Removing composite block, Bonet stud fully embedded in CFRP

Figure 22: Section cut of composite block in upper web-gap region

Experimental Results

Results from the experimental testing are illustrated in Figure 23 and Figure 24. Figure 23 presents the crack patterns in the lower web-gap region recorded at the end of Trial G1.1, before applying the composite block retrofit, and at the end of Trial G1.3, after the crack at the upper web-gap region reached 165 mm (6.5 in.). The rate of crack growth prior to and after the retrofits were applied is illustrated in Figure 24, which shows that the crack propagation in both web-gap regions was eliminated after each retrofit measure.

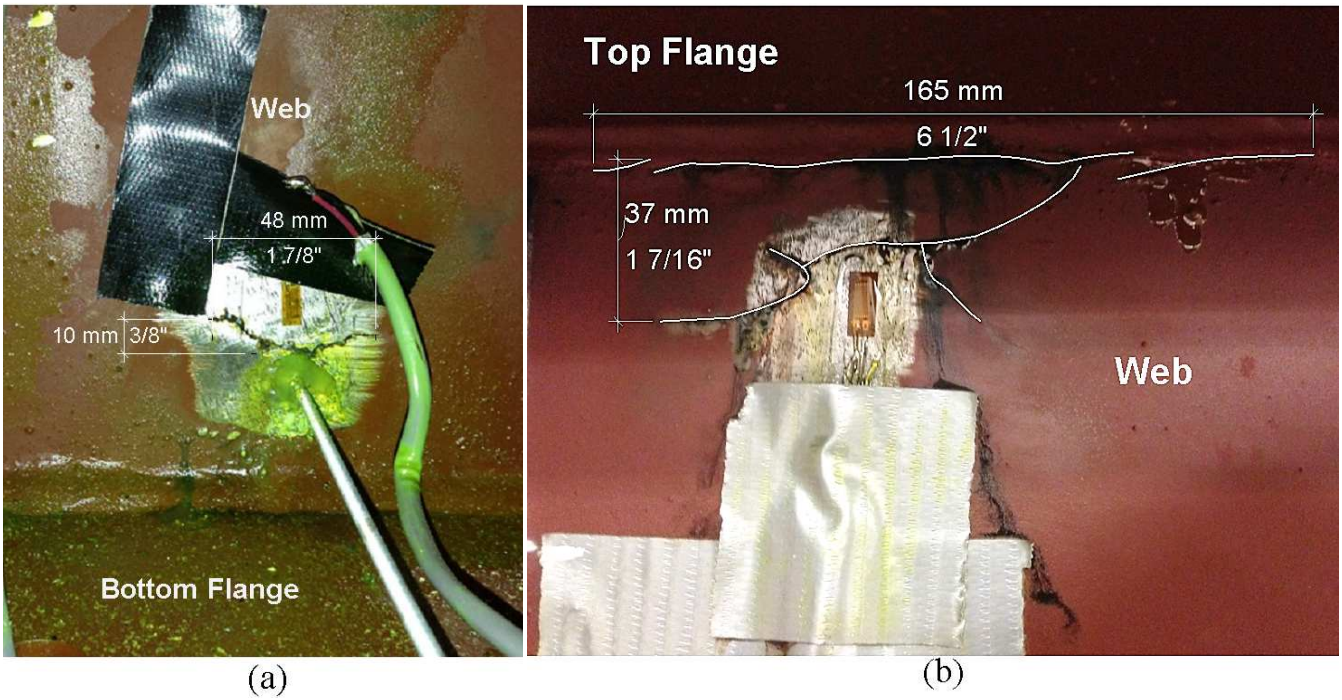

Figure 23: Observed crack patterns in girder subassembly after Trial G1.1 (a: Lower Web-gap Region fascia side) and after Trial G1.3 (b: Upper Web-gap Region fascia side).

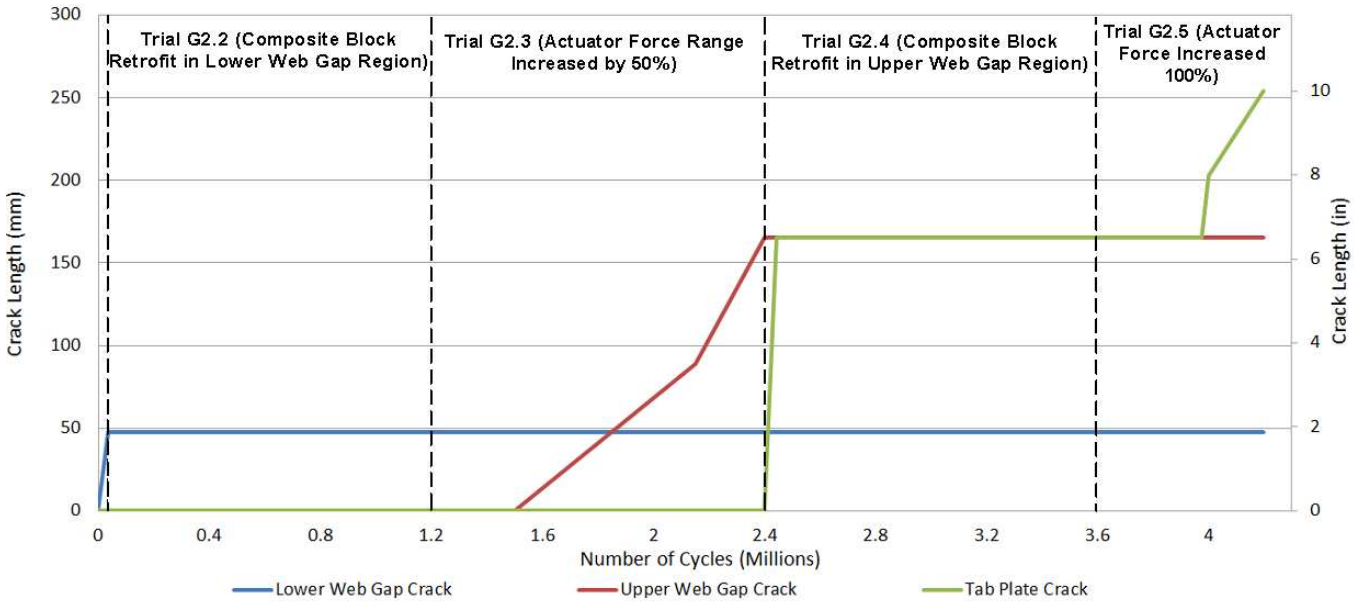

Figure 24: Crack propagation rate as measured on fascia side of girder and tab plate

Figure 25 shows the change in stress recorded during static testing for trials G1.1 and G1.2. The Y-axis gives the stresses which were converted from the strain recorded from the lower fascia strain gage shown in the left of Figure 23. The X-axis is the force recorded from the MTS load cell on the 245 kN (55 kip) actuator. As shown, after the composite block retrofit was applied the stress recorded from the lower fascia strain gage decreased greatly.

Angular rotations on the north half of the fascia side of the girder subassembly were recorded with an array of mirrors and a laser (procedure described in Appendix H). Based off of the rotation calculated at each mirror, the change in stress between mirrors was calculated (procedure described in Appendix I). This data is helpful in viewing how the composite block retrofit successfully stiffened the web-gap region. Figure 26 shows vertical stress changes based off X-axis rotation across the north half of the girder subassembly during Trial G1.1. The lower right corner of Figure 26 corresponds the fascia side of the web-gap region and the stress differential in that region is almost -83Mpa (-12ksi). Figure 27 shows vertical stress changes based off X-axis rotation across the north half of the girder subassembly during Trial G1.2. The block was highly successful in stiffening the web-gap region as the data shows since stress change across the entire girder subassembly was negligible during Trial G1.2.

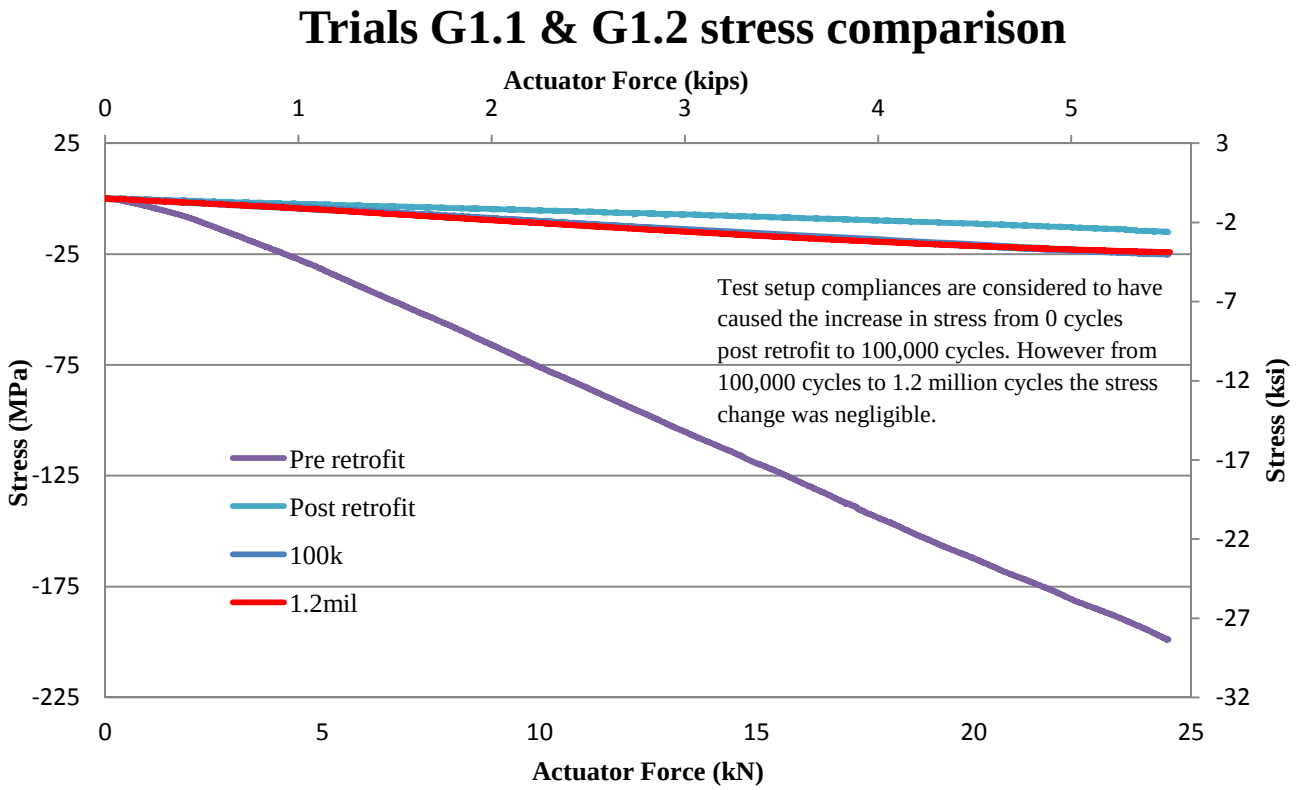

Figure 25: Stress recorded from the lower fascia strain gage vs. Actuator Force during trials G1.1 & G1.2

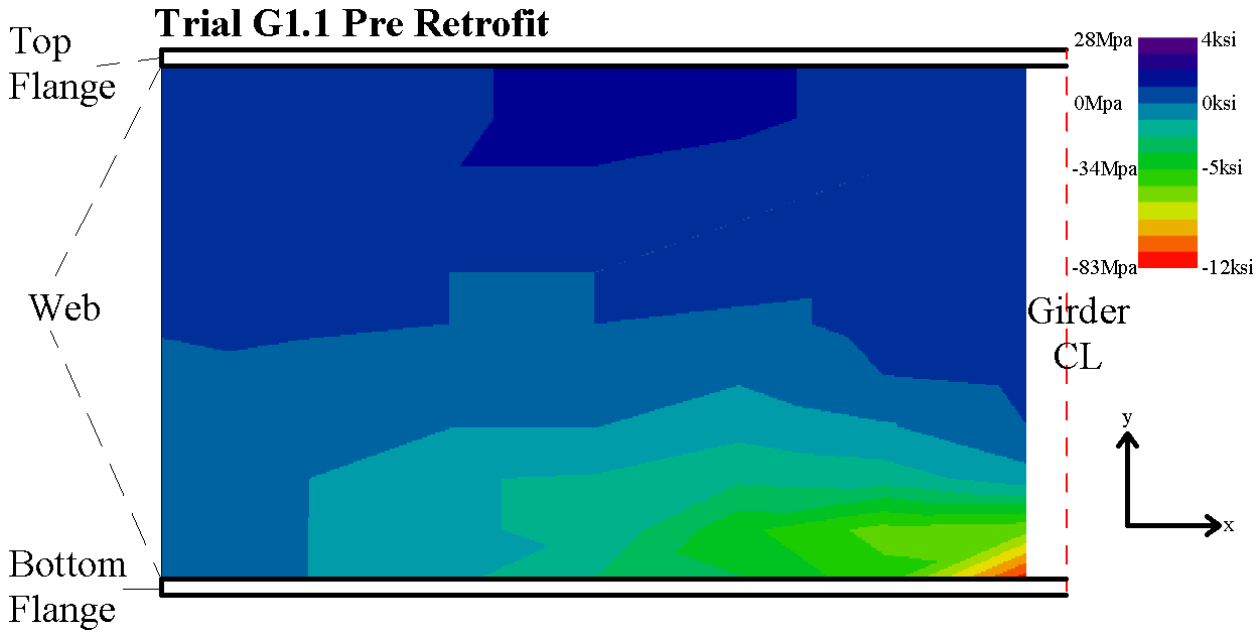

Figure 26: Trial G1.1 vertical stress changes calculated from X-axis rotations across the north half of girder subassembly in pre retrofitted state

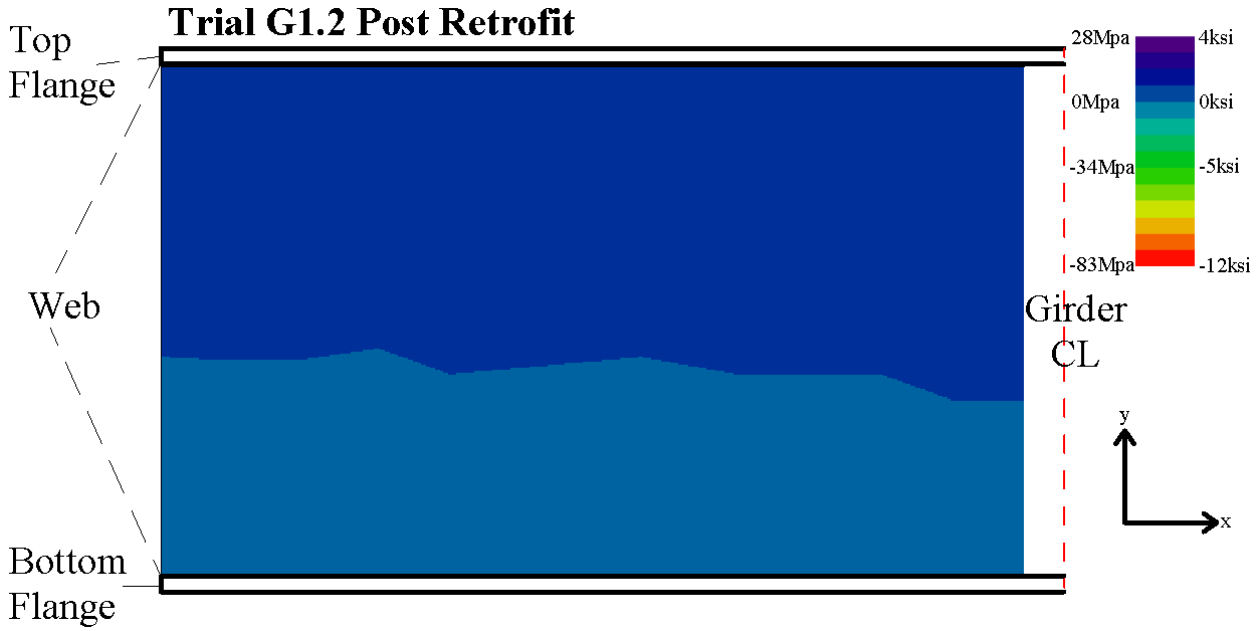

Figure 27: Trial G1.2 vertical stress changes calculated from X-axis rotations across the north half of girder subassembly in post retrofitted state

Figure 28 shows the change in stress during static testing computed from the lower fascia strain gage during Trials G1.1, G1.2, G1.3 and the start of Trial G1.4. Stress was computed by finding the difference in the maximum and minimum strain gage values during static tests and multiplying that difference by the nominal modulus of elasticity of steel, 200,000 MPa (29,000ksi). Before the composite retrofit was applied, the change in stress recorded was almost 200 MPa (29 ksi) in compression. After the retrofit was applied, but before cyclic testing began, the stress dropped to just above 14 MPa (2 ksi) in compression. As shown after the first 100,000 cycles, the change in stress increased to 25.5 MPa (3.7ksi) in compression, this was most likely due to specimen and test setup compliances. The strain gage behind the stiffener on the fascia side of the lower web-gap region,

showed that the lower web-gap region was in compression for the entirety of testing with a compressive stress range varying between 23 MPa (3.4 ksi) and 26 MPa (3.8 ksi) throughout the remainder of Trial G1.2. At the start of Trial G1.3, the compressive stress recorded from the lower fascia strain gage increased to 27Mpa (4.0ksi) due to the increase in actuator force. As Trial G1.3 progressed, the compressive stress in the lower web-gap region decreased as the flexibility of the upper web-gap region increased due to the formation and growth of fatigue cracks in the upper web-gap region. At the end of Trial G1.3, the compressive stress in the lower web-gap region recorded from the lower fascia strain gage was only 1.3Mpa (0.19ksi). Due to the installation of the composite block retrofit in the upper web-gap region, the compressive stress in the lower web-gap region computed from the lower fascia strain gage increased slightly to 7.6Mpa (1.1ksi) at the start of Trial G1.4.

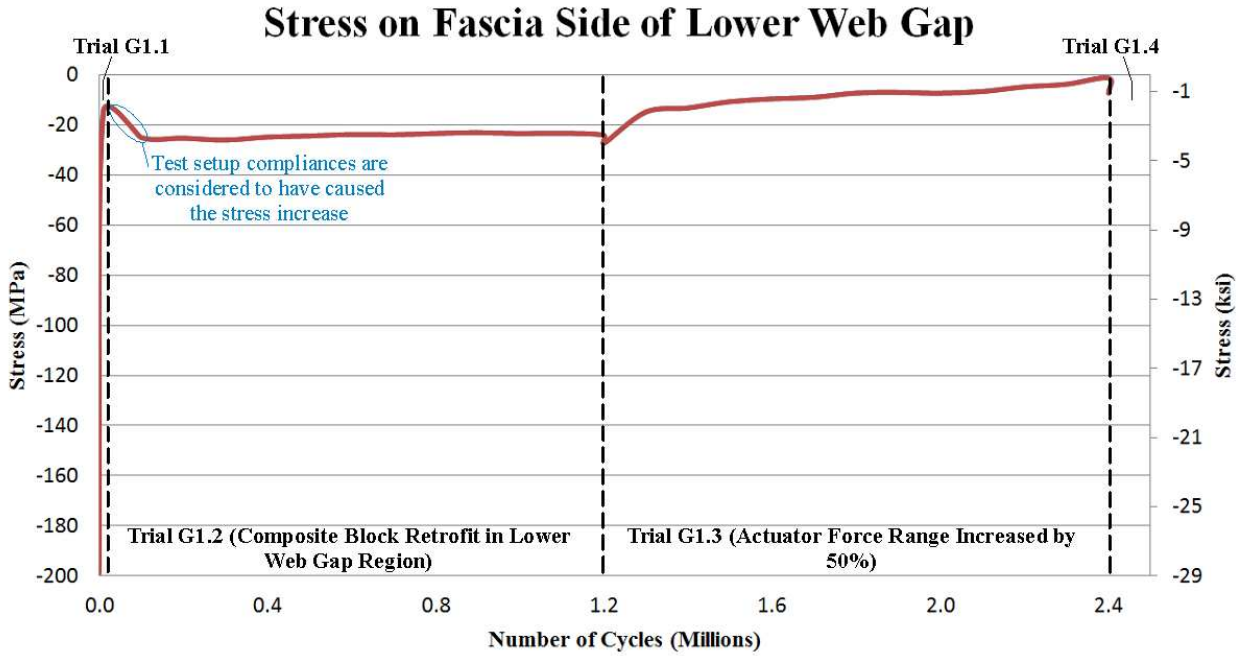

Figure 28: Stress recorded from lower fascia strain gage vs. cycle count for trials G1.1-3 and the start of G1.4

Figure 29 shows stress recorded from the upper fascia strain gage located on the fascia side of the upper web-gap region; this gage can be seen on the right side of Figure 23. It is visible from Figure 29 how the stress in the upper web-gap region slowly increased during Trial G1.2. This stress increase is thought to be due to the composite block installed in the lower web-gap region.

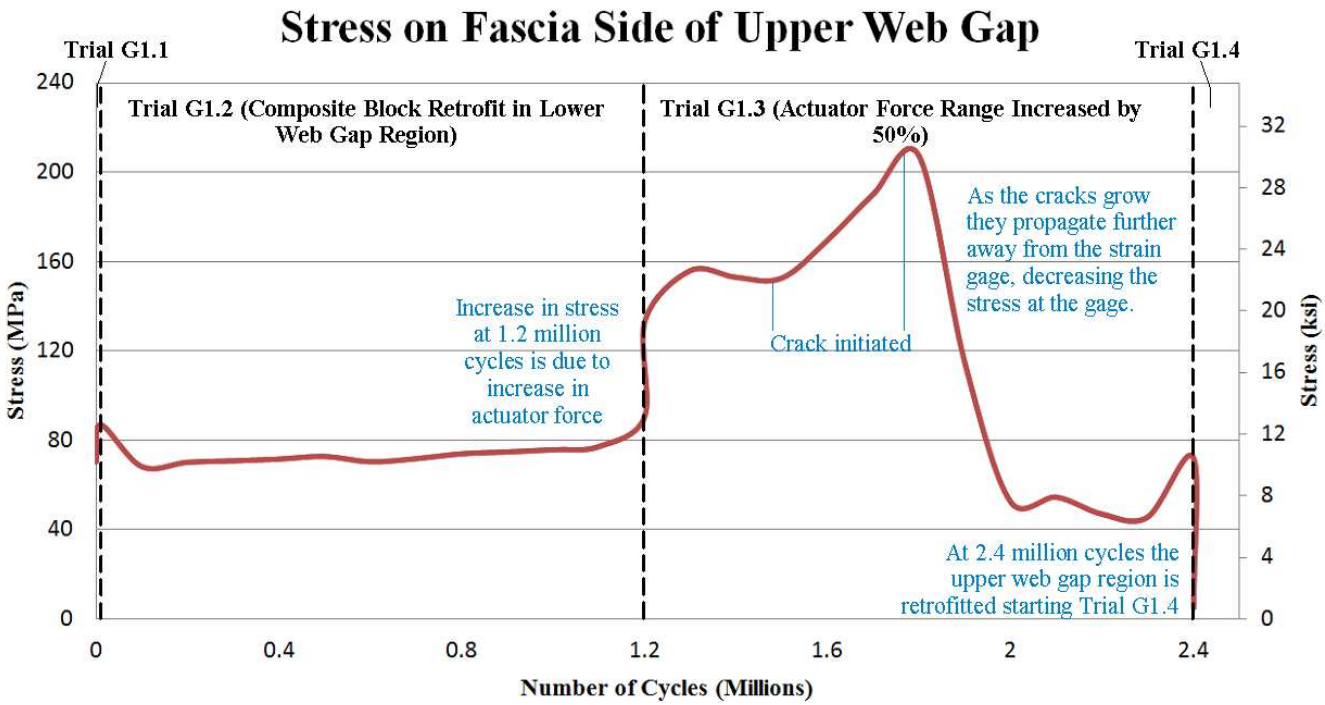

Figure 29: Stress recorded from the upper fascia strain gage vs. cycle count for trials G1.1-3

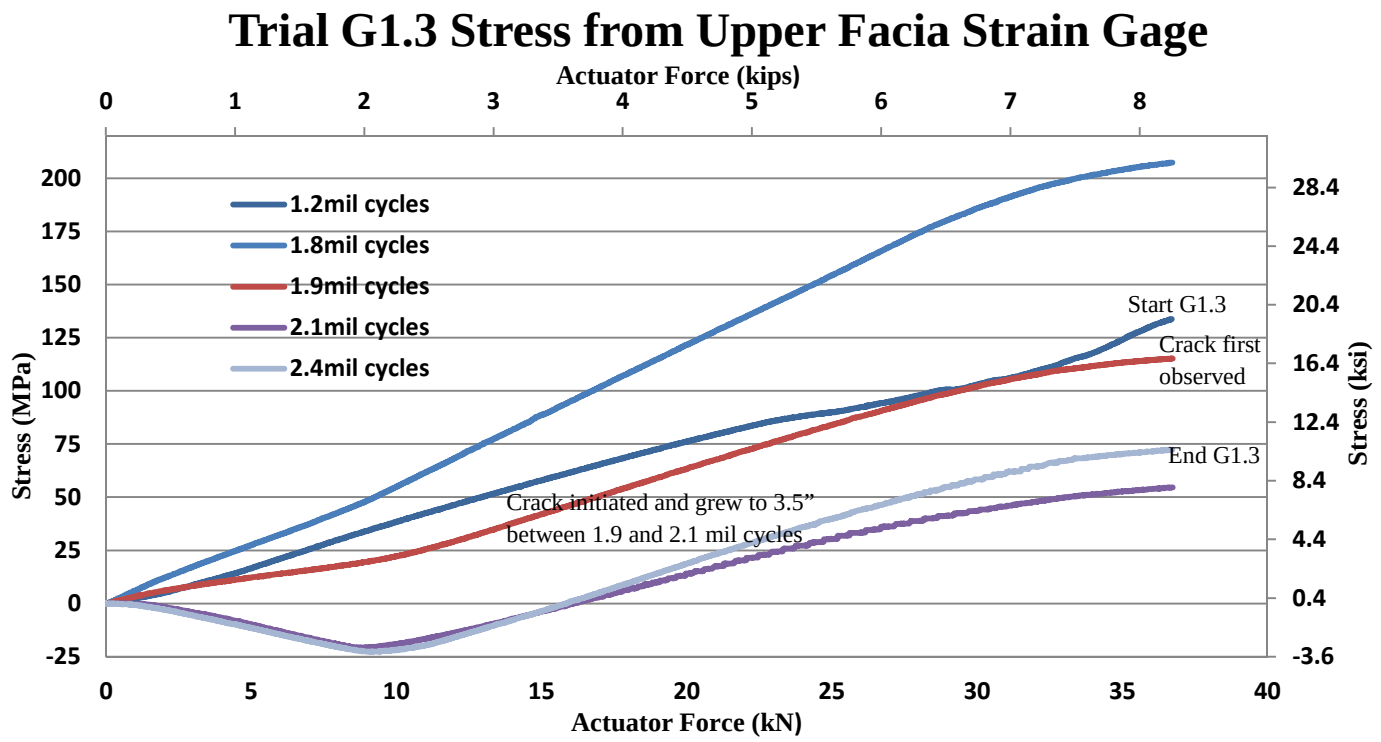

Figure 30: Stress recorded from upper fascia strain gage during trial G1.3

Figure 30 shows the change in stress recorded from the upper fascia strain gage during Trial G1.3. As the cracks in the upper web-gap region grew further and further away from the upper fascia strain gage, the stress recorded by that gage decreased. The change in stresses recorded from the mirror array data proved to be crucial since the upper fascia strain gage was reading relatively low stress values due to its location on the girder web,

even though there was a large crack present in the upper web-gap region. The reason stresses changed from compressive stresses to tensile stresses while the actuator was applying load during static tests taken at 2.1 and 2.4 million cycles became apparent once angular rotation data was recorded from the mirror array. The movement of the laser which reflected off of the mirror closest to the upper web-gap region is shown in Figure 31. As load was being applied the laser started to move in the upwards direction which corresponding to compressive stresses in that area of the web. Then, due to a buckling effect from the crack in the upper web gap region, the laser changed directions and started to move downwards corresponding to tensile stresses in that area of the web. The stress data recorded from the mirror array at the end of Trial G1.3 and at the start of Trial G1.4 can be seen in Figure 32-35.

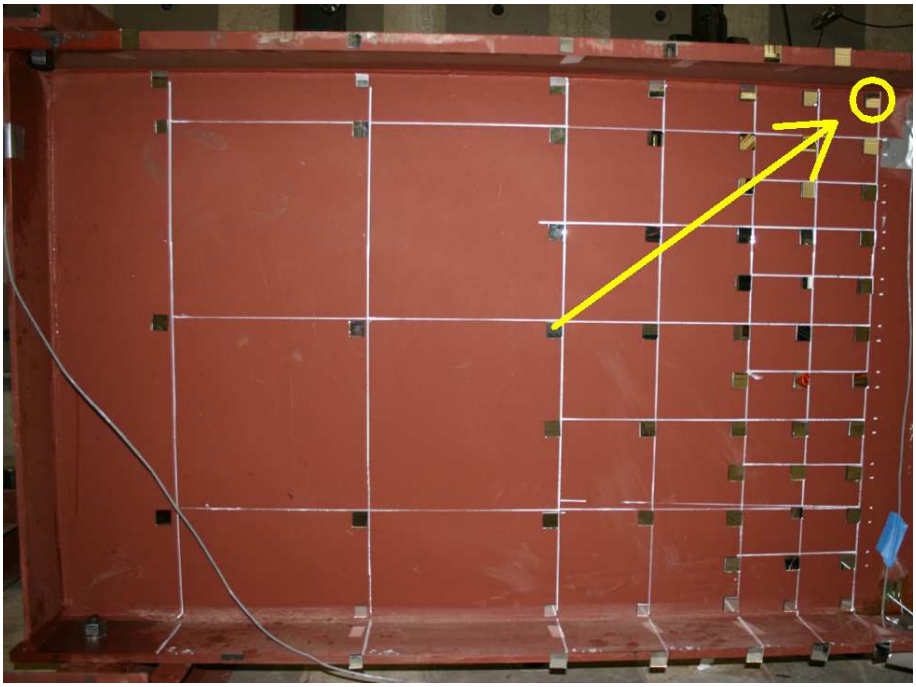

Figure 31: Path of laser (left figure) from the mirror circled in yellow (right figure)

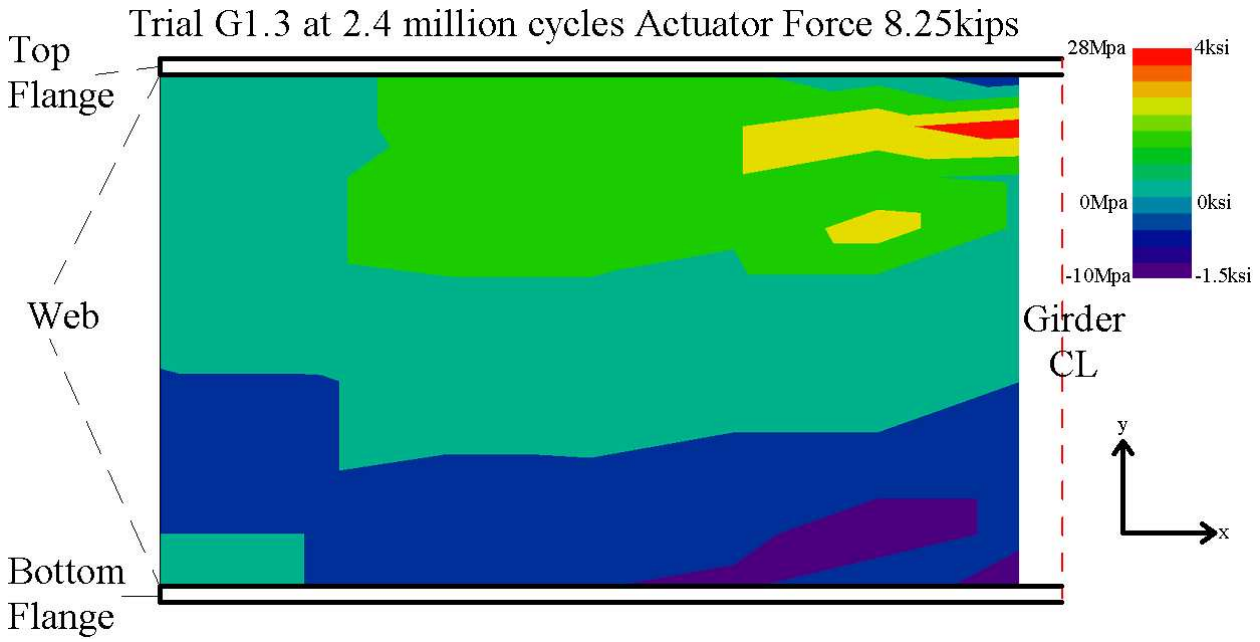

Figure 32: 2.4 million cycles, Trial G1.3, vertical stress changes calculated from X-axis rotations across the north half of girder subassembly

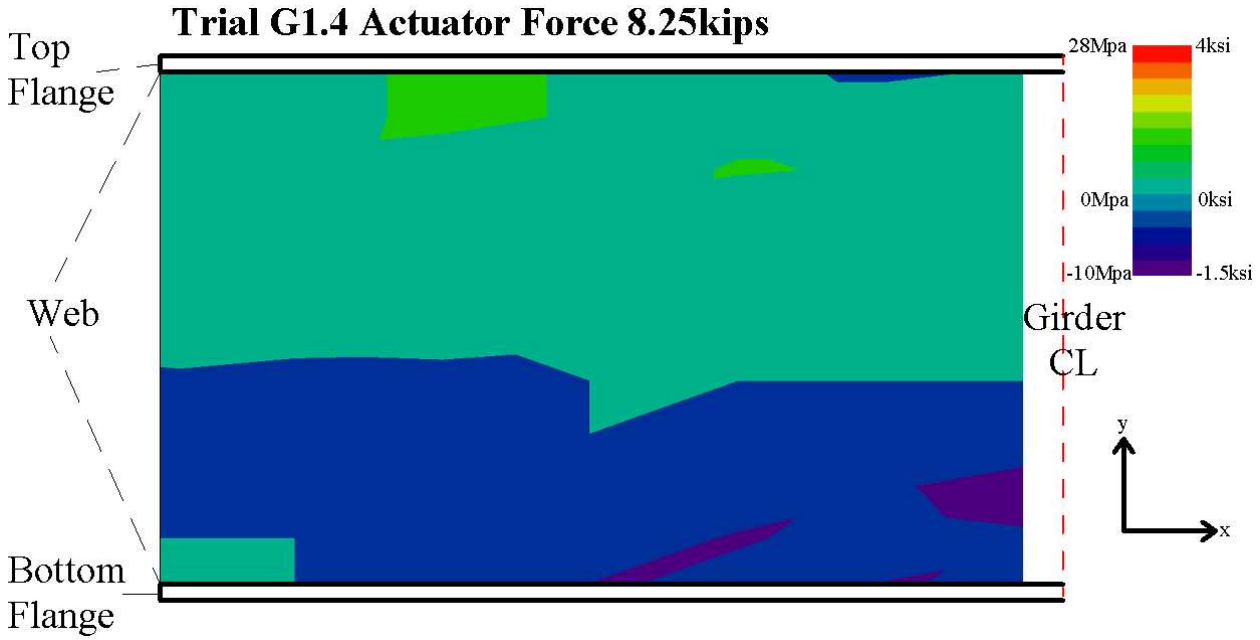

Figure 33: 2.4 million cycles, Trial G1.4, vertical stress changes calculated from X-axis rotations across the north half of girder subassembly after upper composite block retrofit was installed

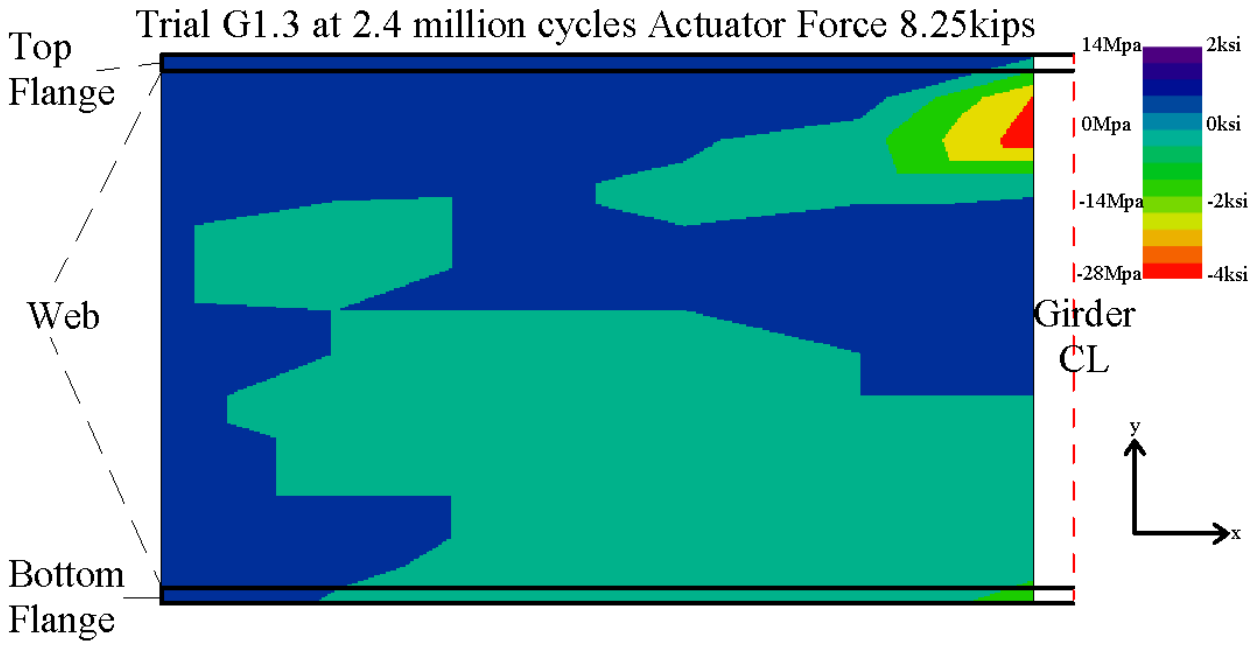

Figure 34: 2.4 million cycles, Trial G1.3, horizontal stress changes calculated from Y-axis rotations across the north half of girder subassembly

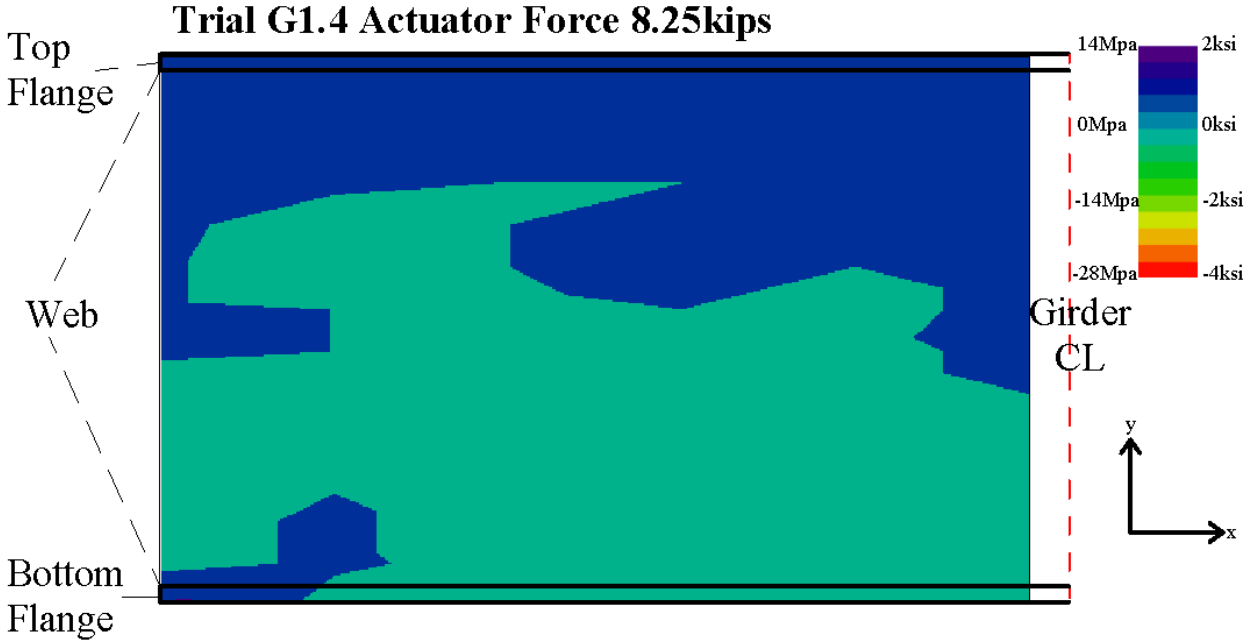

Figure 35: 2.4 million cycles, Trial G1.4, horizontal stress changes calculated from Y-axis rotations across the north half of girder subassembly after upper composite block retrofit was installed

Trial G1.4 began after the composite block retrofit was installed in the upper web-gap region. Figure 36 shows stress recorded from the upper fascia strain gage before and after the composite block retrofit was installed. After the composite block was installed in the upper web-gap region stresses, which were recorded from the strain gage behind the connection stiffener on the fascia side of the upper web-gap region, were reduced by 98%. From both the data taken from the mirror array and the data from the strain gage located in the upper web-gap region it is clear that the composite block was successful in stiffening the upper web-gap region.

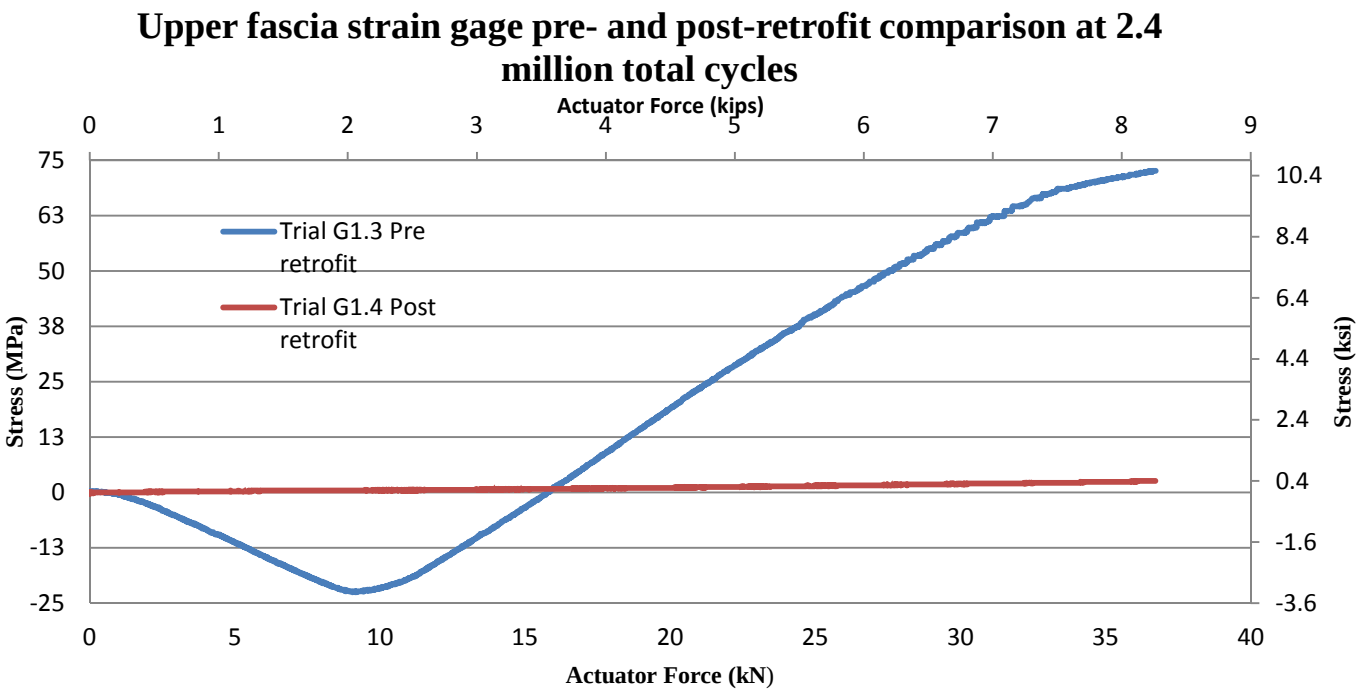

Figure 36: Stress recorded from upper fascia strain gage before and after the composite block was installed in the upper web-gap region

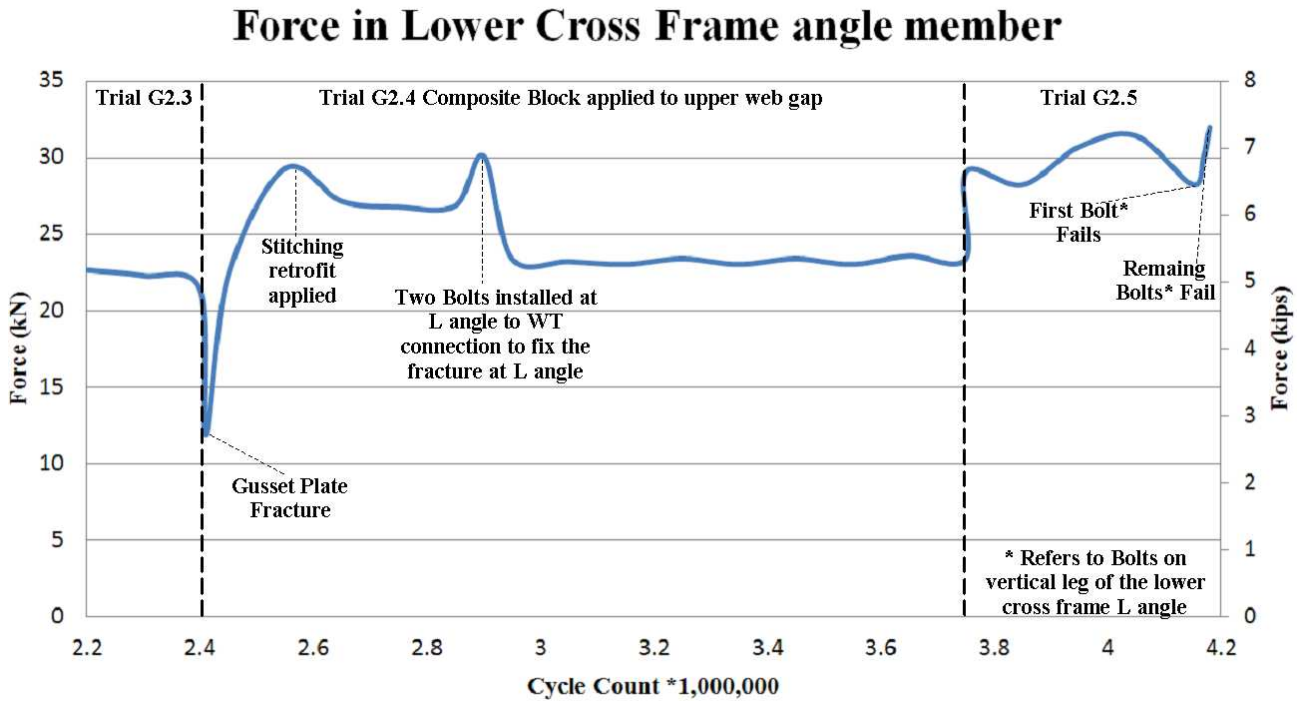

Figure 37: Force in lower cross frame member

Shortly after the upper web-gap region was retrofitted with the composite block retrofit, the tab plate which connected the cross frame to the lower web-gap region fractured. Figure 37 shows the force calculated in the lower member of the cross frame from the strain gage on that member. The force was calculated by converting strain to stress then multiplying the stress by the known cross sectional area of the angle, A=929 mm^2 (1.44 in^2.).

Comparison of Computational Simulations to Experimental Specimen

After the material properties of the composite block retrofit were calculated (Appendix D), and the experimental specimen with a crack in the lower web-gap region was retrofitted, a comparison was done between the stresses computed with the finite element models and the stresses calculated from the strain gage measurements.

The original FE models used to determine the most effective stud geometry included a horseshoe-shaped crack which did not properly represent the crack which formed on the experimental specimen. Figure 38 shows a scaled photo taken of the fascia side of the lower web-gap region. The strain gage shown in Figure 38 was 13-mm (1/2-in.) long. The other dimensions in the photo were scaled using the strain gage, and the crack length was measured.

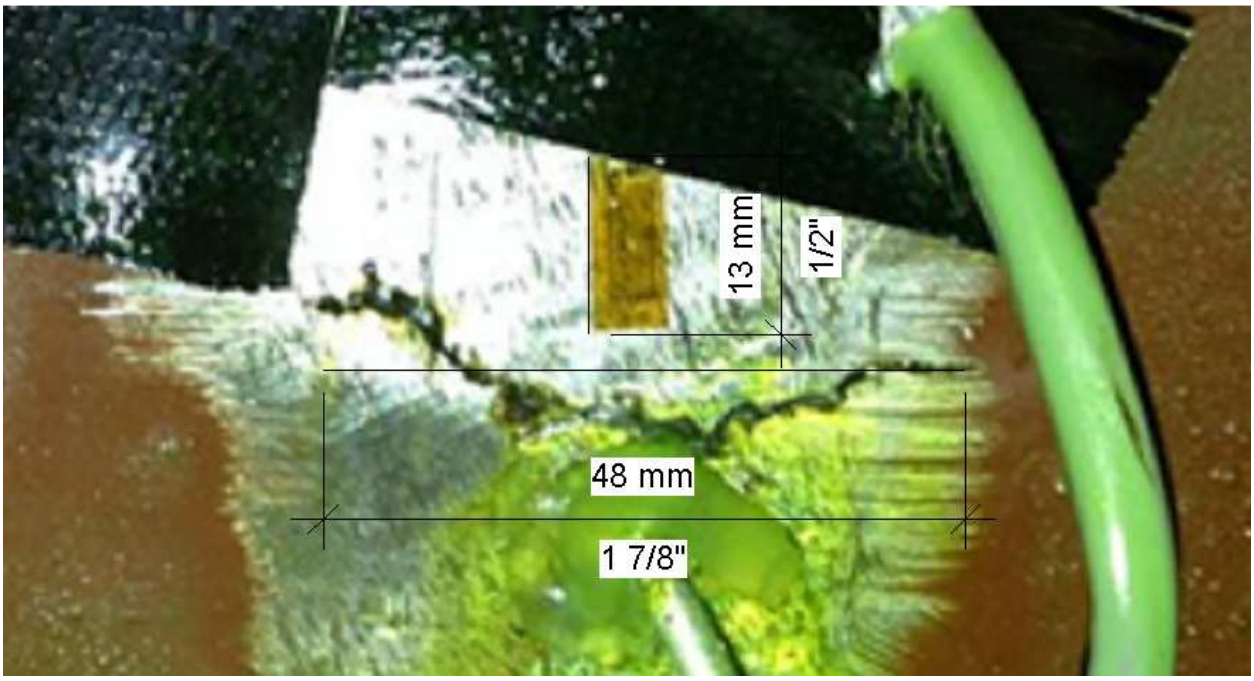

Figure 38: Scaled Photo of Crack in Lower Web-gap Region

The crack was then explicitly modeled in ABAQUS v.6.10.. It was imperative to create a well-structured mesh and to represent the actual crack geometry as faithfully as possible. The meshed web with the updated horseshoe-shaped crack geometry is shown in Figure 39. The edge of lower fascia strain gage on the experimental specimen was centered 6 mm (¼ in.) above the crack. Strain gages average the recorded strain over the area covered by the grid (Vishay Precision Group 2010). Therefore, the stresses used from the analytical model were taken and averaged from an area on the web between 6 mm (¼ in.) and 19 mm (¾ in.), or between 8 and 24 elements, above the center of the explicitly modeled crack. Figure 40 shows a close up view of the updated horseshoe-shaped crack in the unretrofitted FE model with the approximate location of the strain gage superimposed onto it.

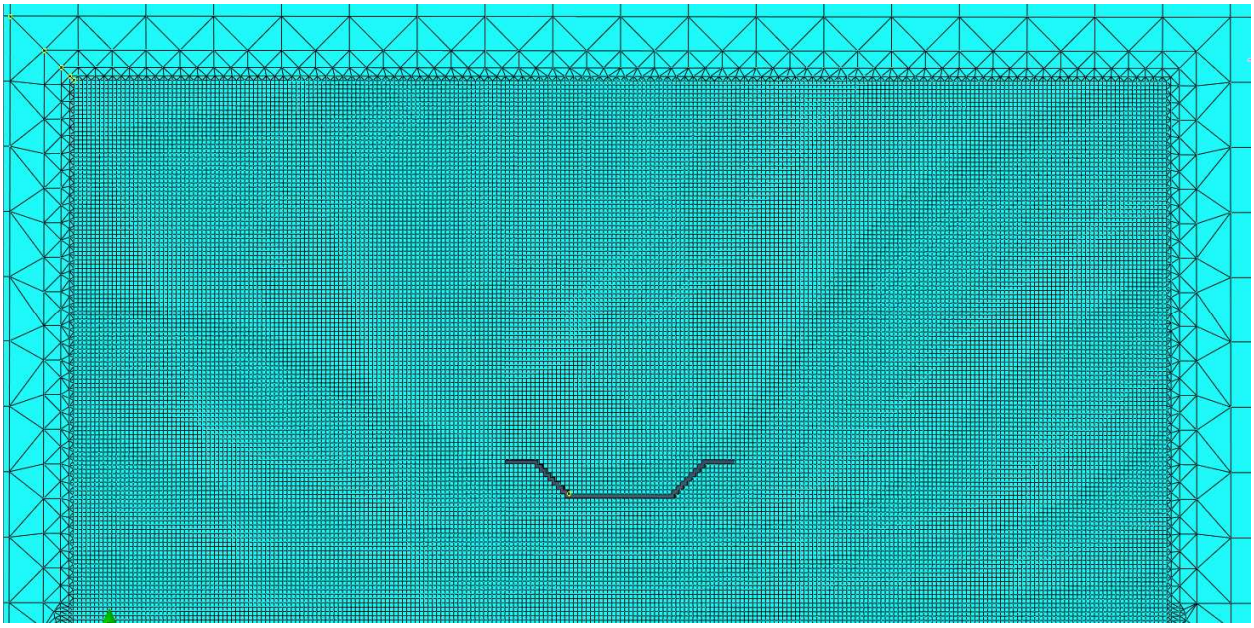

Figure 39: Meshed web with updated crack geometry

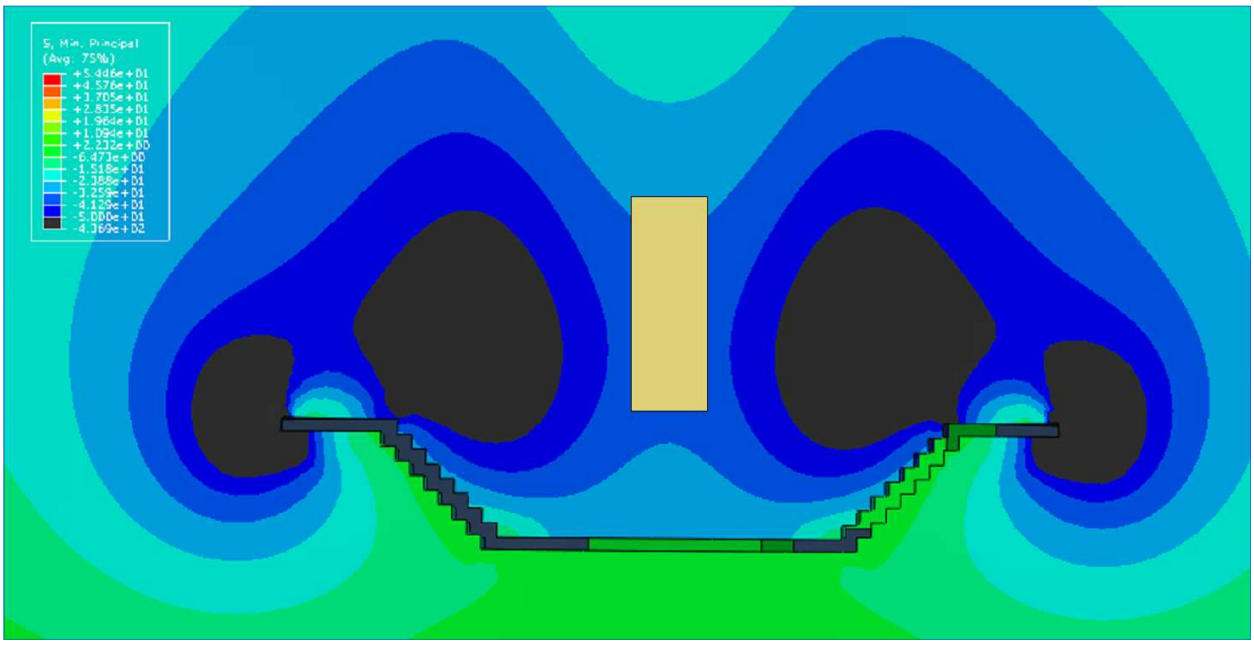

Figure 40: Unretrofitted FEM with strain gage location superimposed in yellow

Minimum principal stress values from the FE models were recorded. These values were then compared with the actual stress values obtained from the strain gage in the experimental setup. These values are shown in Table 1.

	FEM MPa	FEM (ksi)	Experimental MPa	Experimental (ksi)
No retrofit	-250.3	-36.3	-198.8	-28.8
Retrofitted	-9.2	-1.3	-14.9	-2.2
% Stress reduction	0.96		0.92	

Table 1: Comparison of experimentally found and calculated stresses

After comparing the results from the analytical models with the experimentally obtained data it was clear that if properly used FE models could provide an accurate representation of the magnitude of stress reduction that may be expected during physical test trials.

Rather than using a Bonet Stud, an idea was proposed that a bolt may be able to replace the Bonet Stud as a simpler solution to provide the same magnitude of stress reduction. An FEM model was created to compare the effectiveness of a composite block retrofit utilizing bolts rather than Bonet Studs to provide mechanical attachment from the girder flange to the CFRP blocks. The FEM model with the bolt was exactly the same as the model which utilized Bonet Studs except that the bottom "flange" portion of the Bonet Stud was removed, as shown in the right figure in Figure 41. In the updated bolted model all composite to steel interactions between the composite block and its subsequent steel surfaces were recreated before the model was run.

A view of the lower web-gap region with the composite block hidden from view is shown in Figure 41. In Figure 41 the contour stresses and deformed shape limits in both models were set equal. The areas in grey represent stresses above the materials yield strength which is 345 MPa (50 ksi), the deformed scale factor is set to 30. Figure 42 shows the stress path taken along the fascia side of the girder web, in these views the contour stresses were set so areas in grey represent stress above 69 MPa (10ksi) and the deformed scale factor is set to 1. Figure 43 shows the stresses recorded from the stress path shown in Figure 42. Both maximum and minimum stresses are plotted.

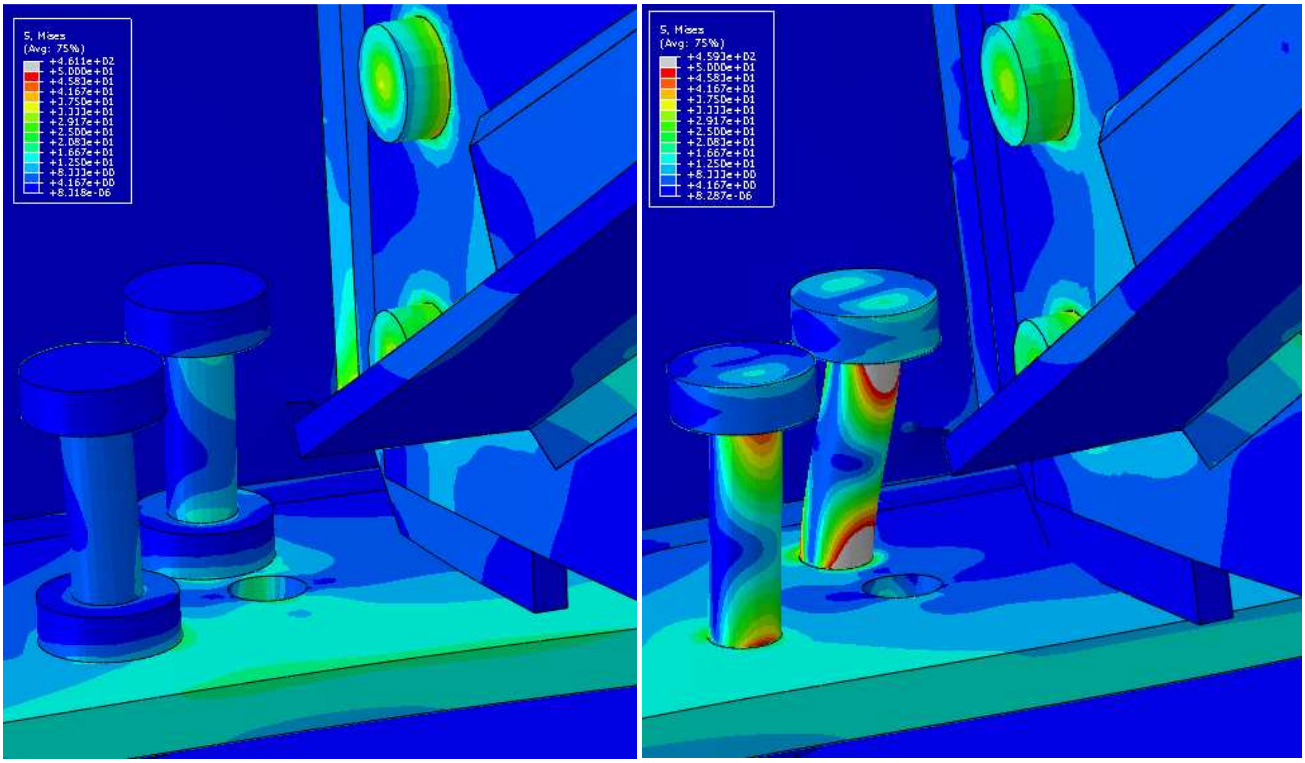

Figure 41: Bonet Stud retrofit (left) vs. retrofit with bolts (right)

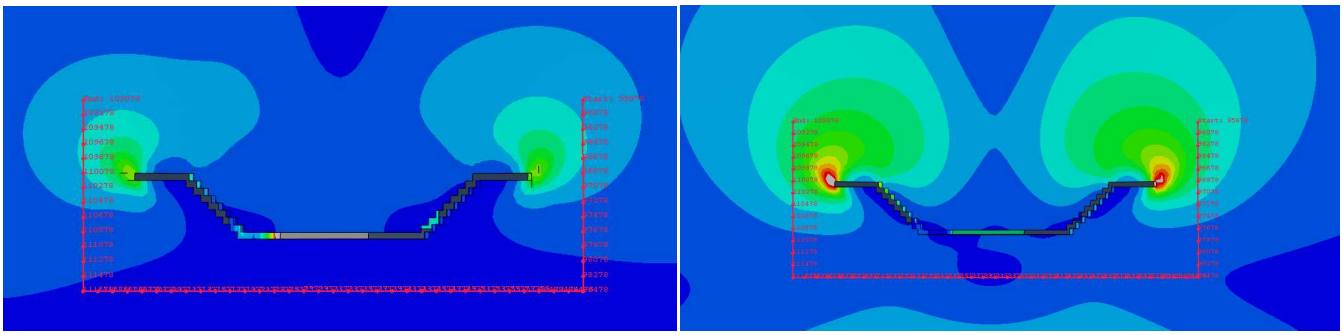

Figure 42: Fascia side of lower web-gap region showing stress path for Bonet Stud retrofit (left) vs. retrofit with bolts (right)

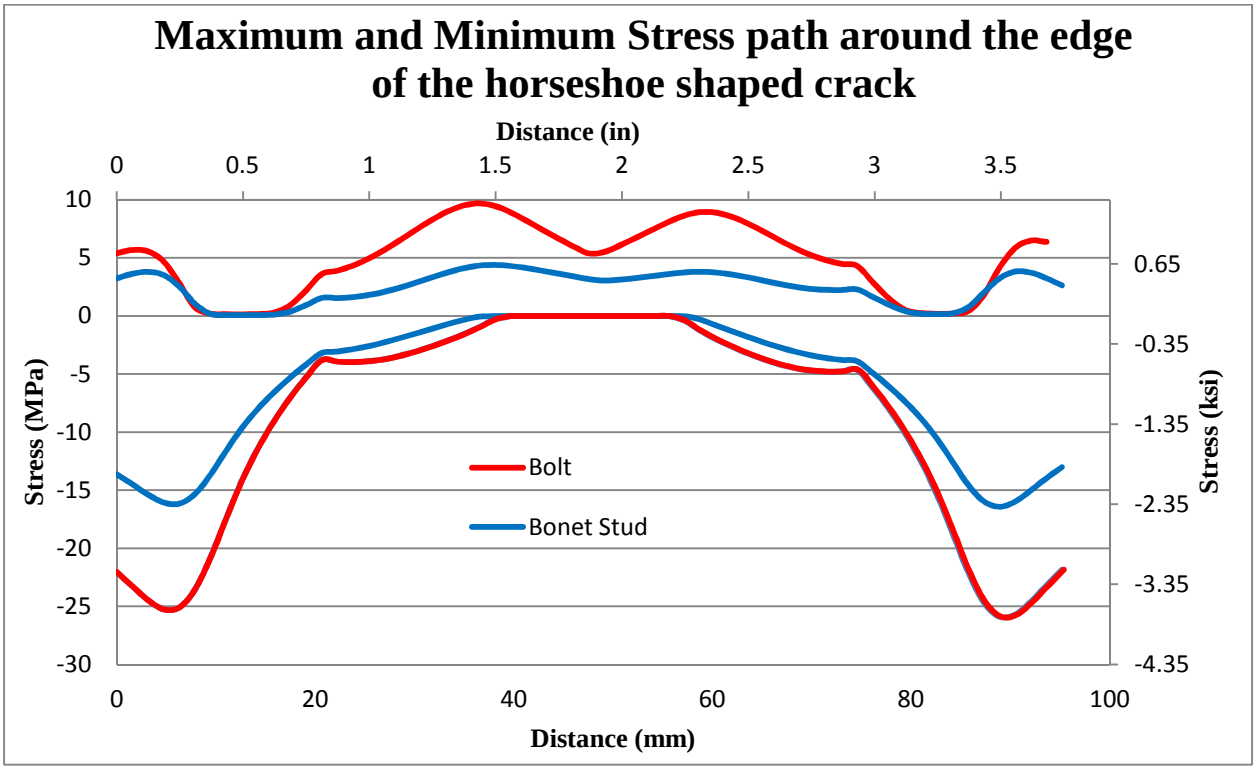

Figure 43: Maximum and minimum stress path along the edge of the crack on the fascia side of girder web

From the both the maximum and minimum stresses plotted from the stress path shown in Figure 42, it is clear that the composite block with the Bonet Studs performed slightly better in terms of reducing stresses along the fascia side of the web in the lower web-gap region. The reason that Bonet Studs performed better than bolts as a mechanical anchorage to connect the CFRP block to the girders flange can be seen in Figure 41. The bolts do not have any surface area to react in bearing against the girders flange. The lack of this bearing surface allows the bolt to bend at the flange-to-bolt shank interaction. The maximum principal stresses in the shank of the bolt where it connects to the flange, were approximately 600 MPa (87 ksi). Since the Bonet Studs are mechanically bearing against the flange, the Bonet Stud does not significantly bend and all stresses in the Bonet Stud are below 138 MPa (20 ksi). From the results of the FE models it is clear that the Bonet Studs are much stiffer than the bolts.

Conclusions

In this study a large body of existing research on FRP materials was reviewed, and subsequently the idea for a composite block retrofit was developed. Utilizing computer simulations, the composite block retrofit geometry was chosen, and was then successfully tested experimentally undergoing over four million high stress fatigue load cycles. The following conclusions were reached:

- Through an extensive review of existing research on FRP materials used to retrofit metal structures, it was concluded that debonding of the bond between FRP and metal surfaces is the primary failure mode when utilizing FRPs to retrofit metal structures. By utilizing the Bonet Studs, which provide mechanical attachment between the metal and FRP, forces are no longer primarily transferred through the FRP to the bond layer. Therefore, debonding of the FRP from the metal surface is no longer a concern.
- The composite block retrofit was successfully utilized in two different locations on a 2.82-meter (9.25-ft.) girder subassembly to retard the growth of fatigue cracks. The composite block was applied in both the lower web-gap region, reducing stresses in that region by 92%, and the upper web-gap region, reducing stresses in that region by 98%. Thus, this process extended the fatigue life of the retrofitted girder considerably, possibly as much as 4 million cycles or more.
- Applying the composite block in the upper web-gap region on the girder subassembly imitates how the retrofit would have to be applied in the field, because in the field the retrofit application process needs to be able to counter the force of gravity.
- When FE models are properly constructed, they can provide a very close representation of the magnitude of stress reduction found in a physical girder subassembly. The analytical computer models constructed for this experiment resulted in a 96% stress reduction in the lower web-gap region from an unretrofitted to retrofitted state, while the physical testing resulted in a stress reduction in the lower web-gap region of 92%. Thus, properly constructed analytical computer models can be used to accurately estimate the expected magnitude of stress reduction when a composite block retrofit is applied onto a girder.
- The large Mode I fatigue crack on the lower web-gap region tab plate was unsuccessfully repaired multiple times by welding, and due to the lack of available surface area on the tab plate, a steel retrofit could not be performed. While researching an alternative to a steel retrofit, a large body of literature was found on utilizing Kevlar stitches to prevent delamination caused by Mode I fracture in laminated composites. This stitching retrofit was then successfully utilized to prevent the crack on the tab plate in the lower web-gap region from opening for over 1.7million fatigue load cycles.

Multiple retrofit techniques to retard the growth of fatigue cracks were developed through multidisciplinary research conducted at the University of Kansas. These retrofit techniques were highly effective at preventing the further growth of existing fatigue cracks caused by distortion-induced fatigue and Mode I fatigue cracks which developed due to the high stress ranges to which the experimental girder

subassembly was subjected. Due to the efficacy of these retrofits, with minimal further experimental testing, they could be formulated for industrial use that could be applied in large quantities on bridges.

Appendix A: Finite Element Modeling techniques used in analytical models.

A detailed finite element model of the 2.82-meter (9.25-ft.) subassembly test system was developed using ABAQUS v.6.10. The models were constructed using three-dimensional solid elements with linear-elastic material properties. Each model contained approximately 2.3 million elements and 77 million degrees of freedom. Steel was specified to have a modulus of elasticity of 200,000 MPa (29,000 ksi) and Poisson's ratio of 0.3. Concrete was specified to have a modulus of elasticity of 27,786 MPa (4030 ksi) and Poisson's ratio of 0.2. The modulus of elasticity of the composite was varied between 13,790 MPa (2000 ksi), 34,474 MPa (5000 ksi) and 68,948 MPa (10,000 ksi) with a Poisson's ratio of 0.2 for all three cases.

The entire steel, concrete and composite assembly was modeled in ABAQUS using primarily hexahedral (C3D8R) elements with varying mesh densities. Elements were sized as small as 0.8 mm (0.03125 in.) near regions of interest while other areas contained element sizes as large as 12.7 mm (0.5 in.). Tetrahedral (C3D4) elements were used to transition between element sizes. The concrete deck used 50.8 mm (2 in.) sized elements.

All parts, including welds, were build up separately then assembled using either surface-to-surface ties if the parts were welded together or when appropriate, hard contacts with a frictional coefficient (0.3 for steel-to-steel and composite-to-steel interactions, or 0.45 for steel-to-concrete interactions) were used to prevent parts from moving through one another during loading. The overall model geometry is presented in Figure A 1.

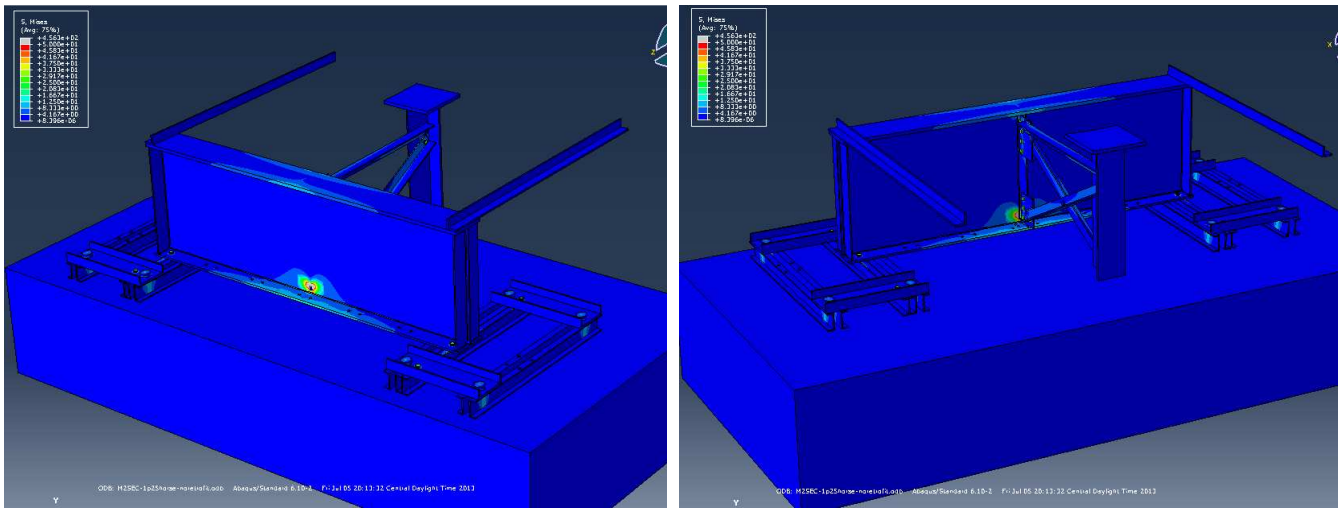

Figure A 1: View of the base finite element model: Left view of fascia side and Right view of stiffener side

Special consideration were taken to ensure the model would be constructed out of 8 node hexahedral elements only using other element types when absolutely necessary. A meshing technique was developed for bolt holes to allow for a clean mesh. Figure A 2 shows the generic bolt hole meshing technique.

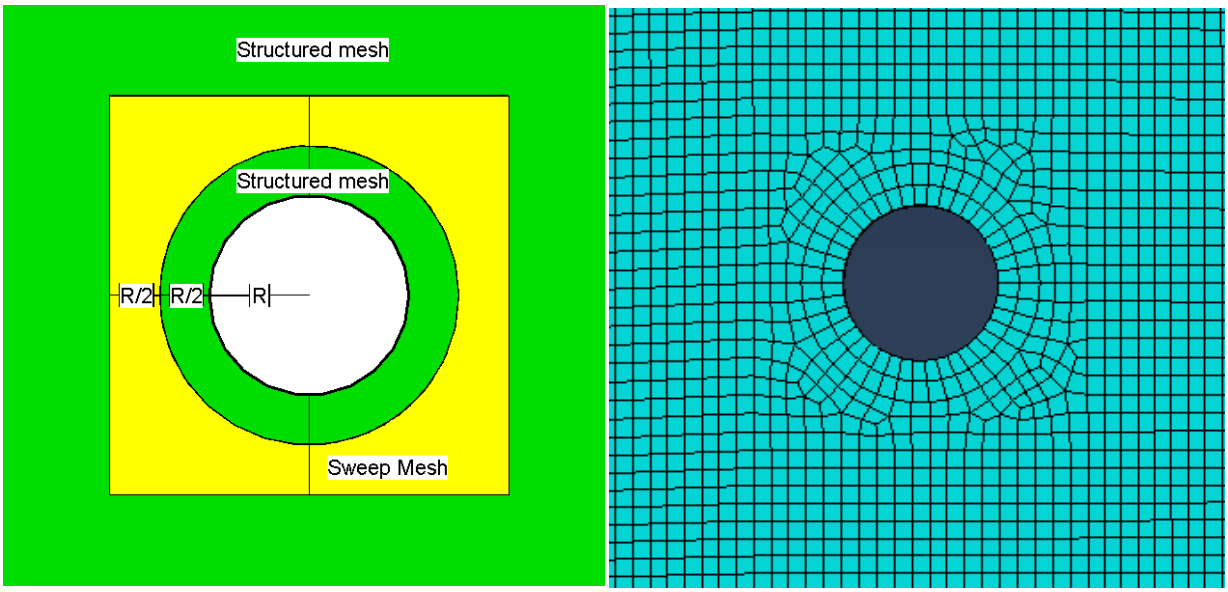

Figure A 2: Bolt hole meshing technique

Bolts were modeled as a revolution part, which was then partitioned into three parts: the shank, nut, and head. The middle of the shank was partitioned in half so the bolt load could be applied to the interior face of the shank. Figure A 3 shows the bolt meshing technique.

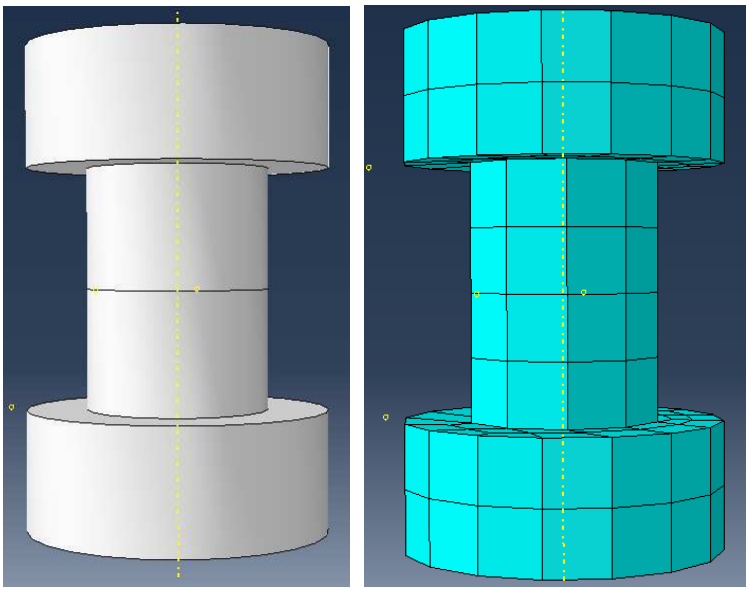

Figure A 3: Bolt meshing technique

The girder web was partitioned to allow for an extremely fine mesh to be located in the web-gap region, and have a smooth transition region to the rest of the part. 13 mm (½ in.) element sizes were used throughout the web, except in the web-gap region. In the web-gap region a 102 x 229mm (4 x 9in.) box was drawn, as shown in Figure A 4. The outer edge of the box had 13 mm (½ in.) element sizes, then another box was drawn 6.4 mm (¼ in) off of the inside faces of the 13mm (½ in.) element size box. This box used 6.4mm (¼ in) element sizes. Smaller boxes which were half the size of the next largest box were subsequently drawn off the inside faces of the larger boxes. This technique continued until the element size on the final box was 0.8mm ($\frac{1}{32}$ in). A 38mm (1 ½

in.) horseshoe crack was explicitly modeled on the web around the weld toe by removing a 0.8mm ($\frac{1}{32}$ in.) section of elements where the horseshoe crack was located.

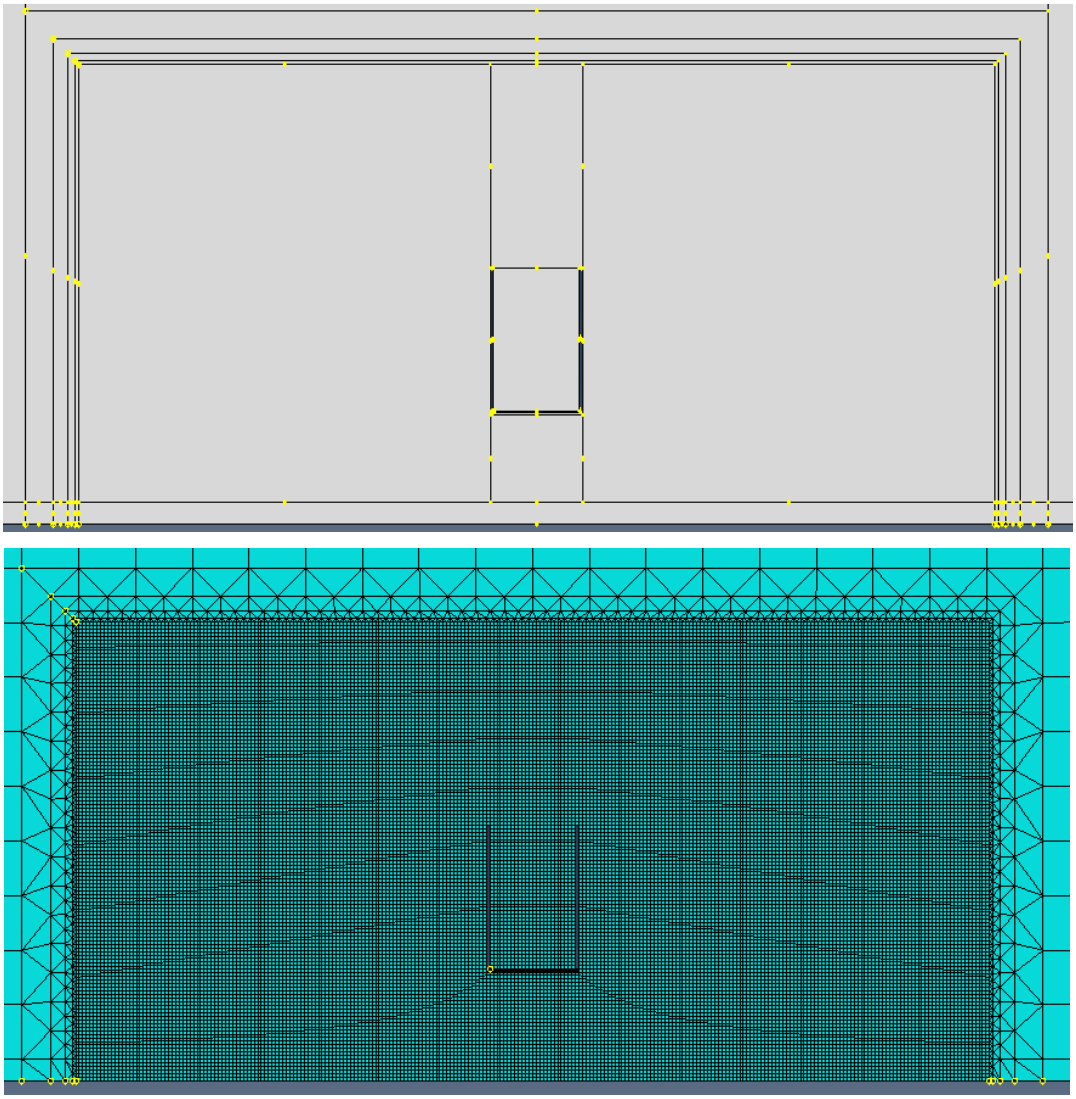

Figure A 4: Girder web meshing technique

The girder flange was partitioned using a similar step down meshing technique like the technique which was used on the web. The majority of the girder had 9.5mm ($\frac{3}{8}$ in.) element sizes except for the area located near the web-gap region where elements were 2.4mm ($\frac{3}{32}$ in.)

Retrofit

The Bonet Stud was modeled the same way as bolts were modeled as shown in Figure A 5. The top face of the lower nut and the bottom face of the stud were tied to their respective faces of the flange. The stud was partitioned so it wouldn't be over constrained since a tie constraint was used to attach the stud to the flange and the rest of the stud had a composite-to-steel interaction with the composite block. The composite block was constructed by placing a 127x152x184mm (5x6x7in.) block on both sides of the stiffener in the web-gap region, when the Bonet Studs were already in place. All parts which were located within the blocks were used to cut the

blocks, removing any material from the blocks which would interfere with parts already in place. The blocks were partitioned to allow the majority of their area to have structured hexahedral elements. Swept hexahedral elements were used around hole locations and a box of tetrahedral elements were located 13mm (½ in) behind the faces of all of the holes to allow for a smooth transition back to structured hexahedral elements. Figure A 5 shows an opaque view of the composite block, green regions represent structured hexahedral elements, yellow regions represent sweep hexahedral elements, and the four small pink regions represent the tetrahedral transition regions. Figure A 7 shows the fully meshed block using 2.4mm ($\frac{3}{32}$ in.) element sizes.

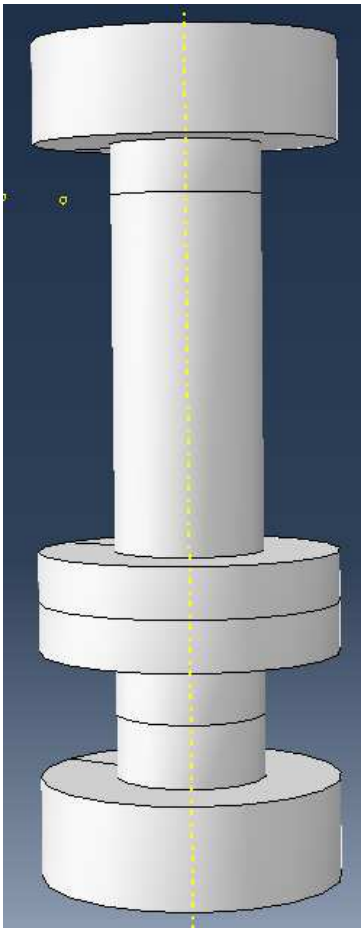

Figure A 5: "Bonet Stud"

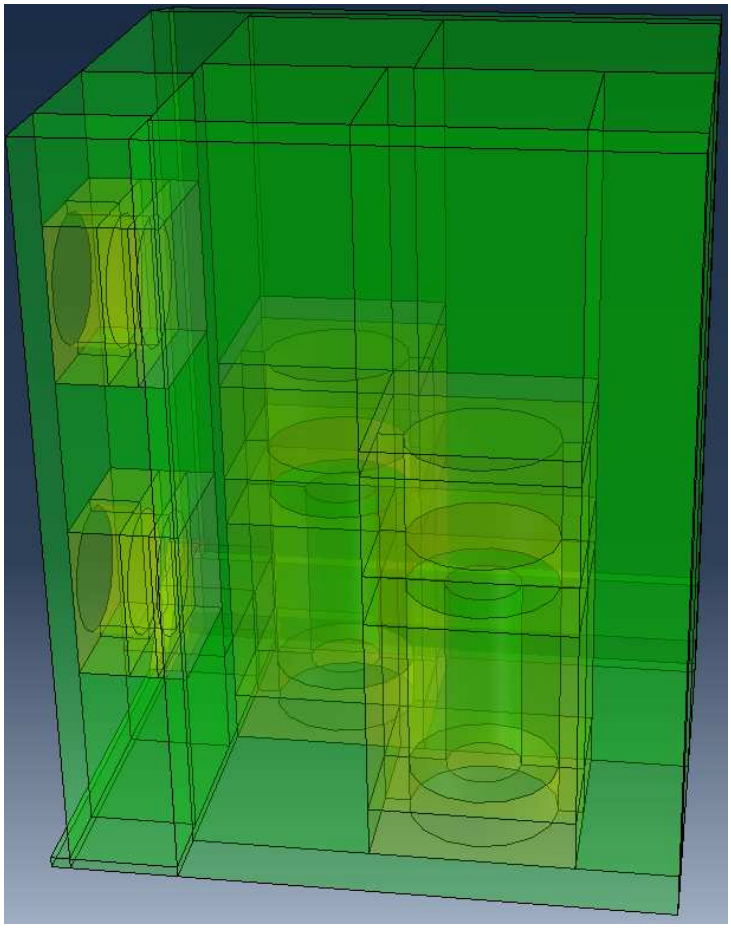

Figure A 6: Opaque view of composite block

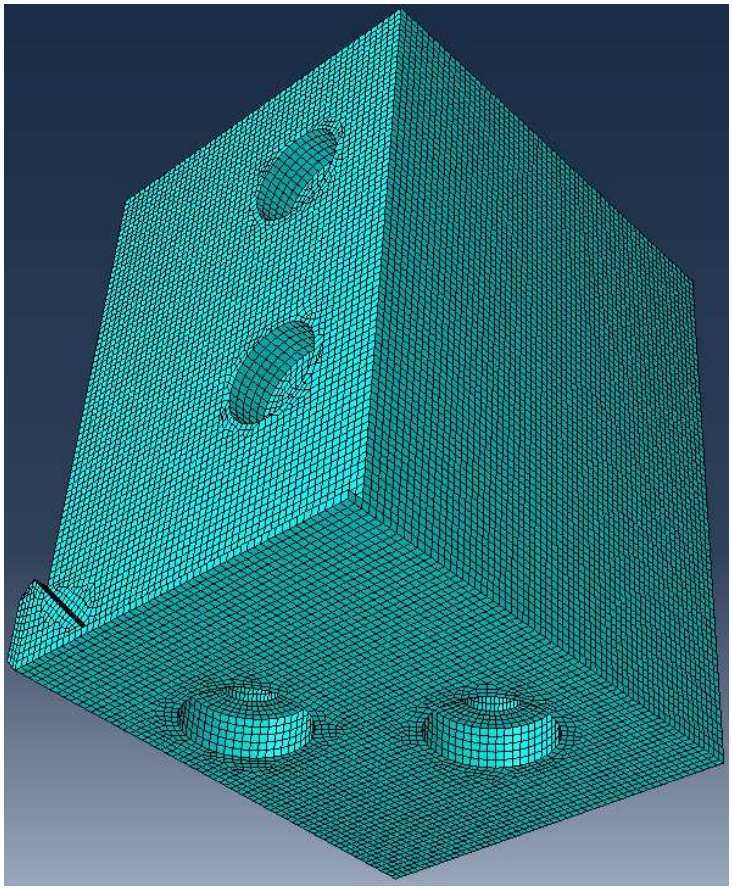

Figure A 7: Composite block meshing

Loading

A bolt load of 107 kN (24kips) was applied onto each bolt as was done in experimental testing. To improve computational efficiency, modeled bolt heads and nuts were connected directly to the surfaces they were in contact with using tie constraints. Bolt tension forces were applied in the second loading step during the computer simulations. Static actuator loading applied in the model correlated with the upper bound load of 24.5kN (5.5kip) from the initial test trial in the experimental test sequence. In the models this load was applied as an upward pressure on a (1x16x16 in) plate which was tied to the WT shape where the cross frame connected into. Actuator loading was applied during the third and final loading step during the computer simulations.

Appendix B: Experimental Setup

The goal of this investigation was to evaluate the effectiveness of the composite block retrofit in a timely and cost effective manner. It was for that reason that the retrofit was tested on a 2.82-meter (9.25-ft.) girder subassembly. There had been numerous tests already preformed at the University of Kansas utilizing 2.82-meter (9.25-ft.) girder subassemblies and there were many spare girders which had yet to be tested. In a laboratory setting it is difficult to replicate the same boundary conditions that exist in a bridge when preforming component testing. The subassembly in this test was placed upside down in order to utilize the strong floor to act as the stiff concrete deck and the unrestrained flange was at the top of the subassembly. Since the concrete deck on a bridge would slightly deflect due to a passing heavy load; this deflection would cause a slight amount of rotation in the top flange of a girder due to the top flange being rigidly attached to the concrete deck. It was thought that a more stringent test for the composite block retrofit would be one that allowed the girder flange to rotate with respect to the connection stiffener. This rotation could cause the composite block retrofit to debond with its respective girder faces faster. To allow the girder flange to rotate the girder was only attached to the strong floor at its two ends.

The girder subassemblies were built-up I shape sections with a height of 918-mm (36-in.), the web had a thickness and height of 10-mm (3/8-in.) and 876-mm (34-1/2-in.) respectively. Both the top and bottom flanges of the girder had a width of 279-mm (11-in.), and thickness of 25-mm (1-in.) and 16-mm (5/8-in.) respectively. The connection plate located in the middle of the girder had a height of 873-mm (34-3/8-in.) a width of 127-mm (5-in.) and a thickness of 10-mm (3/8-in). The connection plate was welded to the web utilizing a 5-mm (3/16-in) weld and had cropped ends of 32-mm (1-1/4-in) with a 3-mm (1/8-in.) gap between the connection plate and the bottom flange. The connection plate was bearing against the inside face of the top flange without any welded connection. Four stiffeners were attached to the girder at each end, on both sides of the web. The stiffeners were fully welded to the web and both flanges with 5-mm (3/16-in.) weld. The stiffeners had a height of 876-mm (34-1/2-in.) a width of 127-mm (5-in.) and a thickness of 10-mm (3/8-in).

The girder subassembly was attached to the strong floor with C5x9 channels. These channels were connected to the girder through fully-tightened 19-mm (3/4-in) diameter A325 structural bolts. To ensure all bolts were fully-tightened TurnaSure Direct Tension Indicator washers were used. The C5x9 channels were post tensioned to the strong floor. The strong floor in M2SEC has a 610x 610-mm (2 x2-ft.) grid of 44.5-mm (1-3/4-in.) threaded holes. Horizontally oriented C10x30 channels were placed on top of the vertically oriented C5x9 channels as shown in Figure B 1. Threaded rods were connected to the floor system and went through 60-mm (2-in.) holes in the C10x30 channels. Nord-Lock MT-175-5/W Super Bolts were used to apply 50kips of pre-tension to the threaded rods effectively securing the specimens floor system to the strong floor.

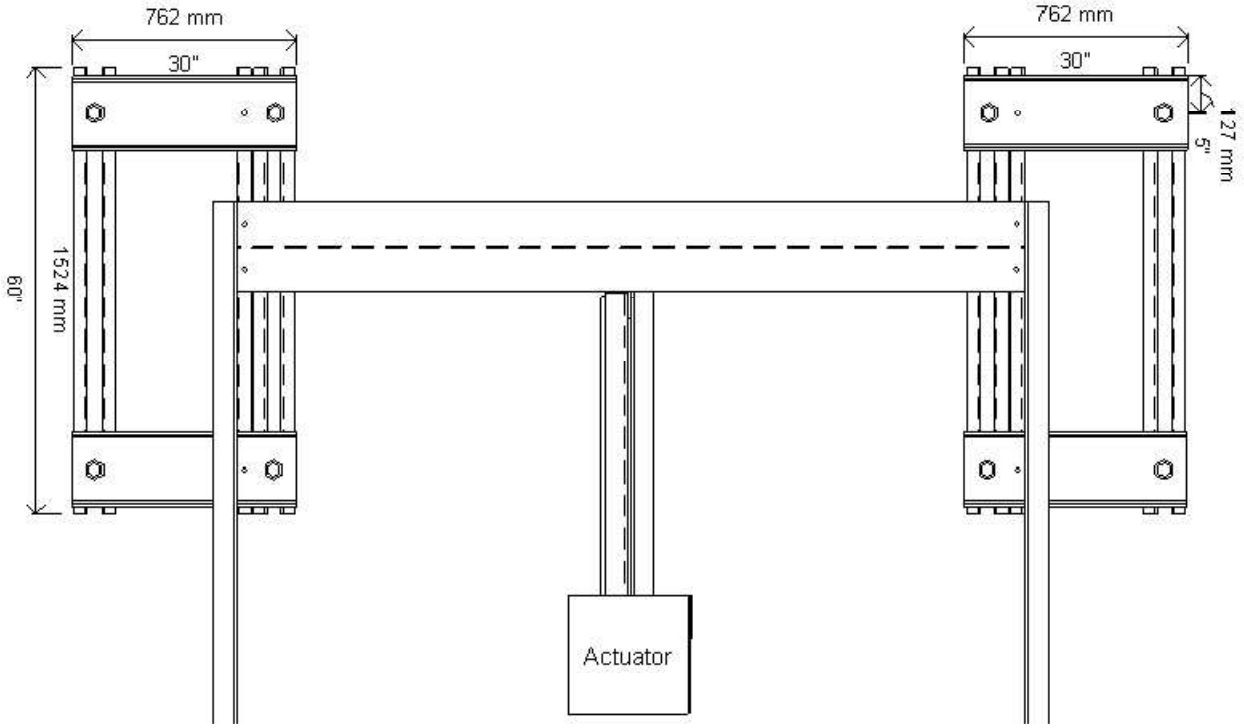

Figure B 1: Plan view of subassembly

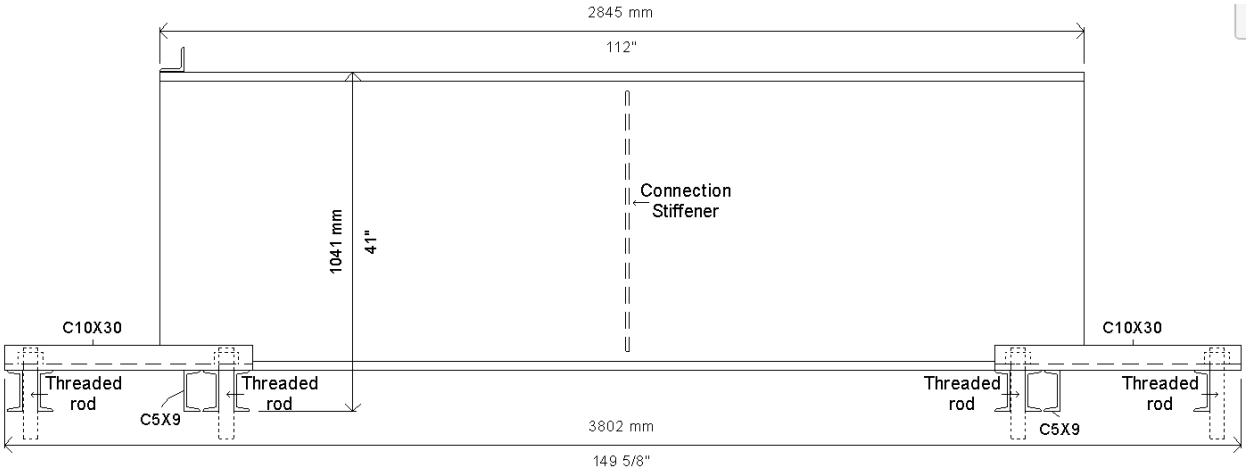

Figure B 2: Elevation view of subassembly

Figure B 3: Side view of subassembly

Bracing members were used to restrain the top flange of the girder from excessive rotation. The bracing members were L76x76x10-mm (L3x3x3/8-in) angles. These angles were attached to the top flange of the girder with two 19-mm (3/4-in.) diameter A325 structural bolts and they were fixed to the strong wall on their opposite side. A cross-frame consisting of three L76-76-10mm (L3x3x3/8-in.) angles, with an X-shape configuration and a horizontal member were used to connect the specimen to the actuator. The cross frame connected into a WT section which was used to stabilized the free end of the cross frame. This successfully prevented bending and warping of the frame while loading the specimen.

When testing began, the free end of the cross frame began to displace horizontally. As the frequency of the actuator increased the horizontal displacement increased and the free end of the cross frame began to move in a circular manner. This caused unintended horizontal rotation at the connection stiffener to web weld. It was believed that this was due to the fact that the girder was only fixed to the floor at its ends. Therefore as the actuator frequency increased it began to approach the natural frequency of the system, causing excess horizontal displacement at the free end of the cross frame.

To prevent this horizontal movement a horizontal movement inhibiting device (HMID) was invented and constructed. The structure for the HMID was constructed out of 19-mm (3/4-in.) steel plate and HSS51x51x6-mm (HSS2x2x1/4) tubular steel. The HMID is shown in Figure B 4. 19-mm (3/4-in.) diameter Steel Flange-

Mounted Ball Bearings were mounted to 152-mm (6-in.) long pieces of HSS steel. 203-mm (8-in.) drive shafts were installed in the ball bearings and the drive shafts were placed snug up against the flange of the WT. 19-mm (3/4-in.) diameter washers were used to create space between the frame of the HMID and the steel tubes which the ball bearings were attached to. The HMID was extremely successful in preventing any horizontal movement at the free end of the cross frame.

Figure B 4: Horizontal Movement Inhibiting Device

Loading

A MTS 244.31 hydraulic actuator (225 kN [55 kips] capacity) powered by a MTS 505.120-G2 120 GPM pump and controlled with a MTS FlexTest 40 Digital Controller delivered cyclic loading to the specimen. A 25-mm (1-in.) thick steel plate was centered under the actuator and bolted to three L angles which were then bolted to the flange and web of the WT shape. Cyclic loading was applied at a rate of 2 Hz for the majority of testing. The

only time the load rate changed was when data from the mirror array was being taken, and at the last 1000 cycles of testing the load rate was changed to 1Hz due to the large actuator displacement.

Instrumentation

The specimen was instrumented such that strain, lateral deflections and specimen rotation could be measured throughout testing. Load and displacement data from the actuator was recorded using the same data acquisition system that was used for all other sensors. The locations for strain gages and linear variable differential transformers (LVDTs) are shown in Figure B 5. LVDTs were powered using a 15V power supply. The strain gages installed were Micro-Measurements WK-06-250BG-350 strain gages and were powered directly through the data acquisition system in a quarter bridge configuration with excitation voltages of 3.3 Volts. Two strain gages were installed on the top and bottom of the fascia side of the web directly behind the connection plate. These two strain gages proved to be crucial when monitoring stress in both the upper and lower web-gap regions.

Synchronizing all data was a critical step it was therefore recorded using a single data acquisition system manufactured by National Instruments (NI cDAQ 9188 with NI 9236 and NI 9239 modules). Utilizing Labview 2011 a protocol was written to read, compress, and record all data into a text file. Appropriate calibration factors were applied within the Labview 2011 protocol which allowed all data to be written in appropriate units.

Data was recorded every 100,000 cycles post retrofit application unless a variable during testing had changed. During the data acquisition process loading was controlled manually progressing from 0 kN (0 kip) to 26.7 kN (6 kip), 37.8 kN (8.5 kip) or 51 kN (11.5kip) depending on what the actuator force range was during fatigue testing. Data was recorded at a sampling rate of approximately 20 samples/second.

Inspection

Inspection of cracking was performed at regular intervals while the specimen was subjected to cyclic loading. Visual inspections as well as evaluation of strain gage data, were utilized as inspection techniques. Magnaflux's Zyglo Penetrant (ZL-27A) was sprayed on the specimen and an ultraviolet flashlight was used to observe the crack openings and tips. When a region of interest was sprayed with dye penetrant during cyclic loading, the cracks in that region would pulse under the ultraviolet light. The cracks were measured with a ruler and dimensioned drawings of the cracks were recorded in a laboratory notebook.

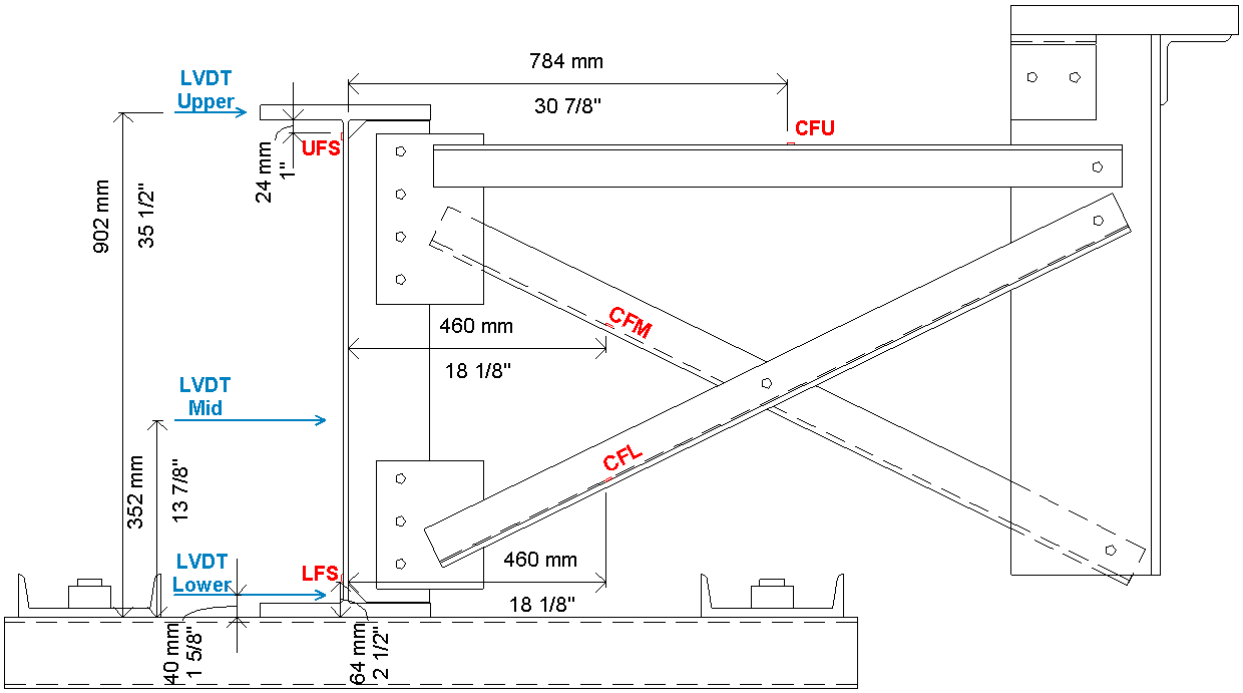

Figure B 5: Section view of instrumentation on experimental subassembly

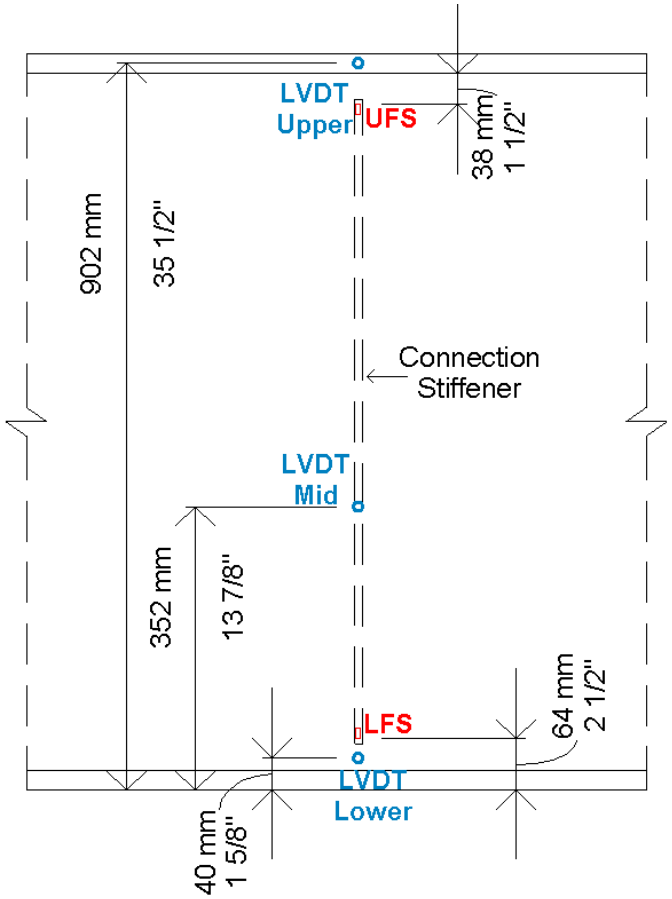

Figure B 6: Fascia side elevation view of instrumentation on experimental subassembly

Appendix C: Lower Composite Block Retrofit Installation

The materials used to apply the lower composite block retrofit were:

1. West System 105 Resin
2. West System 209 Hardener Extra Slow cure
3. Chopped Graphite, 6.3-mm (0.25-in.) fiber length
4. 38-mm (1 1/2-in.) diameter very easy to machine 1215 carbon steel rods
5. 19-mm (3/4-in.) thick plywood
6. 38x89-mm (2x4-in.) lumber
7. Scotch Packing Tape
8. DAP Dynaflex 230 Premium Indoor/Outdoor Sealant
9. 19 liter (5 gallon) plastic bucket
10. Drill Paint Mixer

The composite block retrofit was to be casted on either side of the connection stiffener in the web-gap region. The first task was to fabricate the Bonet Studs. The Bonet Studs were fabricated out of 38-mm (1 ½-in.) diameter 1215 carbon steel rods. A metal lathe was used to machine the steel rods to their proper dimensions. The Bonet Stud geometry is shown in Figure C 1.

Figure C 1: Bonet Stud Geometry

In the locations where the Bonet Studs were installed holes were drilled through the bottom flange of the girder. The surface of the specimen needed to be prepared for the retrofit. This involved using a grinder to grind all of the paint off the specimen in the region where the retrofit would be installed. Figure C 2 shows a dimensioned plan view of the hole location where the Bonet Studs were installed onto the bottom flange of the girder. The two bolts closest to the bottom flange which attached the cross frame's tab plate to the connection stiffener were removed. Bolts 25-mm (1-in.) longer replaced the two bolts which were removed and a nut with

the threads drilled out was placed between the head of the bolt and the connection stiffener. This nut was used to create extra surface area for the CFRP to bond to. The Bonet Studs were then bolted to the bottom flange. The bolts were fully-tightened as indicated by TurnaSure Direct Tension Indicator washers. The entire region was then cleaned with Acetone. The prepared web-gap region with the Bonet Studs installed is shown in Figure C 3.

Figure C 2: Location of holes where Bonet Studs will be located

Figure C 3: Web-gap region prepared for the composite block retrofit

The composite block retrofit had the following dimensions 127x152x178-mm (5x6x7-in.) the block extended 127-mm (5-in.) off the web, 152-mm (6-in.) off the stiffener, and was 178-mm (7-in) tall. A mold was constructed to contain the composite during casting. The mold was constructed out of 16-mm (5/8-in) thick plywood which was cut to its proper size and then wrapped in packing tape in order to prevent the composite from bonding with the plywood. All of the edges of the mold were then caulked with Dap Dynaflex 230 Premium Indoor/Outdoor sealant in an attempt to prevent the composite from leaking during casting. The caulk was given 2 days to dry before the composite was casted. Figure 3 shows the constructed mold.

A 15% carbon fiber by volume ratio was chosen for the composite block retrofit based off the results and casting process of the composite tension test specimens. The volume of each block was 3441-cm^3 (210-in^3) giving a total volume of the two blocks of 6883-cm^3 (420-in^3). Based off the 15% fiber volume ratio 1032-cm^3 (63-in^3) of carbon fibers were required leaving 5850-cm^3 (357-in^3) of Epoxy required. As specified by West Systems the ratio of the 105 resin to 209 hardener should be 3 parts resin to 1 part hardener. Therefore, the volume of resin and hardener was 4388-cm^3 (268-in^3) and 1463-cm^3 (89-in^3) respectively. The density of the carbon fibers, West system 105 Resin and West System 209 hardener were 27.68 g/mL, 1.142 g/mL and 0.968 g/mL respectively. All of the materials were weighed out on an Explorer Pro max 22000g scale with $1/10^{th}$ gram accuracy. The total weight of materials was, 1857.5 grams of fibers, 5011.6 grams of resin and 1415.0 grams of hardener.

After all materials were weighed out the resin and hardener was mixed together, a drill attached paint mixer was used to mix the two liquids together for 30 seconds. After the liquids were mixed the fibers were slowly

added. A paint stick was used to mix the fibers and the epoxy together. After all fibers were added the composite was mixed for 5 minutes. Figure C 4 shows the composite mixture after 5 minutes of mixing.

Figure C 4: CFRP mixture after mixing

The CFRP mixture was then put into the mold at the web-gap region. The experimenter took handfuls of the composite and shoved it into the mold until the composite was flush with the top of the box as shown in Figure C 5. A 127x152-mm (5x6-in.) piece of 16-mm (5/8-in.) thick plywood wrapped in packing tape was placed on the top of the box. A 667-mm (26 ¼-in.) long 51x102-mm (2x4-in.) was wedged up against the underside of the girder's top flange. This 51x102-mm (2x4-in.) was used to push the plywood piece on top of the box into the form in order to compact the composite and insure there wouldn't be any air pockets present in the block. Clear epoxy then began to leak through the form insuring that the block was under pressure as shown in Figure C 6. The temperature in the lab when the block was casted was 24.3-C° (75.7-F°).

Figure C 5: CFRP inside mold

The block was given nine full days to cure. On the 10th day of curing the plywood mold was removed. A crowbar and hammer was used to remove the mold from the block. Figure C 7 shows the mold being removed and the fully cured composite block. Testing of the composite block retrofit commenced shortly after the wooden mold was removed and the lab space was cleaned.

Figure C 6: Epoxy leaking out of mold insuring air pockets wouldn't be present in the block

Figure C 7: Cured composite block

Appendix D: ASTM D3039 – 08 Standard test method for Tensile Properties of Polymer Matrix Composite Materials.

Some of the material properties calculated in the following report are not what would be theoretically expected. The fibers in the FRPs tested, are randomly oriented. The ASTM procedure used was for FRPs which are uniaxial oriented or biaxial oriented. There is no current ASTM procedure for FRPs utilizing randomly oriented fibers. A literature review was performed and there was no available data found on material tests conducted with FRPs utilizing randomly oriented fibers.

If this test is to be repeated, the material properties should be calculated using a block with similar dimensions to the composite block retrofit. On all four sides of the block there should be a strain gage oriented both longitudinally and transversely. The loading protocol should put the block in compression.

14.1 The test was performed on a Baldwin 120 BTE472961model.

14.1.1 Date of issue of test method was 2008 utilizing test method D3039/D3039M-08.

14.1.2 The test was performed on 22 August 2013 in Learned Hall, Room 1167 at the University of Kansas.

14.1.3 The test operator was Eric Bonet.

14.1.4 There were no anomalies noticed during testing.

14.1.5 Materials used:

Impregnated Chopped Carbon fiber

Filament diameter: 7.2 microns (0.283 mils)

Fiber areal weight: 1.81 g/cc (0.065 lb/in^3)

Matrix type: Random

Prepreg matrix content: CST The Composites Store 0.25” Chopped Carbon Fiber Filler

Prepreg volatiles content: West systems 105 Epoxy Resin, West Systems 209 Extra Slow Hardener

14.1.6 The tensile specimens were molded on 16 July 2013. They were removed from the molds on 20 July 2013. They were fabricated using a mold constructed of 16-mm (5/8-in) thick plywood. The plywood was sealed with clear packing tape in order to prevent the composite to bonding with the plywood. The mold was rectangular with dimensions of 24x50x305-mm (1x2x12-in.) and it was held together with 29-mm (1.125”) wood screws. 286.4 grams of West systems 105 resin, 80.9 grams of West Systems 209 hardener and 106 grams of CST 6-mm (0.25-in.) chopped carbon fiber filler were measured out into separate containers. This ratio gave a 15% by volume fiber ratio, and conformed to the West Systems standard of 3 parts resin to 1 parts hardener. The hardener was then added to the resin and resin/hardener was mixed thoroughly for 30 seconds. The carbon fibers were then slowly added and stirred for another 5 minutes. After the composite was poured into the molds, steel “C” clamps were applied in order to place the composite under pressure to remove any air pockets. They were allowed to

cure in the molds for 9 days. The specimens were then removed from their molds and sanded on a rotating disk sander to refine their final dimensions.

14.1.7 The orientation of the carbon fiber in the specimens is random. The fibers are 6-mm (1/4-in.) long.

14.1.8 The chopped carbon fibers accounted for 15% of the composite volume.

14.1.9 The Carbon fiber is chopped and therefore there are no plies.

14.1.10 No nondestructive evaluation tests were performed.

14.1.11 Method of Preparing test Specimens:

The test specimens were labeled 1 through 4 with a number written on tape which was taped to each specimen. The specimen geometry is approximately 24x50x305-mm (1x2x12-in.). See 14.1.15 for specimen specific dimensions. The specimens were fabricated using a wooden mold as described in 14.1.6. The specimens were not cut and they were clamped directly into the Baldwin 120 testing apparatus. There were no tabs used.

14.1.12 The Baldwin 120's Transducer was last calibrated on 8 January 2013 using a Strain type calibration test. The results show it Passed Class B-1- 100% Range in Tension mode.

14.1.13 The machine used was a Baldwin 120 BTE472961 model, with Baldwin BD120WGf Flat Wedge Grip. The grips were aligned using a 19-mm thick, 51-mm wide (3/4x2-in.) wide piece of steel. Data was recorded at a rate of 20 Hz utilizing a NI cDAQ 9188 chassis with NI 9236 and NI 9239 modules.

14.1.14 Due to the grips being aligned with a piece of steel a system alignment test was not performed.

14.1.15 Dimensions of each test specimen are as follows:

Specimen 1					Specimen 2				
Width		Thickness		Length	Width		Thickness		Length
in	Tolerance %	in	Tolerance %	in	in	Tolerance %	in	Tolerance %	in
1.979	1.0	0.881	0.6	11.945	1.957	0	0.929	0.1	11.760
1.988	0.1	0.875	0		1.958	0.1	0.928	0.2	
2.000	1.1	0.869	0.6		1.956	0.1	0.933	0.3	
1.989	AVG	0.875	AVG		1.957	AVG	0.930	AVG	
Specimen 3					Specimen 4				
Width		Thickness		Length	Width		Thickness		Length
in	Tolerance %	in	Tolerance %	in	in	Tolerance %	in	Tolerance %	in
1.961	0.2	0.730	0.1	11.905	1.985	0.7	0.738	0.7	11.830
1.964	0.1	0.728	0.1		1.976	0.2	0.729	0.2	
1.965	0.2	0.729	0		1.974	0.4	0.725	0.6	
1.963	AVG	0.729	AVG		1.978	AVG	0.731	AVG	

Figure D 1: CFRP tension test specimen dimensions

14.1.16 The specimens were left unconditioned during testing and the moisture content was unknown.

14.1.17 Relative humidity of testing laboratory: 76% RH

Relative temperature of testing laboratory: 31.7°-C (89.0°-F).

14.1.18 There was no Environmental chamber used. The test was performed in the structures lab in Learned Hall at the University of Kansas. The specimens were acclimated to the lab for one week before the test was performed.

14.1.19 There were 4 specimens tested.

14.1.20 The speed of testing was controlled by the Bladwin 120. The Baldwin 120 applied a tensile load of 4.45kN/min (1kip/min) until failure. Testing took between 4-6minutes depending on the specimen tested.

14.1.21 Two Strain Gages were placed on each specimen one gage was oriented longitudinally the other transversely. The gages were centered on the specimen on the larger face. Strain gage data was recorded using a NI 9236 card reader which internally created a Full Wheatstone bridge, with one leg of the bridge being replaced with a strain gage. Each gage was calibrated using Labview 2012.

14.1.22 The Strain Gages utilized were Micro-Measurements General Purpose Strain Gages, EA-06-250BF-350/P. The gages were 350.0 Ohms +- 0.5%. The gage length and width was 6.35-mm (0.25-in.) and 9.525-mm (0.375-in.) respectively. Temperature was compensated was performed in the Labview 2012 software. The transverse sensitivity of the gages was (+0.2 +-0.2)%. The resistance of the lead wire wasn't recorded since Labview 2012 calibrates all gages with the lead wires attached. No correction factors were used.

14.1.23 Stress vs. Strain Plots shown below.

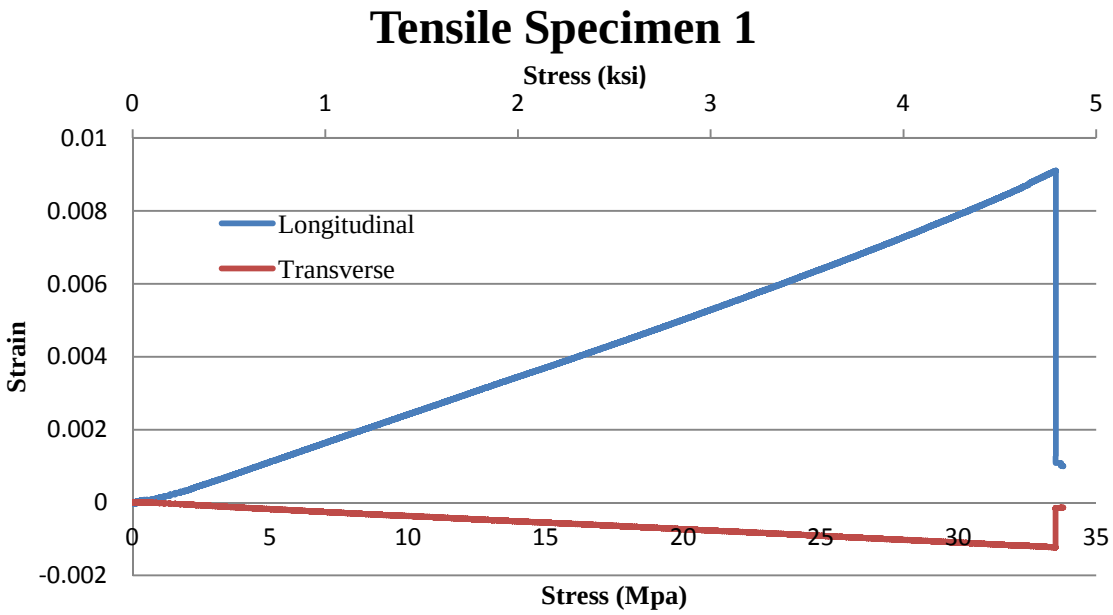

Figure D 2: Stress strain curve tensile specimen 1

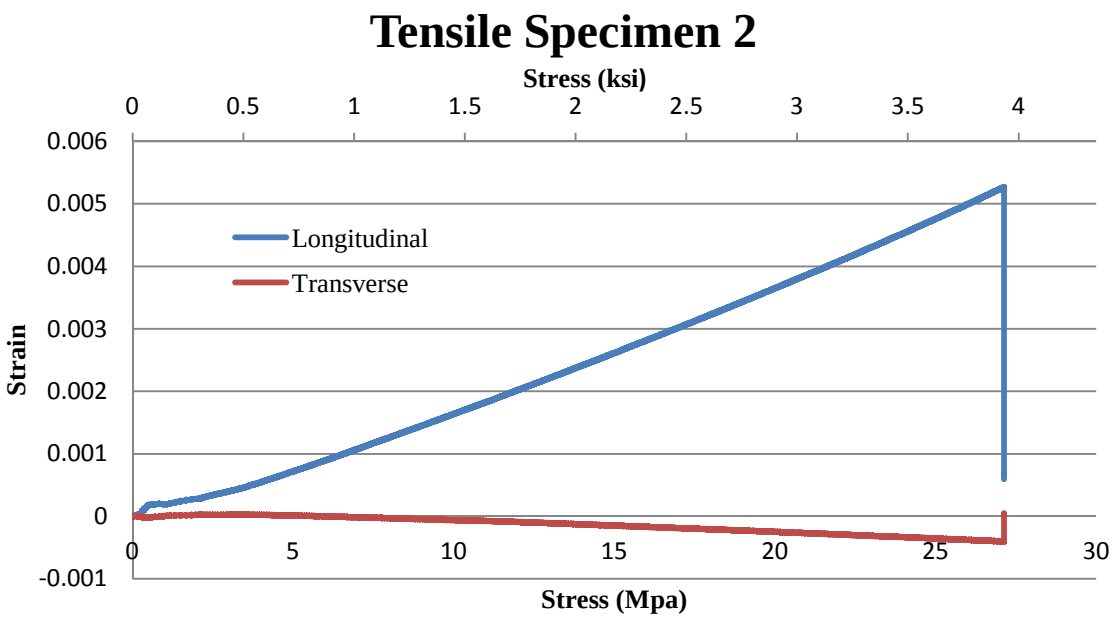

Figure D 3: Stress strain curve tensile specimen 2

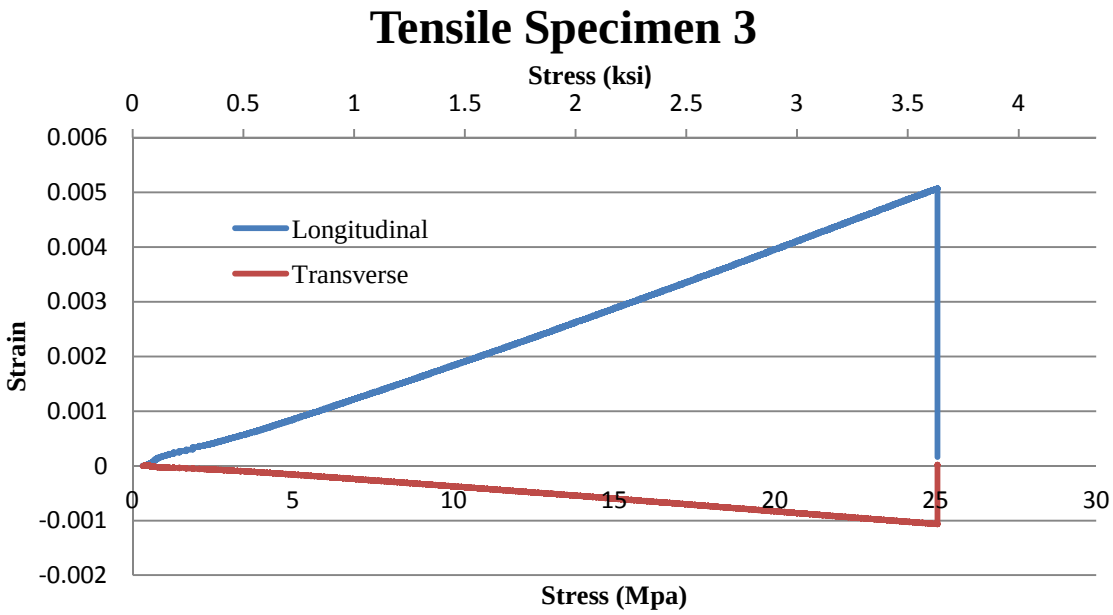

Figure D 4: Stress strain curve tensile specimen 3

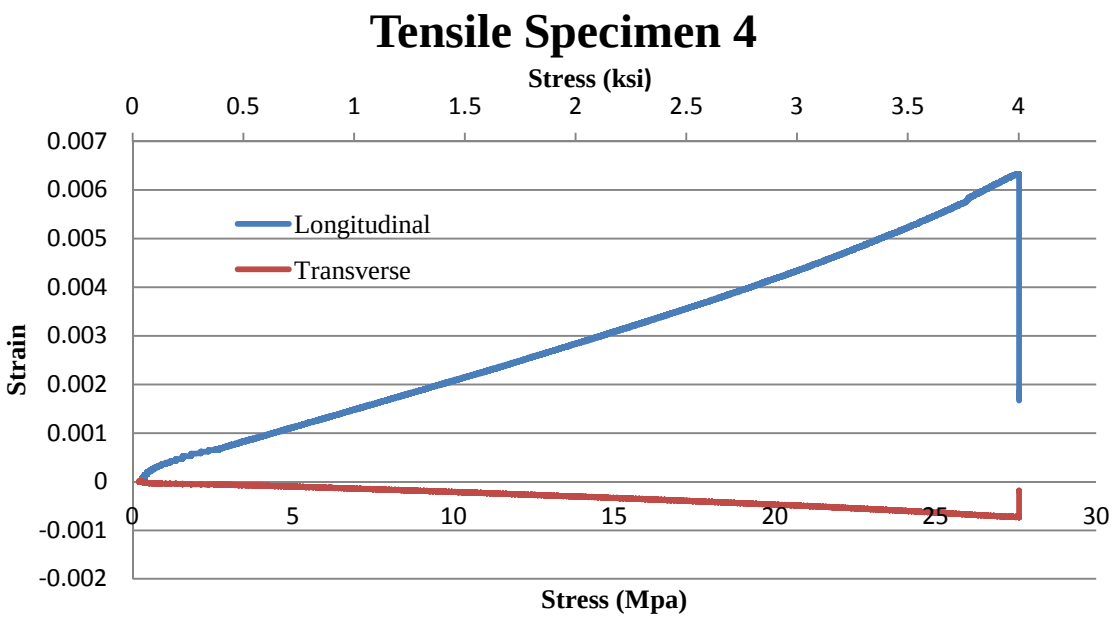

Figure D 5: Stress strain curve tensile specimen 4

14.1.24 Bending was not calculated for the specimens.

14.1.25

Specimen #	Fu (ksi)	Standard Deviation	Coefficient of Variation
1	5.66	0.792	0.184
2	3.93		
3	3.63		
4	4.00		
Average	4.308		

14.1.26

Table D 1: CFRP tensile specimen's ultimate strength

Specimen #	Lateral Failure Strain	Standard Deviation	Coefficient of Variation	Transverse Failure Strain	Standard Deviation	Coefficient of Variation
1	0.00910	0.00161	0.249	-0.001230	0.00032	-0.373
2	0.00527			-0.000399		
3	0.00508			-0.001061		
4	0.00632			-0.000728		
Average	0.00644			-0.00085		

Table D 2: Strains at failure

14.1.27 The Strain range used to calculate chord modulus and Poisson's ration was 1000με to 3000με

14.1.28 Chord modulus was used

14.1.29

Specimen #	Echord	Standard Deviation	Coefficient of Variation
1	566.21	71.827	0.104
2	744.65		
3	714.41		
4	731.61		
Average	689.222		

Table D 3: Modulus of elasticity

14.1.30 The chordwise definition was used for Poisson's ratio.

14.1.31

Specimen #	v	Standard Deviation	Coefficient of Variation
1	0.145	0.048	0.335
2	0.089		
3	0.217		
4	0.118		
Average	0.142		

Table D 4: Poisson's ratio

14.1.32-33 Transition strain was not determined

14.1.34

Specimen #	Failure Mode
1	LWB
2	GAT
3	LGM
4	LGM

Table D 5: Failure mode and location

Photographs of tension specimen fabrication and testing

Figure D 6: 25x51x305 mm (1x2x12 in) Tension specimens curing

Figure D 7: Removing cured specimen from mold

Figure D 8: Sanding specimen

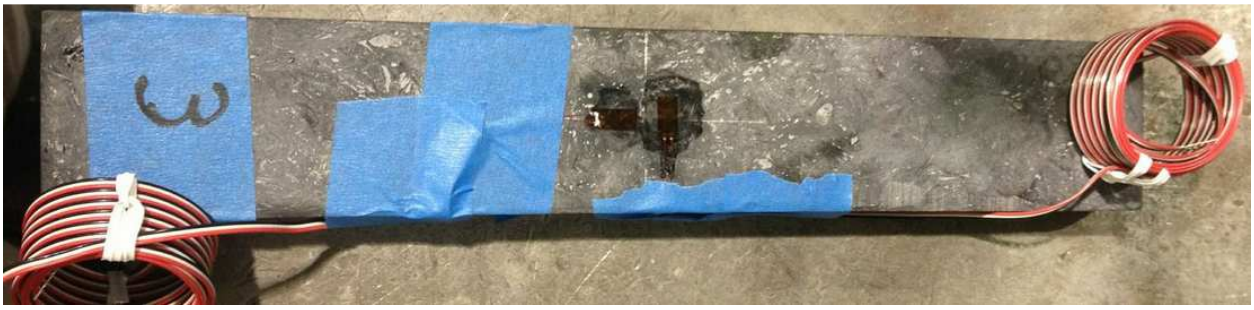

Figure D 9: Strain Gages installed in tension specimen

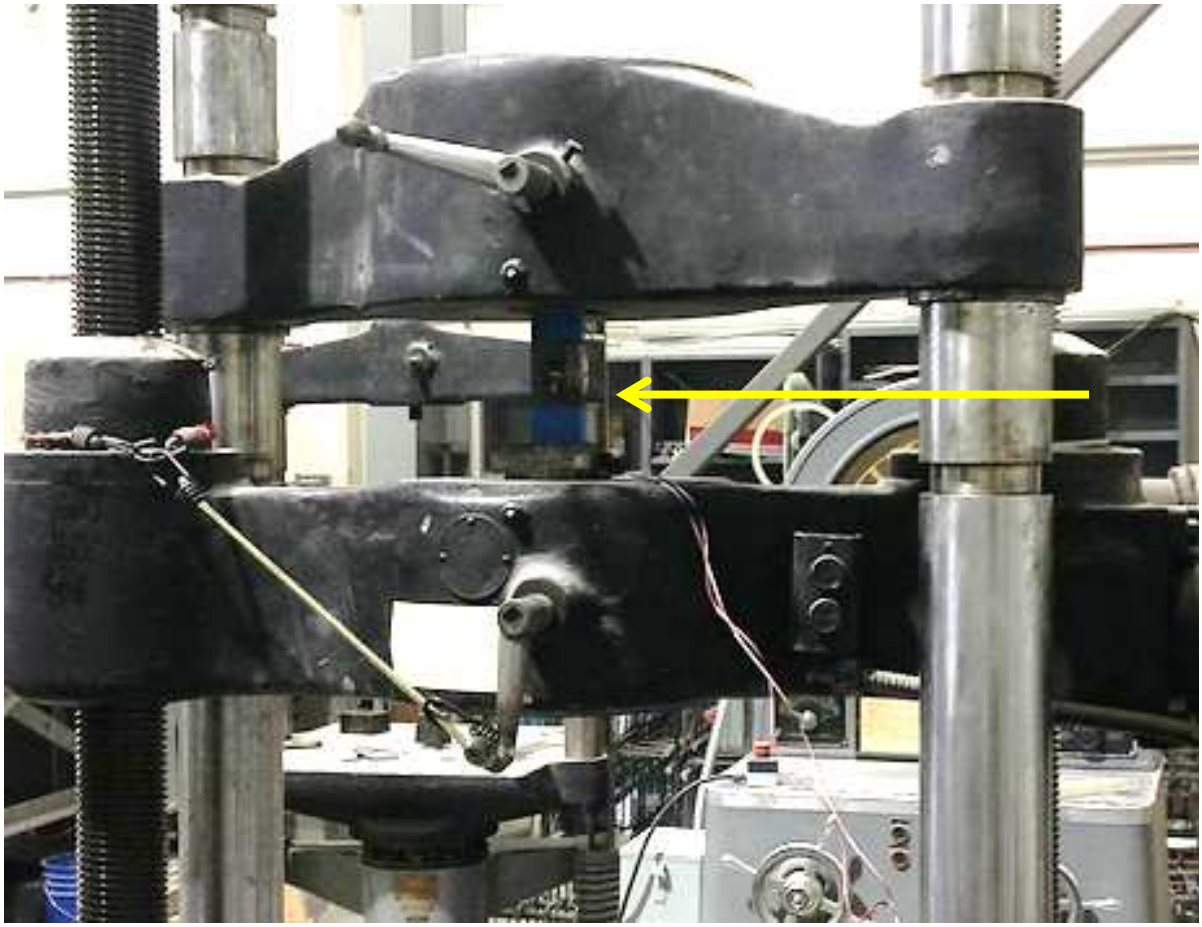

Figure D 10: Testing Tension Specimens

Appendix E: ASTM D5961-13 Standard Test Method for Bearing Response of Polymer Matrix Composite Laminates.

14.1.1 The test method preformed was ASTM D5961-13

14.1.2 The procedure used was Procedure A, Double, Tension. All specimen configurations were the same however because the composite used randomly oriented fibers the specimen geometry needed to be increased. The w/D ration remained at 6 and the D/h ratio was 1.3 since the average specimen thickness was 19-mm (3/4-in.) and the hole diameter was 25-mm (1-in.). The specimen was tested in the unstabilized configuration (No Support Fixture).

14.1.3 Testing was conducted at the University of Kansas in the Fracture and Fatigue lab in M2SEC on the 29th and 30th of August 2013.

14.1.4 Testing was conducted by Eric Bonet.

14.1.5 Other than the increasing the specimen size due to the randomly oriented fibers, there were no variations in the testing methods.

14.1.6 Materials used:

Impregnated Chopped Carbon fiber
Filament diameter: 7.2 microns (0.283 mils)
Fiber areal weight: 1.81 g/cc (0.065 lb/in^3)
Matrix type: Random
Prepreg matrix content: CST The Composites Store 0.25” Chopped Carbon Fiber Filler
Prepreg volatiles content: West systems 105 Epoxy Resin, West Systems 209 Extra Slow Hardener

14.1.7 The tensile specimens were molded on 19 July 2013. They were removed from the molds on 28 July 2013. They were fabricated using a mold constructed of 16-mm (5/8-in) thick plywood. The plywood was sealed with clear packing tape in order to prevent the composite from bonding with the plywood. The mold was rectangular with dimensions of 19x152x305-mm (3/4x6x12-in.) and it was held together with 29-mm (1.125”) wood screws. A 24-mm (1-in.) diameter hole was cut through the two faces of the mod the center of the hole was 76-mm (3-in.) from the top of the specimens and centered horizontally. The composite was casted with the 24-mm (1-in.) diameter rod in place. 634.5 grams of West systems 105 resin, 179.4 grams of West Systems 209 hardener and 226 grams of CST 6-mm (0.25-in.) chopped carbon fiber filler were measured out into separate containers. This ratio gave a 15% by volume fiber ratio, and conformed to the West Systems standard of 3 parts resin to 1 parts hardener. The hardener was then added to the resin and resin/hardener was mixed thoroughly for 30 seconds. The carbon fibers were then slowly added and stirred for another 5 minutes. After the composite was

poured into the molds, steel “C” clamps were applied in order to place the composite under pressure to remove any air pockets. The specimens were allowed to cure in the molds for 7 days. The specimens were then removed from their molds and sanded on a rotating disk sander to refine their final dimensions.

14.1.8 The orientation of the carbon fiber in the specimens is random. The fibers are 6-mm (1/4-in.) long.

14.1.9 The chopped carbon fibers accounted for 15% of the composite volume.

14.1.10 The Carbon fiber is chopped and therefore there are no plies.

14.1.11 No nondestructive evaluation tests were performed.

14.1.12 Method of Preparing test Specimens:

The test specimens were labeled 1 through 5 with a number written on painters tape which was taped to each specimen. The specimen geometry is approximately 19x152x305-mm (3/4x6x12-in.). See 14.1.17 for specimen specific dimensions. The specimens were fabricated using a wooden mold as described in 14.1.7. The specimens were not cut and they were clamped directly into the Instron Model 1334 testing apparatus. There were no tabs used.

14.1.13 The fasteners used were 25-mm (1-in.) diameter rods which were installed in the specimens before casting took place. Appropriately sized nuts and washer were used to secure the rod to the metal bearing plate. Due to the large size of the rods and fasteners and the fact that they were put under a small amount of force, the nuts and washers were reused for each specimen.

14.1.14 Since no hole was drilled in the specimen the only cleaning method was done directly after the specimens were removed from their molds. Which was sanding the edges down to prevent the experimenter from cutting his hands while working with the specimens.

14.1.15 The Instron Model 1334 was last calibrated on 30 April 2008. The extensometer used was calibrated on 28 August 2013 using a Pratt & Whitney Supermicrometer G-2100.

14.1.16 The test machine used was an Instron Model 1334, the Instron uses hydraulic grips and the grip pressure was 10,340kPa (1500psi). The grips on the Baldwin were aligned using 19-mm. (3/4-in.) thick steel plate. Data was recorded at a rate of 20 Hz utilizing a NI cDAQ 9188 chassis with a NI 9239 module.

14.1.17 Dimensions of each test specimen are as follows:

Specimen 1					Specimen 2				
Width		Thickness		Length	Width		Thickness		Length
in	Tolerance %	in	Tolerance %	in	In	Tolerance %	in	Tolerance %	in
5.984	0	0.814	0.55	12.000	5.946	2.225	0.676	1.825	11.750
5.986	0.2	0.809	0.05		5.952	1.625	0.695	0.075	
5.977	0.7	0.805	0.35		5.982	1.375	0.705	1.075	
5.989	0.5	0.806	0.25		5.993	2.475	0.701	0.675	
5.984	AVG	0.809	AVG		5.968	AVG	0.694	AVG	
Specimen 3					Specimen 4				
Width		Thickness		Length	Width		Thickness		Length
in	Tolerance %	in	Tolerance %	in	In	Tolerance %	in	Tolerance %	in
6.02	1.475	0.851	0.1	11.875	6.046	0.075	0.668	2.475	11.813
5.996	0.925	0.866	1.4		6.042	0.475	0.689	0.375	
5.998	0.725	0.83	2.2		6.046	0.075	0.709	1.625	
6.007	0.175	0.861	0.9		6.053	0.625	0.705	1.225	
6.005	AVG	0.852	AVG		6.047	AVG	0.693	AVG	

Specimen 5				
Width		Thickness		Length
in	Tolerance %	in	Tolerance %	in
6.035	1.175	0.698	0.525	11.955
5.998	4.875	0.696	0.325	
6	4.675	0.722	2.925	
6.02	2.675	0.721	2.825	
6.013	AVG	0.709	AVG	

Table E 1: CFRP bearing specimens dimensions

14.1.18 Since each specimen was casted with a 24-mm (1-in.) rod inside of it. All holes were exactly 24-mm (1-in.) because the rods used were fabricated out of the same 24-mm (1-in.) stock rod. Each specimen's hole diameter to thickness ratio is shown in Table E 2.

Hole to Diameter to thickness ratio			
Specimen #	Hole Diameter (in)	Thickness (in)	Ratio
1	1	0.809	1.237
2	1	0.694	1.440
3	1	0.852	1.174
4	1	0.693	1.444
5	1	0.709	1.410
AVG	1	0.751	1.341

Table E 2: Hole diameter to thickness ratio

14.1.19 Loading type was tensile, there was no support fixture used. The gap between plates was 19-mm (3/4-in.) which was created with a 19-mm (3/4-in.) steel plate.

14.1.20 Travelers were not used and the specimen was left unconditioned.

14.1.21 The temperature in the testing lab was 20°-C (68°-F), the relative humidity was 58%.

14.1.22 An environmental chamber wasn't used the specimens were left in the lab for four days before testing began.

14.1.23 Five specimens were tested

14.1.24 The Instron Model 1334 applied a tensile load of 4.45kN/min (1kip/min) until failure. Testing took between 7-11 minutes depending on which specimen was tested.

14.1.25 The extensometer used had arms which were spaced 24-mm (1-in.) apart. The extensometer was centered horizontally on the specimen and the lower arm of the extensometer was placed on the composite 146-mm (5 3/4-in.) from the top of the specimen. The upper arm of the extensometer was 24-mm (1-in.) above the lower arm. The extensometer had four 350 Ohm 6-mm (1/4-in) strain gages longitudinally oriented, one on each face of the two arms. They were wired in a wheat stone bridge configuration and connected to a 5V power supply and the Data acquisition system.

14.1.26 Bearing stress/bearing strain curves are shown below:

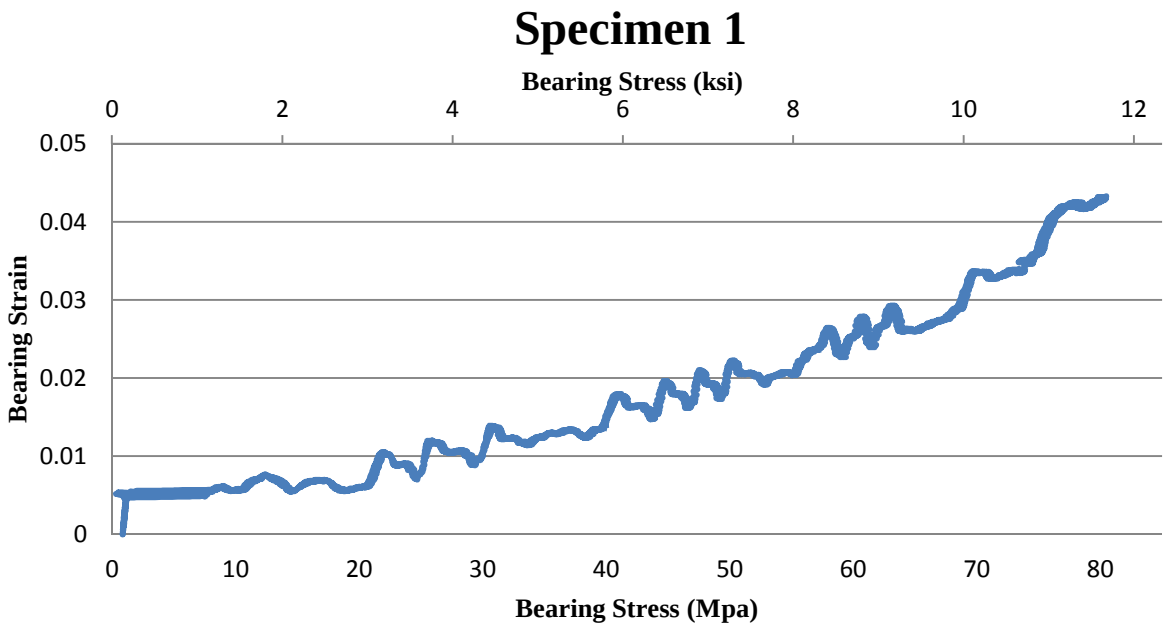

Figure E 1: Stress strain curve for bearing specimen 1

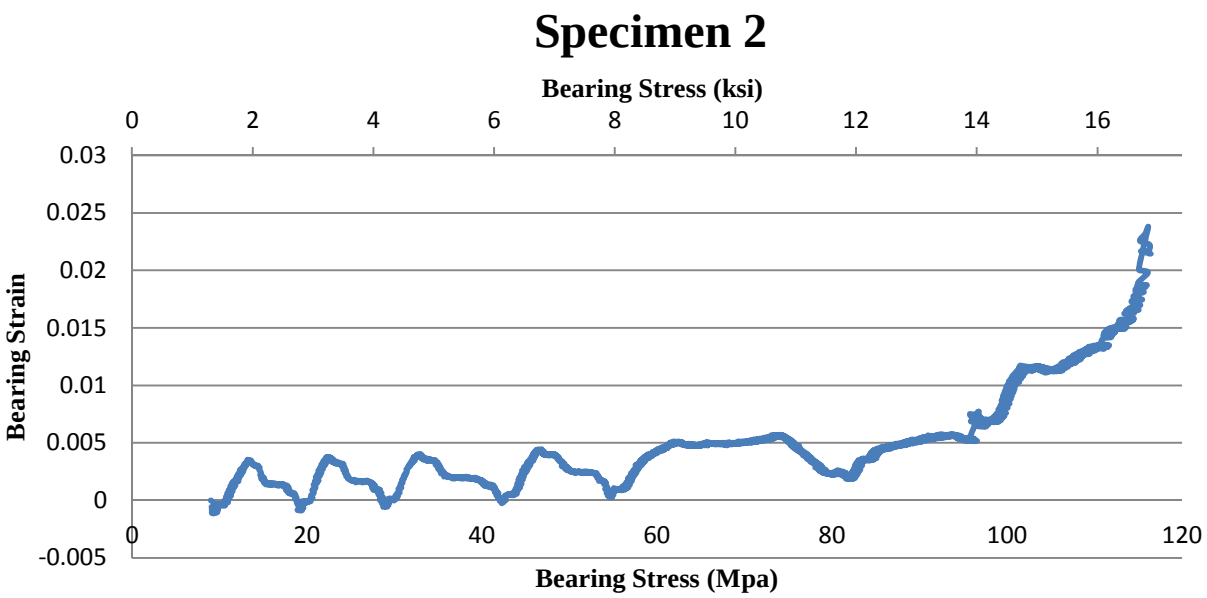

Figure E 2: Stress strain curve for bearing specimen 2

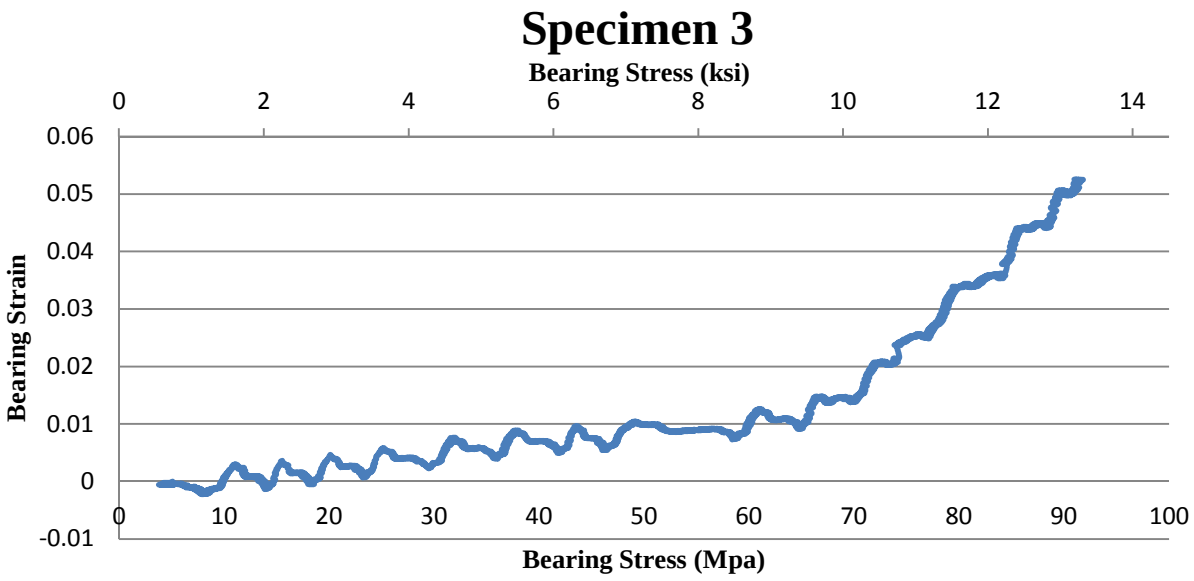

Figure E 3: Stress strain curve for bearing specimen 3

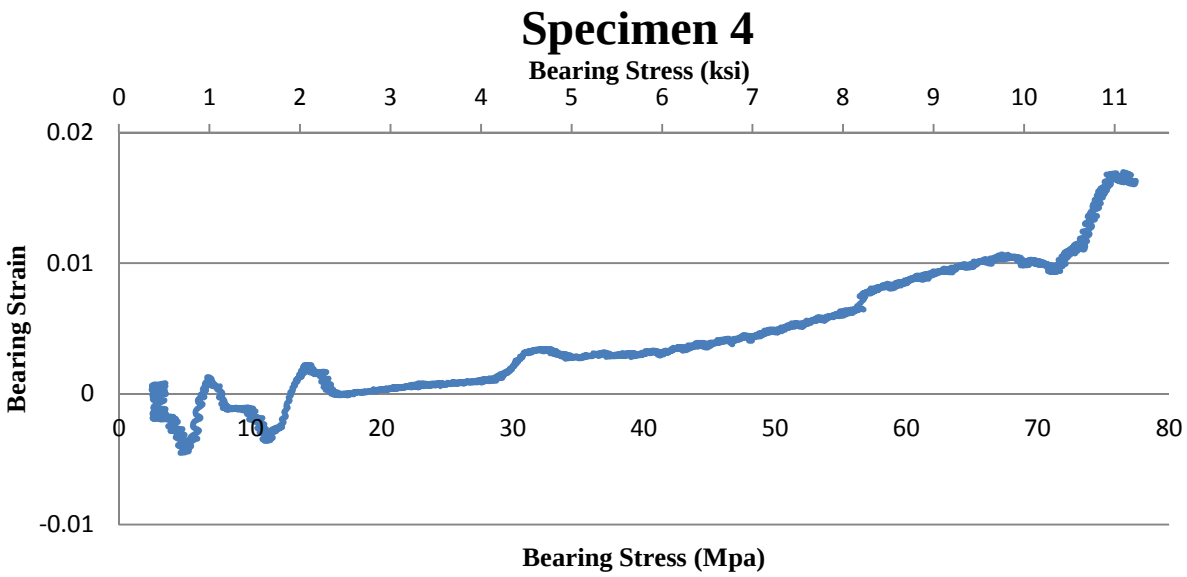

Figure E 4: Stress strain curve for bearing specimen 4

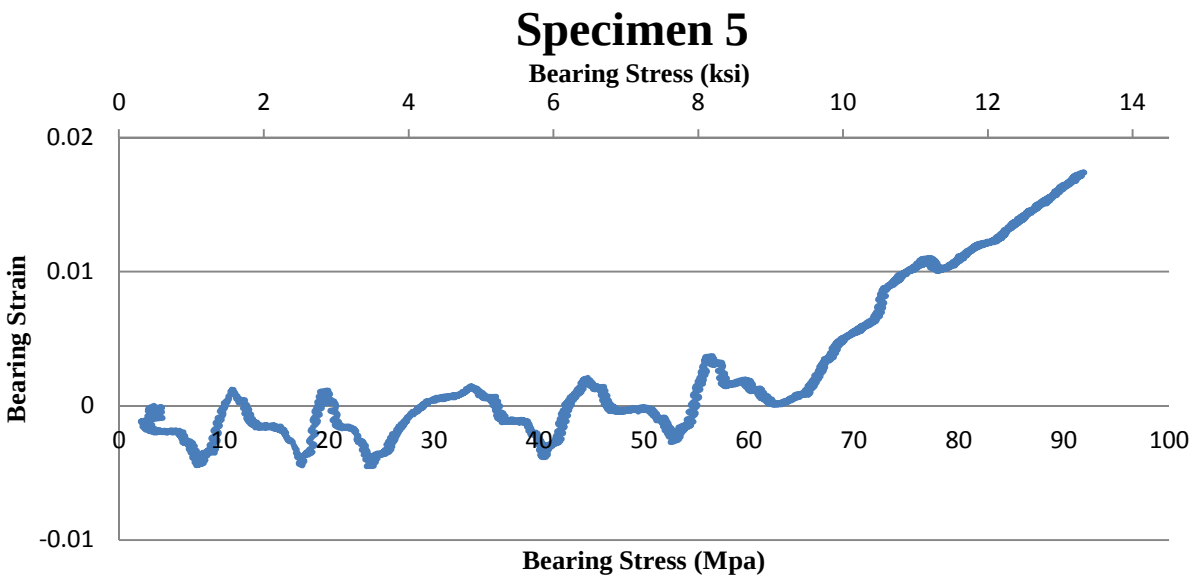

Figure E 5: Stress strain curve for bearing specimen 5

14.1.27

Ultimate Bearing Strengths			
Specimen #	F^{bur} (ksi)	Standard Deviation	Coefficient of Variation
1	9.440	1.435	0.144
2	11.723		
3	11.347		
4	7.784		
5	9.456		
AVG	9.950		

Table E 3: Ultimate bearing strength

14.1.28

Ultimate Bearing Strains			
Specimen #	F^{bur} (in/in)	Standard Deviation	Coefficient of Variation
1	0.043	0.014	0.470
2	0.024		
3	0.053		
4	0.017		
5	0.017		
AVG	0.031		

Table E 4: Ultimate bearing strain

14.1.29-30 The offset bearing strength was not determined.

14.1.31 The initial peak bearing strength was not determined.

14.1.32 The Instron fast track 8800 controller which was used to run the Instron model 1334 was unable to output load and displacement simultaneously. For this reason Force/displacement curves were not created.

14.1.33-34 Ultimate force and failure force occurred simultaneously shown in Table E 5.

Ultimate/Failure Force	
Specimen #	P^{max}
1	9.440
2	11.723
3	11.347
4	7.784
5	9.456
AVG	9.950

Table E 5: Bearing specimens ultimate force

14.1.35 The failure mode and location of failure for each specimen is given in Table E 6.

Specimen #	Failure Mode
1	L(above bottom grip)
2	L1I
3	M(bl)1I
4	B1I
5	B1I

Table E 6: Failure mode and location

Photographs of bearing specimen fabrication and testing

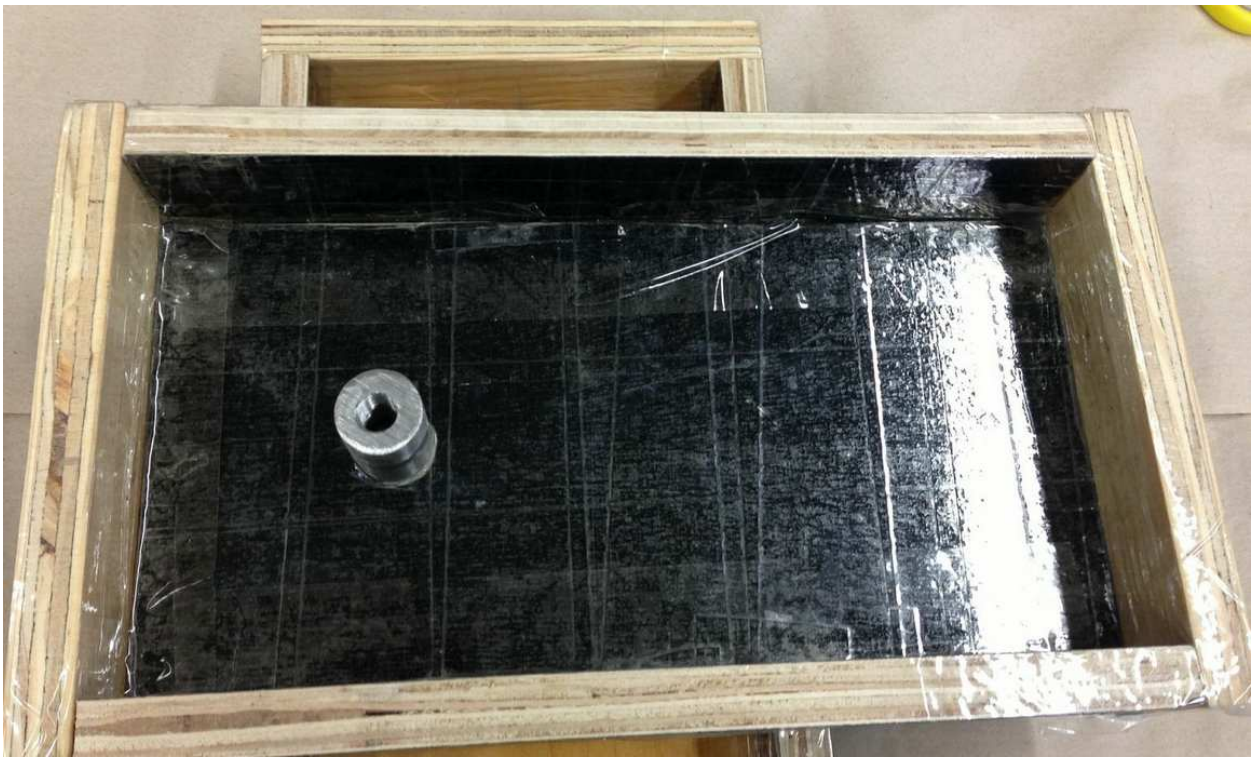

Table E 7: Mold for bearing specimen

Table E 8: Casting bearing specimen

Table E 9: Bearing specimens curing

Table E 10: Test setup for bearing specimens

Table E 11: The tested bearing specimens

Appendix F: Upper Composite Block Retrofit Installation

The installation of the upper composite block retrofit was very similar to the procedure described in Appendix C. The materials used to apply the retrofit were:

1. West System 105 Resin
2. West System 209 Hardener Extra Slow cure
3. Chopped Graphite, 6.3-mm (0.25-in.) fiber length
4. 38-mm (1 1/2-in.) diameter very easy to machine 1215 carbon steel rods
5. 19-mm (3/4-in.) thick plywood
6. 38x89-mm (2x4-in.) lumber
7. Scotch Packing Tape

8. DAP Dynaflex 230 Premium Indoor/Outdoor Sealant
9. 19 liter (5 gallon) plastic bucket
10. Drill Paint Mixer

The first task preformed when installing the upper composite block retrofit was to fabricate the Bonet Studs. The same fabrication process was used as described in Appendix C. Once the studs were fabricated four holes in total were drilled through the top flange at the locations where the Bonet Studs would be located. Figure F 1 shows a plan view of the locations where holes were drilled through the top flange, in preparation for the installation of the Bonet Studs.

Figure F 1: Location of holes where Bonet Studs will be located.

After the holes were drilled the surface was then prepared for the retrofit to be installed. This involved using a grinder to grind all of the paint off the specimen in the region where the retrofit would be installed. The two bolts closest to the top flange which attach the cross frame's tab plate to the connection stiffener were removed. Bolts 25-mm (1-in.) longer replaced the two bolts which were removed and a nut with the treads drilled out was placed between the head of the bolt and the connection stiffener. The Bonet Studs were then bolted to the top flange, the bolts were fully tightened as indicated by TurnaSure Direct Tension Indicator washers. The entire region was then cleaned with Acetone. Figure F 2 shows the upper web-gap region with the surface prepared and the Bonet Studs installed.

Figure F 2: Upper web-gap region composite block retrofit preparation

The upper composite block retrofit had the following dimensions 127x152x178-mm (5x6x7-in.) the block extended 127-mm (5-in.) off the web, 152-mm (6-in.) off the stiffener and 178-mm (7-in) from the bottom face of the top flange. A mold was constructed in order to contain the composite during casting. The mold was constructed out of 16-mm (5/8-in) thick plywood which was cut to its proper size and then wrapped in packing tape in order to prevent the composite from bonding with the plywood. All of the edges of the mold were then caulked with Dap Dynaflex 230 Premium Indoor/Outdoor silicon sealant in an attempt to prevent the composite from leaking during casting. The caulk was given 2 days to dry before the composite was casted. Figure F 2 shows the constructed mold. Applying the composite block in the upper web-gap region on the girder subassembly imitates how the retrofit would have to be applied in the field, because in the field the retrofit application process needs to be able to counter the force of gravity. In the upper web-gap region the composite was put into the mold from a 127x102-mm (5x4-in.) tunnel located on the side of the block mold, rather than from above the mold like what was done in the lower web-gap region.

The exact same composite mix design which was used for the instillation of the composite block retrofit in the lower web-gap region was used for the installation of the composite block retrofit in the upper web-gap region. See Appendix C for more information.

After the composite was mixed it was put into the mold at the upper web-gap region. Handfuls of composite were shoved through the tunnel created in the mold until the composite extended well beyond the dimensions of the box. A 127x102-mm (5x4-in.) piece of 16-mm (5/8-in.) thick plywood wrapped in packing tape was placed inside the tunnel. A 51x102-mm (2x4-in.) was wedged against the inside face of the exterior

stiffener and the 127x102-mm (5x4-in.) piece of 16-mm (5/8-in.) thick plywood. This 51x102-mm (2x4-in.) was used to push the plywood piece in the tunnel of the box further into the form, in order to compact the composite and insure there wouldn't be any air pockets present in the block. Clear epoxy then began to leak through the form insuring that the block was under pressure as shown in Figure F 3. The temperature in the lab when the block was casted was 24.3-C° (75.7-F°).

The composite was given nine full days to cure. On the 10th day of curing the plywood mold was removed. A crowbar and hammer was used to remove the mold from around the block. Figure F 4 shows one of the fully cured blocks installed in the upper web-gap region. Testing of the upper composite block retrofit commenced shortly after the mold was removed and the lab space was cleaned.

Figure F 3: Upper composite block retrofit curing in the form.

Figure F 4: Fully cured upper composite block retrofit

Appendix G: Kevlar Stitching Retrofit Installation

There are many locations on structures where welding is either geometrically too difficult to preform, too dangerous due to combustibles nearby, or continue to fail due to fatigue at welds. If welding cannot be performed another possible route to take to connect two or more structural elements would be stitching the elements together. The specimen tested in M2SEC had a 165-mm (6.5-in.) mode 1 crack located on the tab plate which connected the cross frame to the connection stiffener. The primary stress path was perpendicular to the direction of the crack. The crack was repaired with a full penetration 5-mm (3/16-in.) arc weld on three separate occasions and it broke all three times. Since welding the crack together was not a viable solution, a stitching retrofit was applied.

The goal of the stitching retrofit was to create a load path from the cross frame directly to the girder, while bypassing the tab plate. Four (5/8 in.) diameter holes were drilled through the composite block and web in the lower web-gap region, so that there were two holes oriented vertically on either side of the connection stiffener. After the holes were drilled, a grinder was used to remove any sharp edges created from drilling. Two (3/8-in.) holes were then drilled on the horizontal leg of the angle, which was welded to the fractured tab plate and three (3/8-in.) holes were drilled on the vertical leg of that angle. Five fully threaded Grade 5, Medium Strength Steel (3/8-in.) diameter screws with a minimum Rockwell hardness of C25 and a minimum tensile strength of (120ksi) (McMaster-Carr) were then installed in the holes and fully tightened with crescent wrenches. Before the screws were installed, a washer was placed against the screw head, then a nut was run down the screw threads so the washer was locked in place, this allowed a space to be created between the cross frame and the washer so the stitching would not slide out of place when it was wrapped around the screw.

The materials used to apply the stitching retrofit are:

1. West System 105 Resin
2. West System 206 Hardener Slow Cure
3. Grade 5, Medium Strength (3/8-in.) diameter fully threaded screws
4. Grade 8 steel (3/8-in.) Diameter Hex Nuts
5. General Purpose Washers-USS and SAE (Type A) (3/8-in.) diameter Plain Steel Washers
6. Aramid Yarn, Denier 1510
7. 12k Carbon Fiber Tow
8. 1 metal clothes hanger

Originally, the stitching was going to combine the 12k Carbon Fiber and the Aramid Yarn. The two materials were going to be spun together as shown in Figure G 1. After one attempt at spinning the two threads together it proved to be much too difficult and time consuming. The Carbon Fiber threads were too brittle and kept breaking. It was then decided to use only the Aramid Yarn in the stitching retrofit. The Aramid yarn was unraveled in a 3.7m (12-ft.) section and folded back on itself 32 times, so there were 64 total

strands of Armid Yard for the 1.8m (6-ft.) long stitch. The Armid Yarn was then coated with the West Systems epoxy. The epoxy was made by combining the 105 resin with the 206 hardener in a 5:1 ratio by volume. The liquids were then vigorously mixed for 30 seconds.

Figure G 1: 12k Carbon Fiber and Aramid Yarn spun together

The MTS actuator was powered on and a compressive load of (1kip) was applied to the cross frame. This successfully created a post tensioning affect. After the retrofit was installed and the compressive actuator load was removed. The threads were then stitched through the predrilled holes in the composite block and web using a metal clothes hanger which was taken apart and made into a giant sewing needle. The threads passed through the top hole, were wrapped around one of the bolts and were then passed through the bottom hole. This procedure continued until approximately 0.3m (1-ft.) of the stitch was left. This 0.3m (1-ft.) section was then tightly wrapped around the stitching on the stiffener side as shown in Figure G 2, the thin piece of metal which can be seen sticking out of the stitch is the clothes hanger. This processed was repeated for the other side of the cross frame until there were two separate stitches on either side of the angle on the cross frame. The stitching on the fascia side of the girder was then tied together with a small piece of Aramid Yarn. The remaining epoxy which was mixed earlier was then coated on the exposed stitches.

The entire process took under three hours. It took approximately two hours to drill, clean and install screws in their respective holes. Drilling through the composite block was surprisingly very easy. However, the drill bit became dull after the four holes were drilled. The stitching process was done very quickly after the idea of using the 12k Carbon Fiber was disregarded.

Figure G 2: Kevlar stitching retrofit north stiffener side

Figure G 3: Kevlar stitching retrofit south stiffener side

Appendix H: Rotation on Fascia Side of Girder

A simple, cost effective and accurate way to measure specimen rotation at a given location is through the use of an array of mirrors and a laser. This is done by reflecting a laser off of a rotating object and measuring the displacement of the laser in both the horizontal and vertical direction. The displacement of the laser is then used to calculate the rotation of the object. This procedure was performed on the 2.82-meter (9.25-ft.) subassembly tested in the Fracture and Fatigue lab in M2SEC to accurately observe how the stiffness of the specimen changed when any variable on the specimen was altered.

Before specimen rotation could be accurately recorded, the design and construction of a mirror array system was performed. Figure 9-1 shows the location of every mirror (shown as blue squares) placed on the fascia side of the girder subassembly. The mirror array was only placed on the north half of the girder since the girder was symmetric about the connection stiffener. The connection stiffener was located at the center of the girder. Since the retrofits were placed on the connection stiffener, the region behind the connection stiffener on the fascia side of the girder was the region of interest. To save time, mirrors were placed in a tight 76-mm (3-in.) by 76-mm (3-in.) grid at the region of interest and further away from the region of interest the mirrors were not spaced as closely together.

Rotation at every mirror location was found using the following procedure:

1. The MTS Actuator was commanded to cycle at 0.25Hz at the load range which was being tested.
2. A Pittsburgh 16” Laser Level with Swivel Head was oriented so its laser would reflect off of one of the mirrors on the specimen to a grid of 6-mm (¼-in.) by 6-mm (¼-in) squares located on the opposite wall.
3. The displacement of the laser was recorded to a 3-mm (1/8-in.) tolerance in both the horizontal and vertical direction. If the laser was moving in the upward vertical direction as the actuator was moving in the upward direction the vertical change in distance was recorded as being positive.
4. The horizontal and vertical displacement of the laser was recorded into a premade Microsoft Excel sheet. This sheet converted the recorded change in displacement to a rotation utilizing Equation H 1. The difference in the two equations is due to the different distances from the flange and web of the girder subassembly to the opposite wall where the laser was reflected onto

$$\text{Flange Mirror} = \frac{\operatorname{atan}\left(\frac{x}{407\text{in}}\right)}{2} = \qquad \text{Web Mirror} = \frac{\operatorname{atan}\left(\frac{x}{402\text{in}}\right)}{2} =$$

Equation H 1: Calculate angular rotation from flange or web mirror

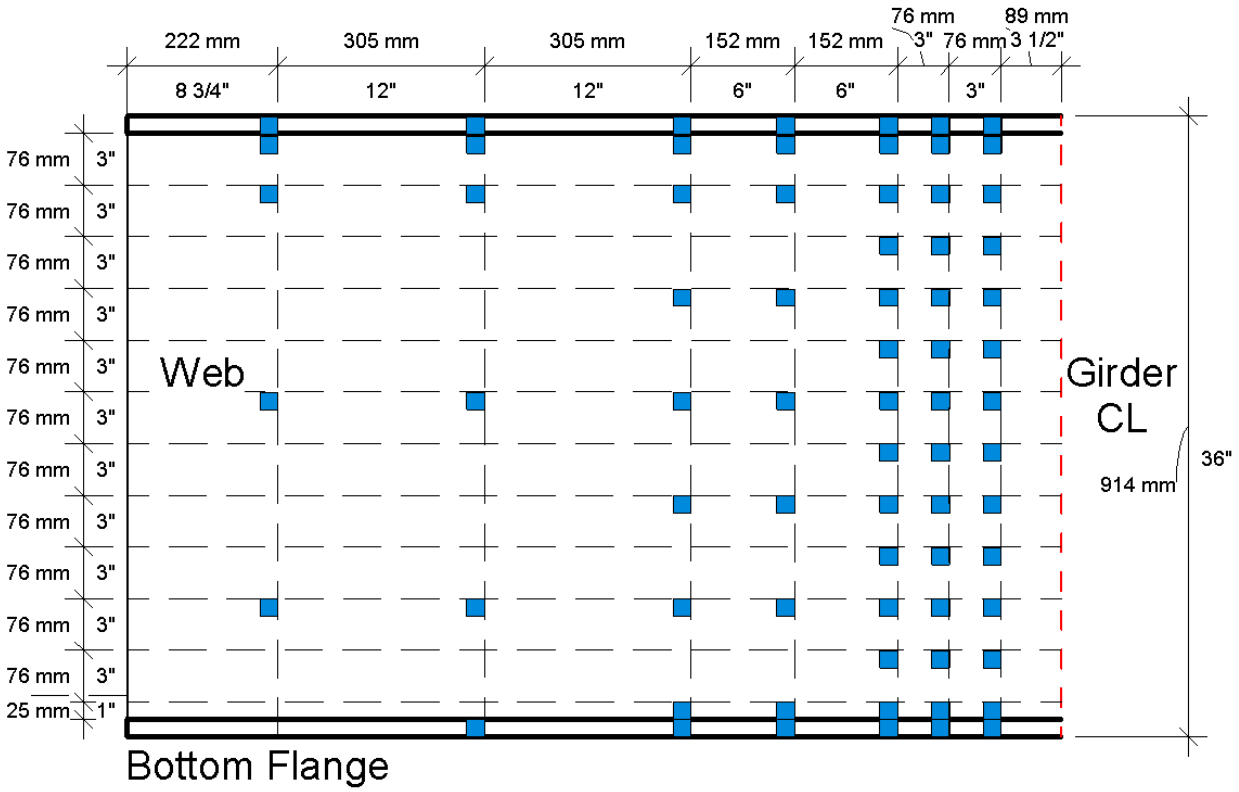

Figure H 1: Location of mirrors on fascia side of girder subassembly

Figure H 2: Assembled mirror array

The entire process of calculating the angular rotation from the mirror array took between two and three hours. Once all the data was recorded, PTC's MathCAD version 15 was utilized in order to create surface contour plots which made it easy to visualize the data recorded from the mirror array.

Figure H 4-10 show the seven different times that data from the mirror array was recorded for rotation about the girders X-axis. The figure on the left shows an elevation view of the north half of the girder subassembly and the figure on the right shows a section cut of the rotation at the girders center line, behind the connection stiffener. The contours are based off the maximum and minimum angular rotation from all seven different plots. It can be easily seen how successful the block was in stiffening the lower web-gap region by viewing the Pre and Post Retrofit figures. These figures were made utilizing excel to record the laser displacement and convert that displacement into rotation. The rotational data was then imported into Mathcad version 15, where it was made into a 3D surface plot, these plots were then exported to Autodesk Revit 2014 where they were applied over line drawings of the north half of the girder subassembly.

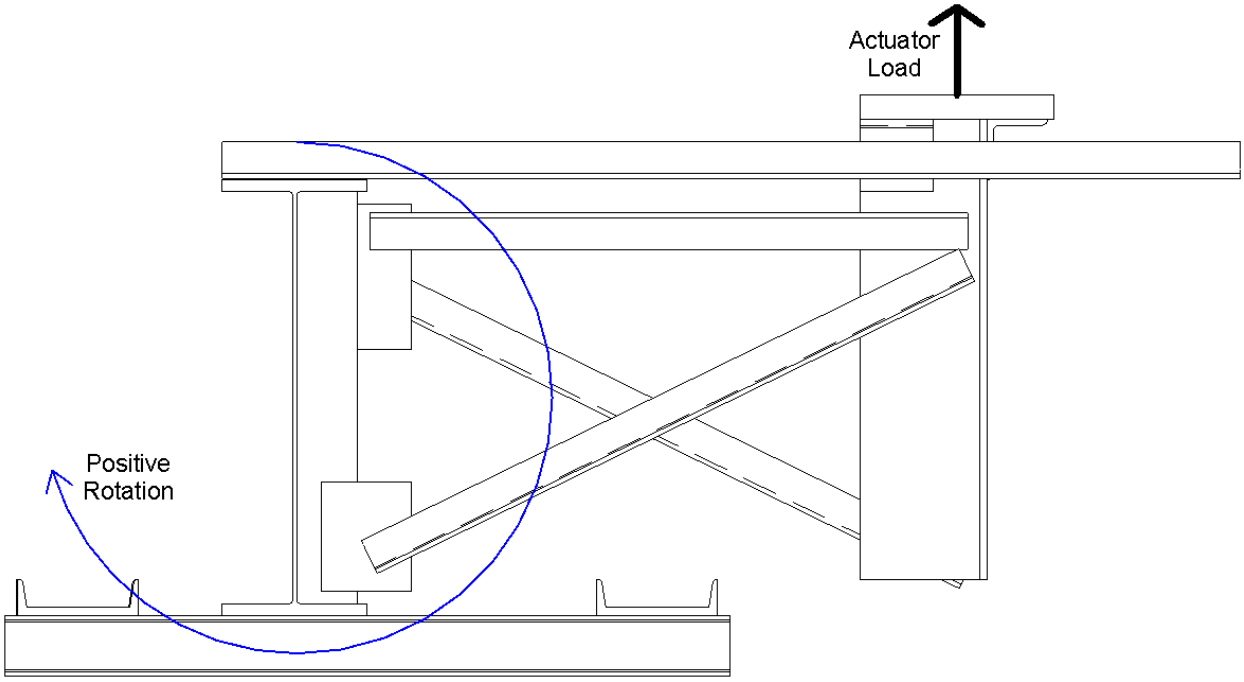

Figure H 3: Direction of rotation about the girders X-axis

X-axis rotation contours

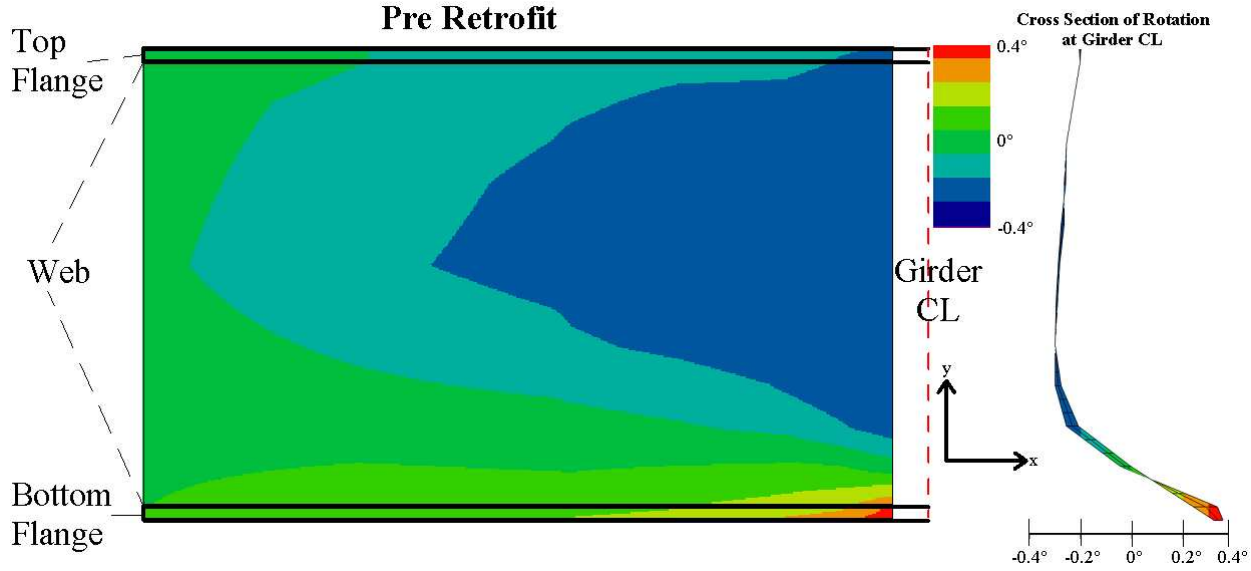

Figure H 4: X-axis rotation contours, pre retrofit

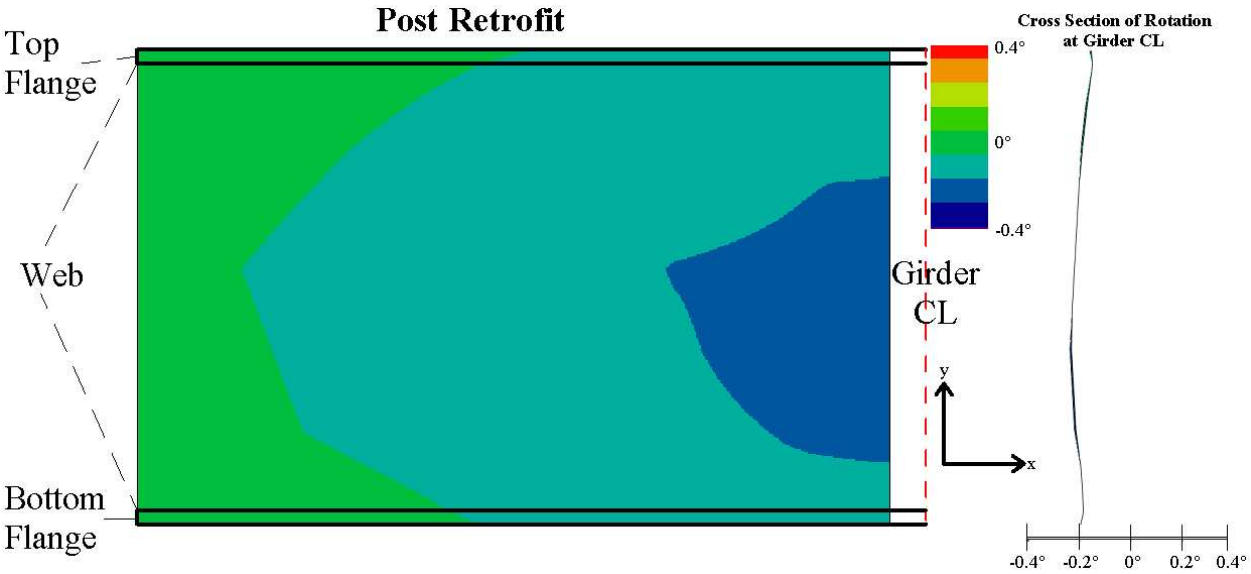

Figure H 5: X-axis rotation contours, after the composite block retrofit was installed in the lower web-gap region

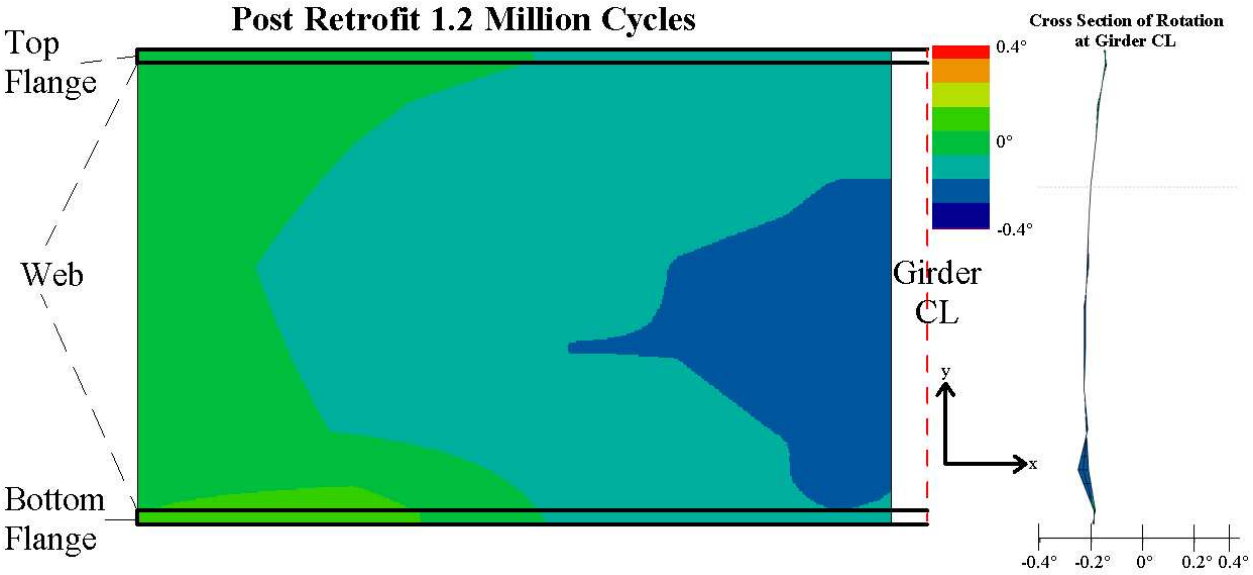

Figure H 6: X-axis rotation contours, post retrofit 1.2 million total cycles

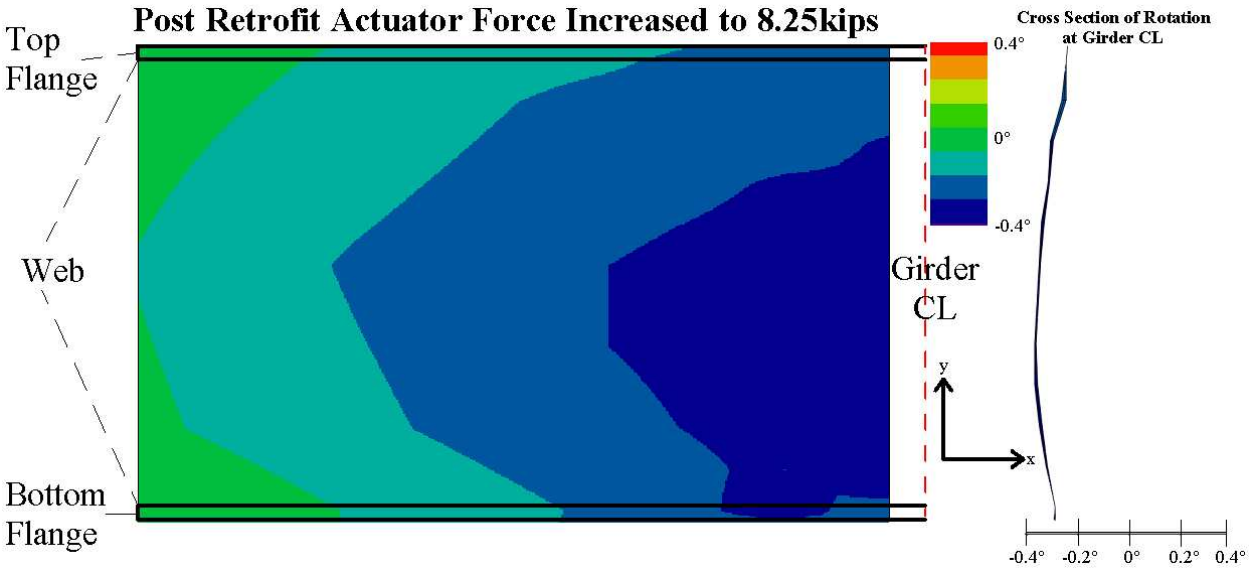

Figure H 7: X-axis rotation contours, post retrofit 1.2 million total cycles actuator force increased by 50%

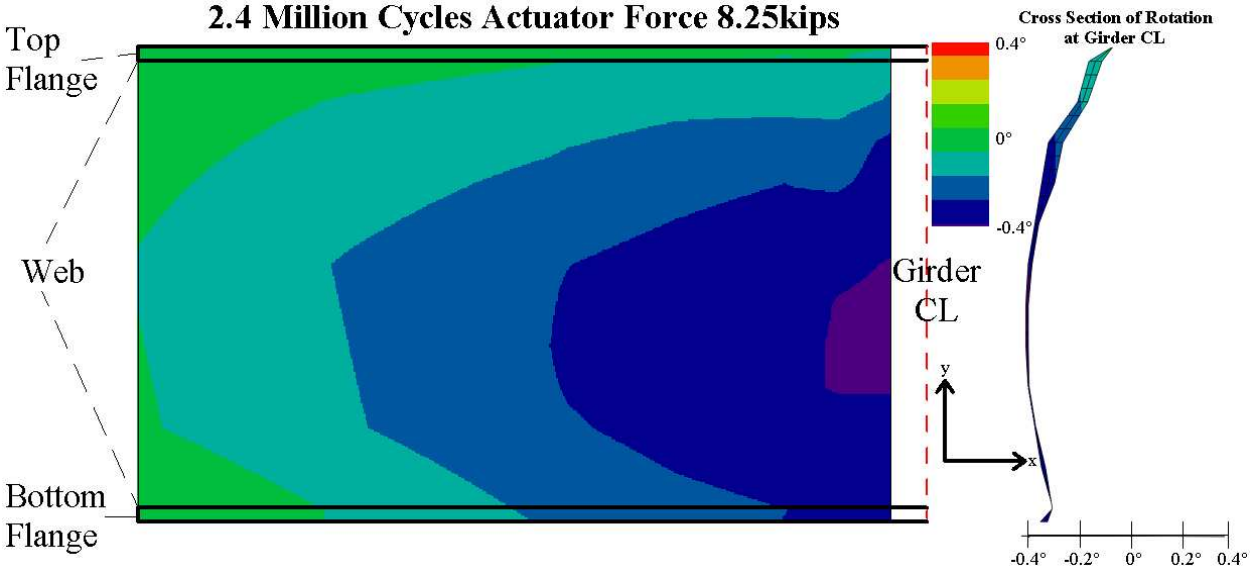

Figure H 8: X-axis rotation contours, post retrofit 2.4 million total cycles actuator force increased by 50%

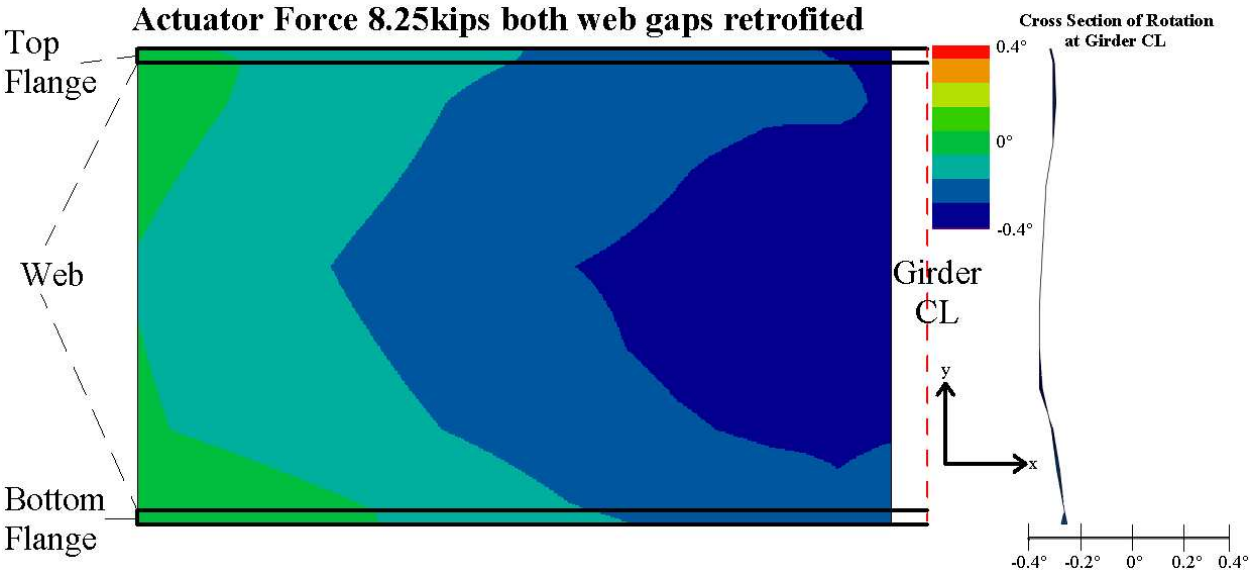

Figure H 9: X-axis rotation contours, 2.4 million total cycles, upper web-gap region retrofitted

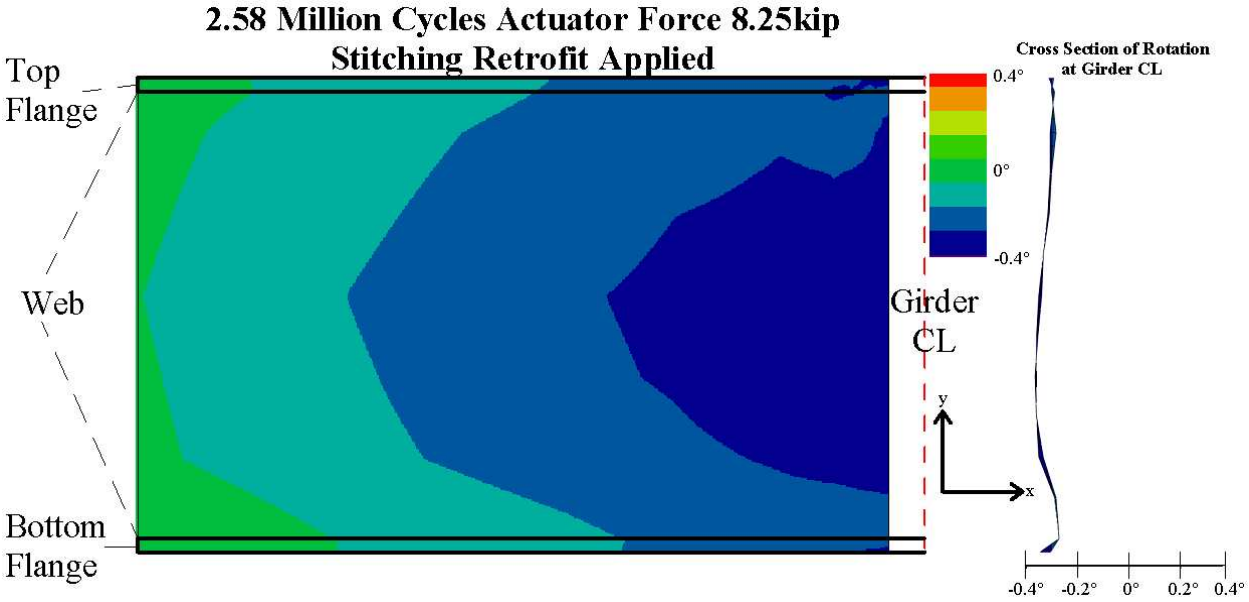

Figure H 10: X-axis rotation contours, post retrofit 2.58 million total cycles stitching retrofit applied

Figure H 12-18 show the seven different times that data from the mirror array was recorded for rotation about the girders Y-axis. The process to create the contour plots for Y-axis rotation was exactly the same as the process to create the contour plots for X-axis rotation.

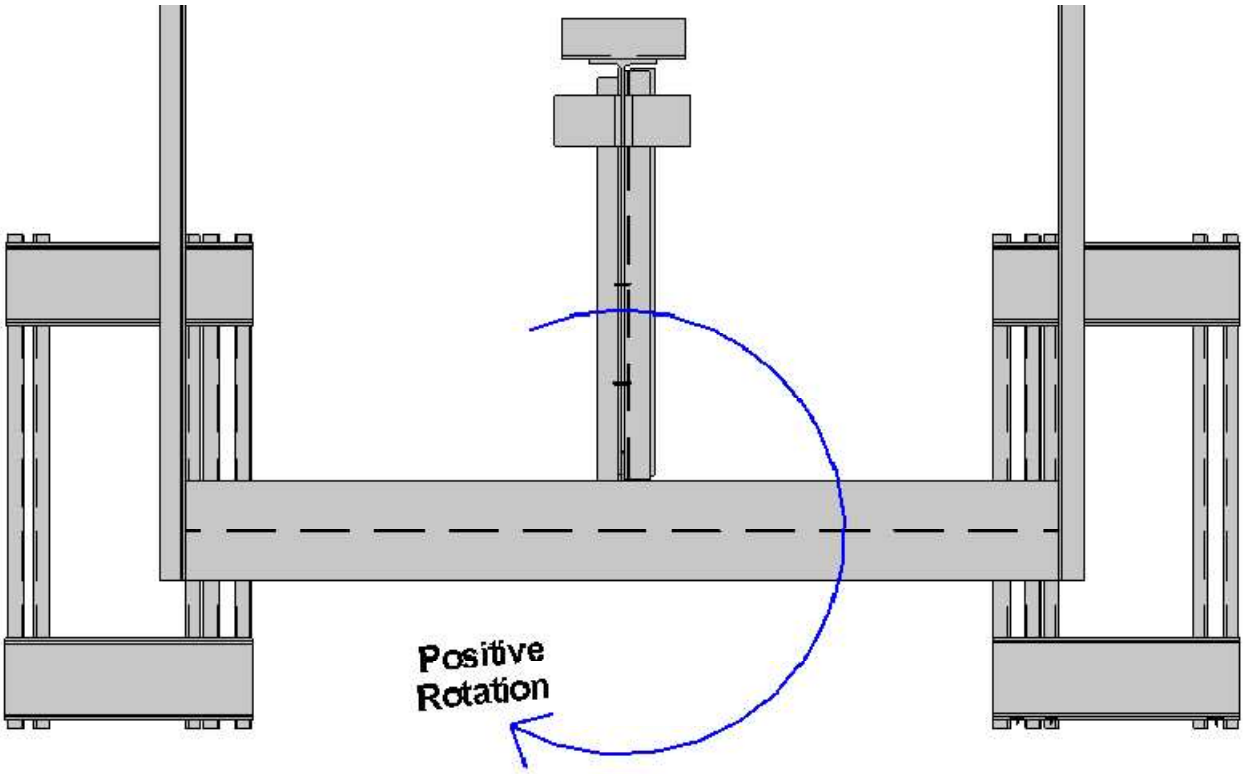

Figure H 11: Direction of rotation about the girders Y-axis

Y-axis rotation contours

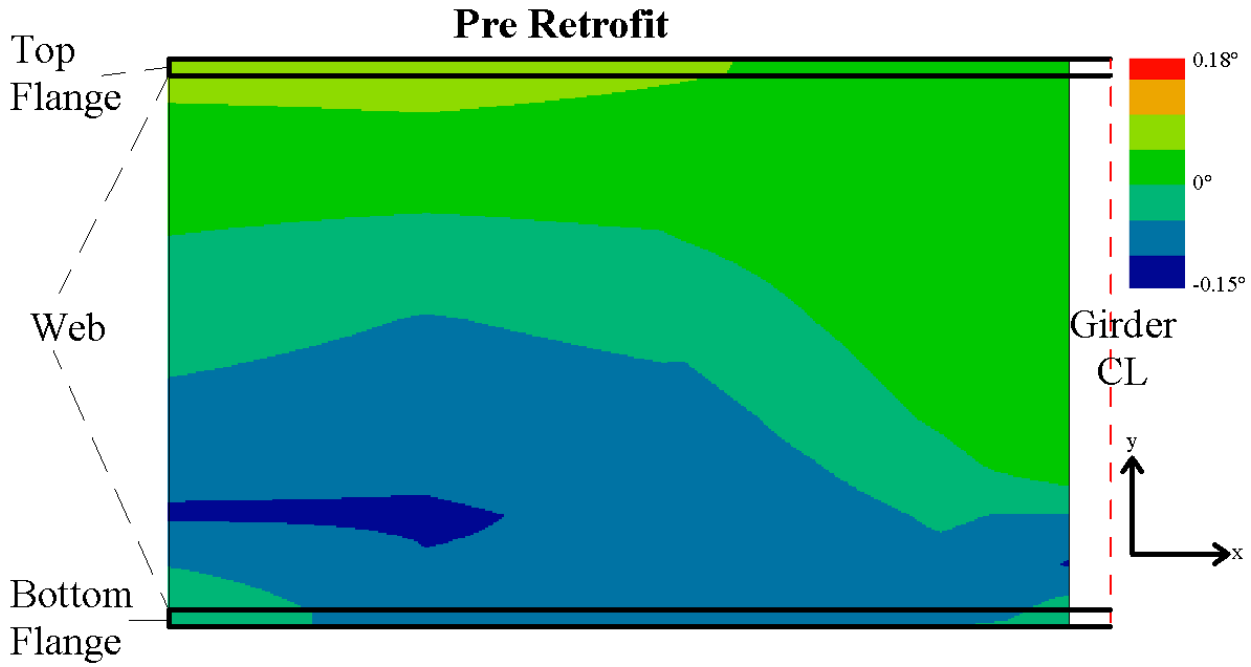

Figure H 12: Y-axis rotation contours, pre retrofit

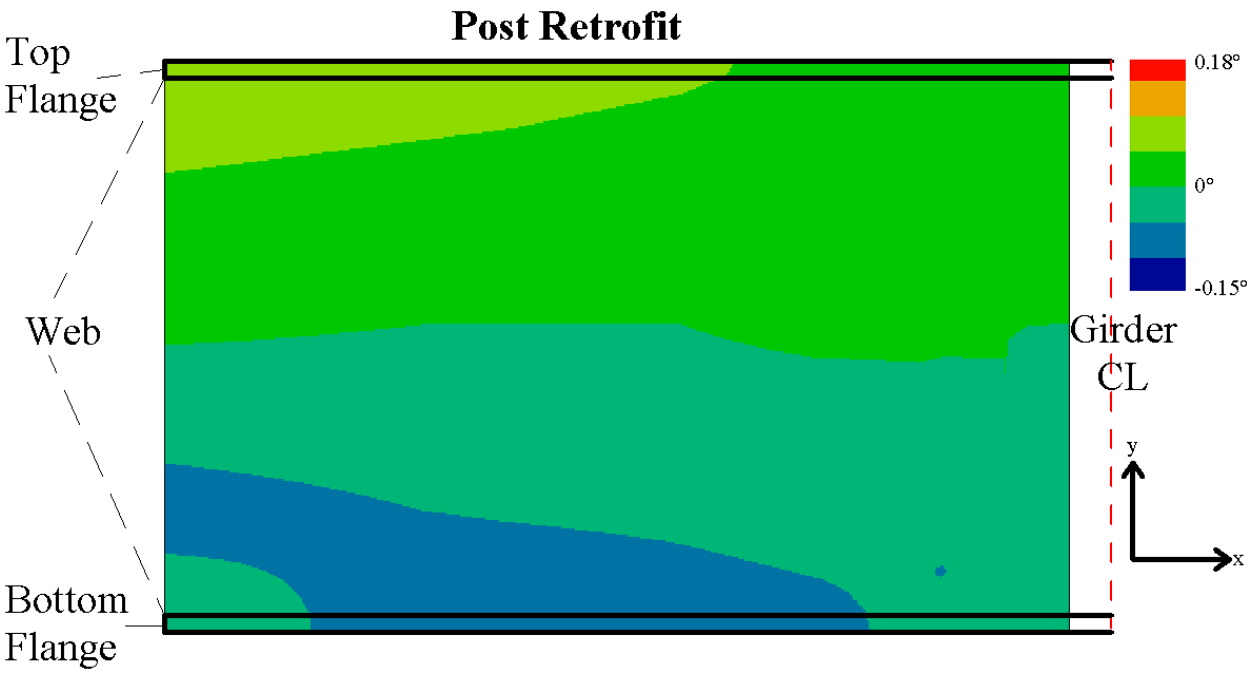

Figure H 13: Y-axis rotation contours, after the composite block retrofit was installed in the lower web-gap region

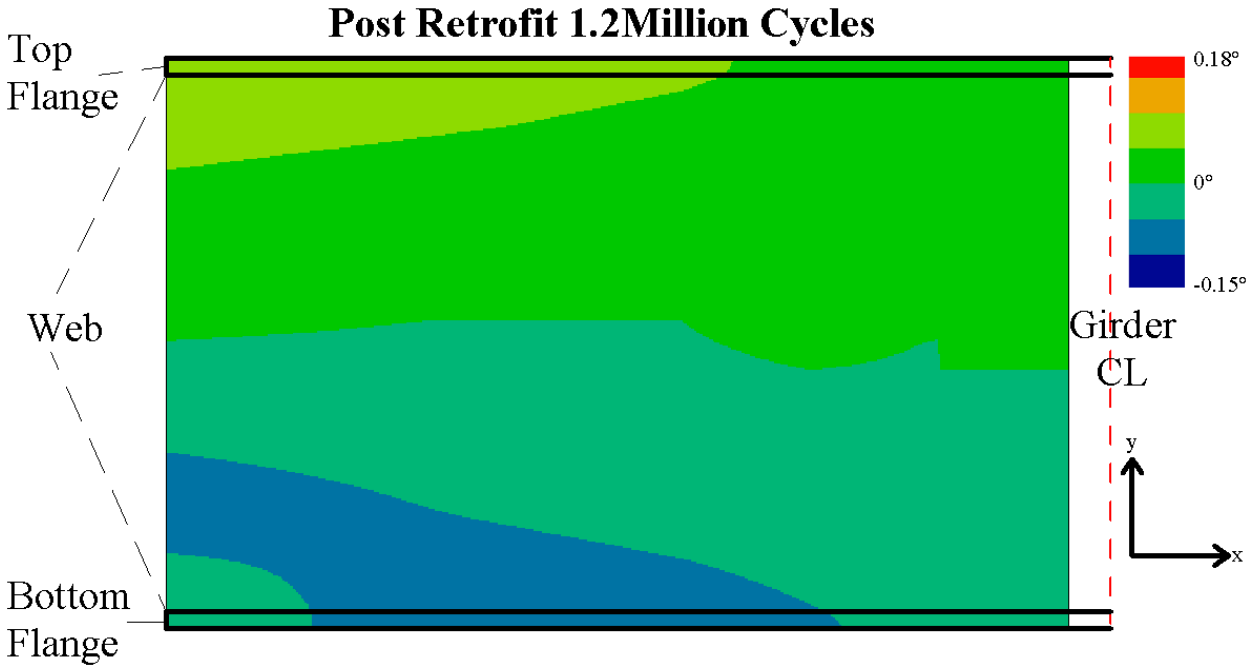

Figure H 14: Y-axis rotation contours, post retrofit 1.2 million total cycles

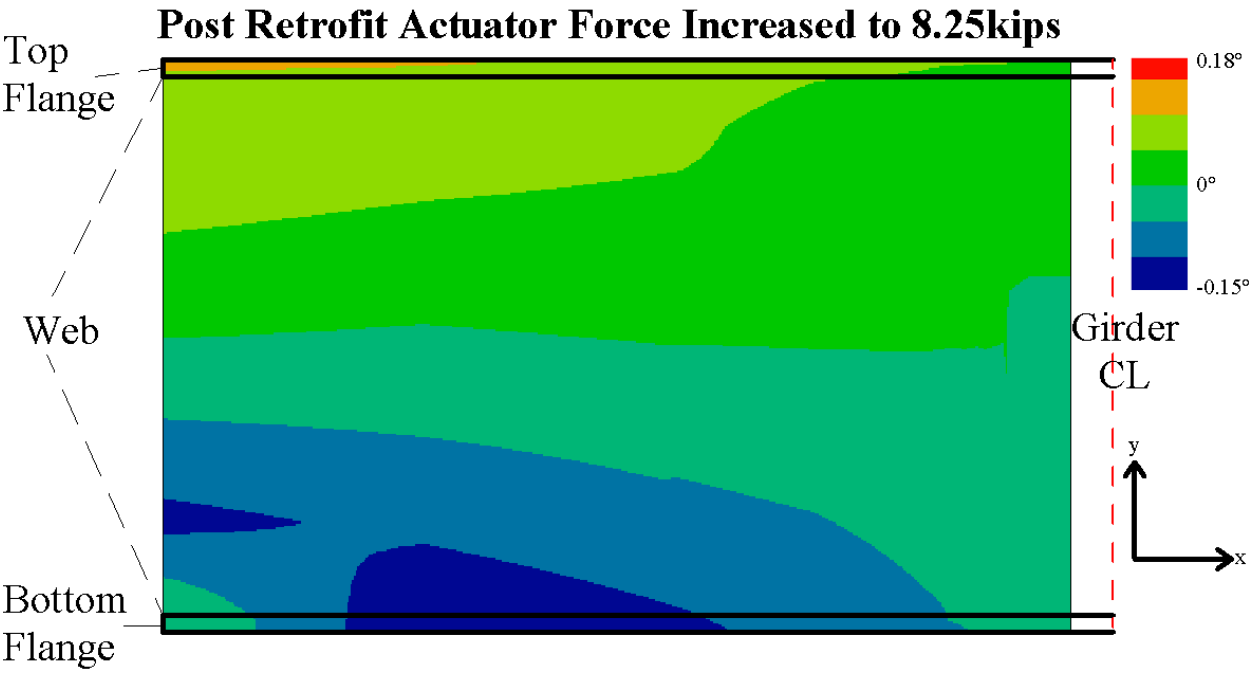

Figure H 15: Y-axis rotation contours, post retrofit 1.2 million total cycles actuator force increased by 50%

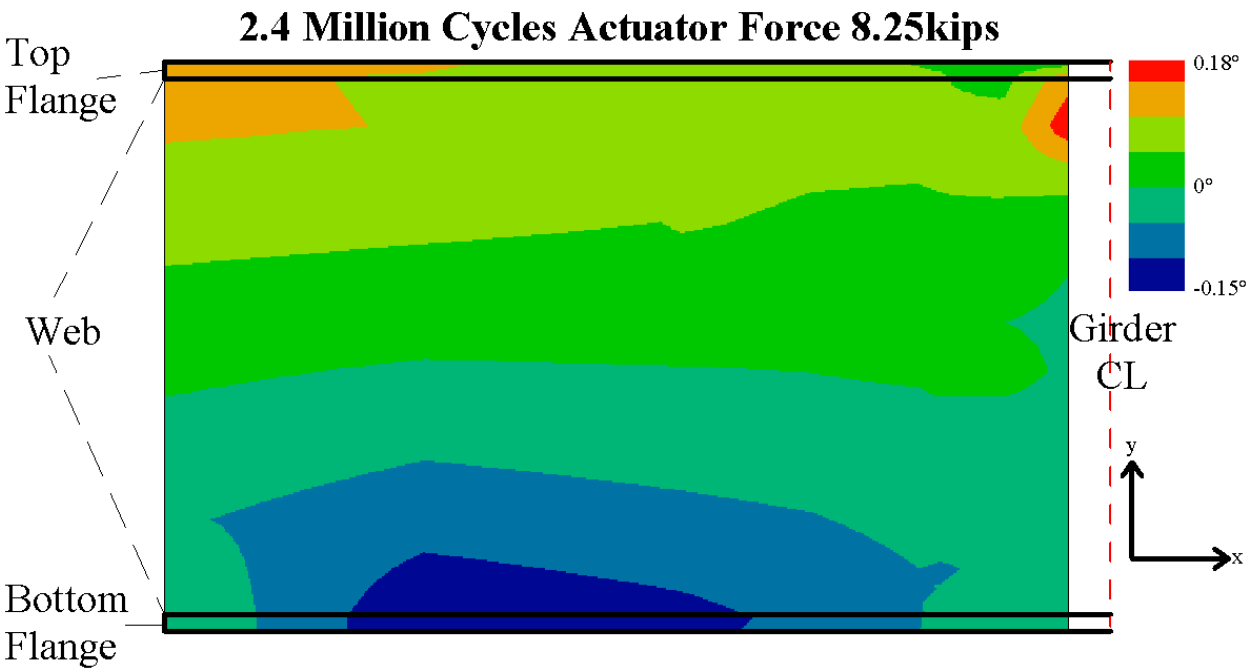

Figure H 16: Y-axis rotation contours, post retrofit 2.4 million total cycles actuator force increased by 50%

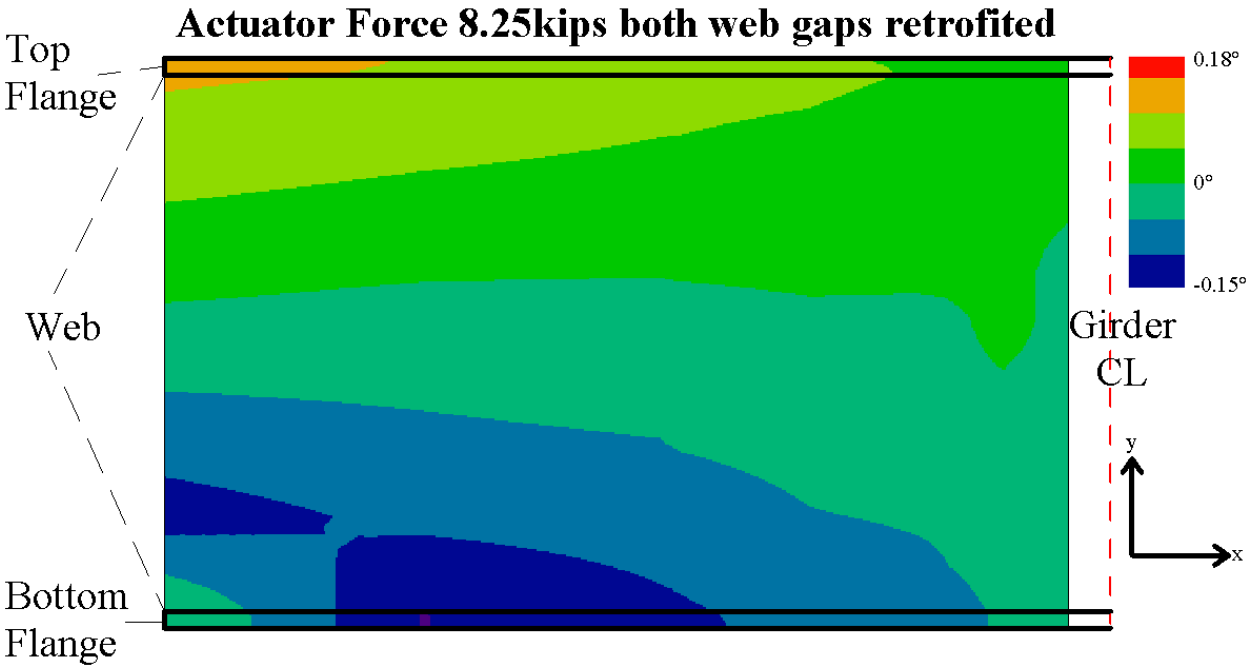

Figure H 17: Y-axis rotation contours, 2.4 million total cycles, upper web-gap region retrofitted

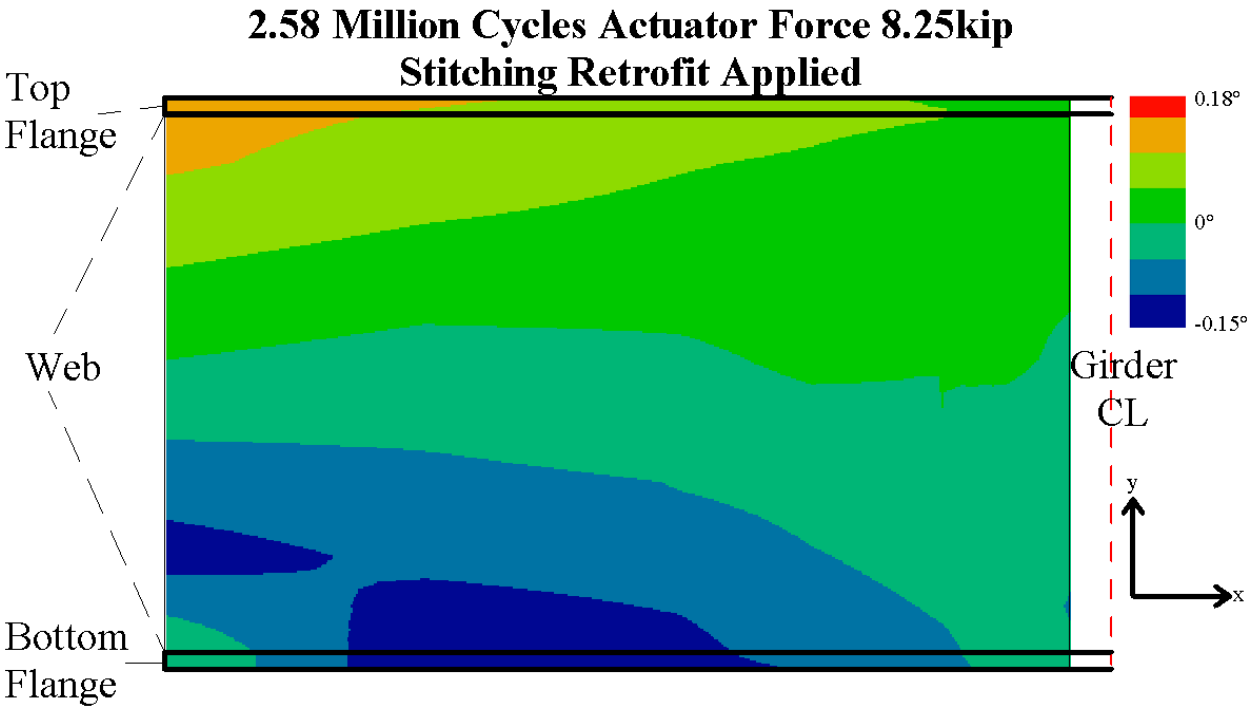

Figure H 18: Y-axis rotation contours, post retrofit 2.58 million total cycles stitching retrofit applied

Appendix I: Relative Stresses on Fascia Side of Girder Subassembly

Utilizing angular rotation data, the change in stress between mirrors can be calculated. Figure I 1 shows the array of mirrors on the north half of the fascia side of the girder subassembly. Each mirror was assigned an X and Y coordinate and the change in vertical and horizontal distance between mirrors is referred to as ΔY and ΔX respectively.

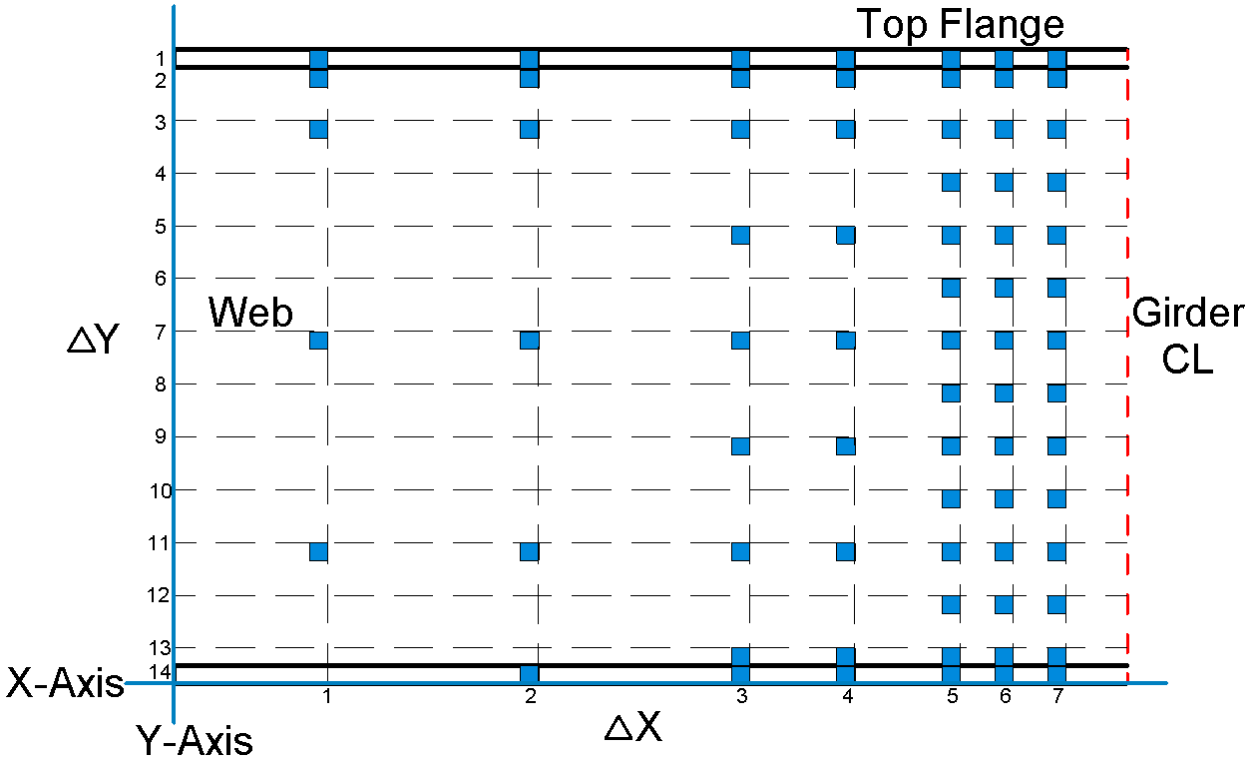

Figure I 1: Mirror array numbering

The equations on the following pages show how change in vertical stress between mirrors was calculated based off of X-axis rotation and change in vertical distance between mirrors. The same equations were used to calculate change in horizontal stress between mirrors. However in those equations X-axis rotation was substituted with Y-axis rotation and change in vertical distance between mirrors was substituted with change in horizontal distance between mirrors. It is important to note that change in vertical stresses between mirrors were not calculated on either of the flanges.

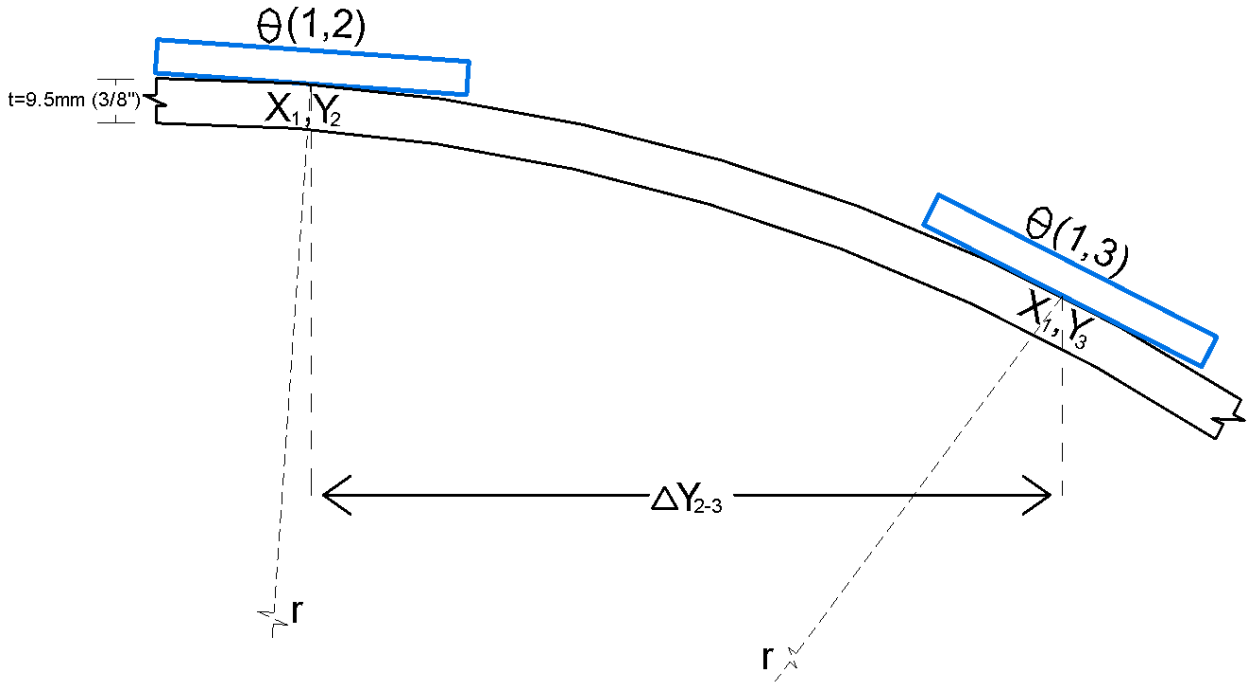

Figure I 2: Distance between mirrors

$$\alpha_{1,2-3} = \theta_{1,2} - \theta_{1,3}$$ Equation I 1: Solve for change in rotation between two mirrors

$$k = \frac{\alpha}{\Delta y}$$ Equation I 2: Solve for curvature between two mirrors

$$r = \frac{1}{k}$$ Equation I 3: Solve for radius

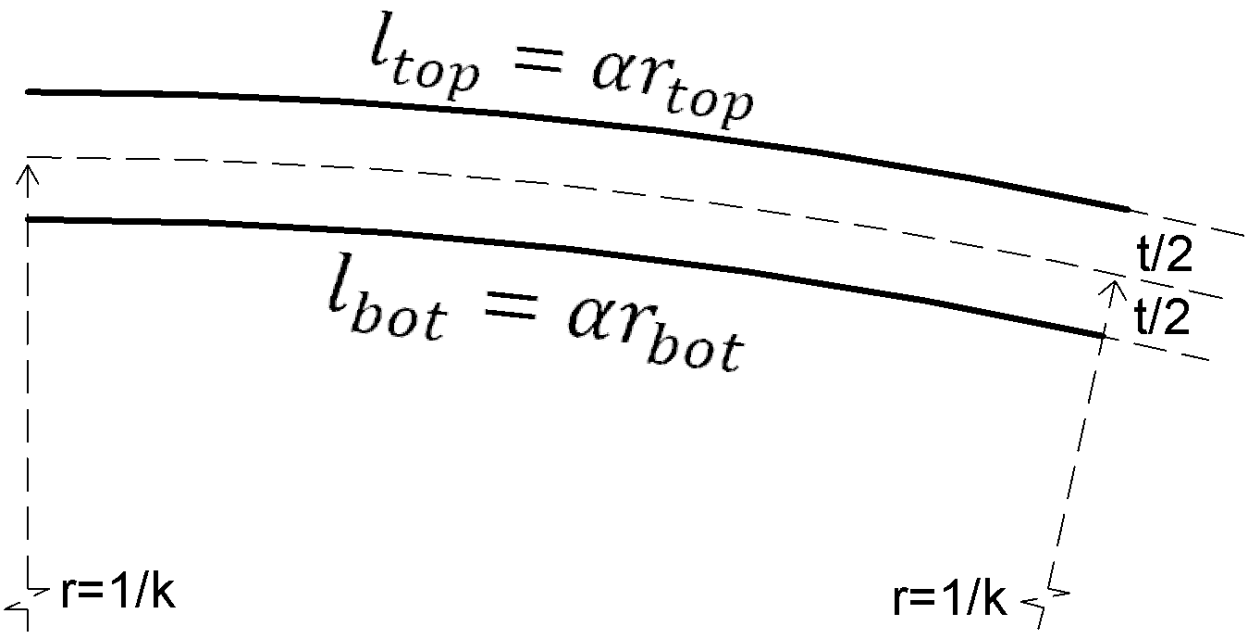

Figure I 3: Radius of curved specimen

$$\Delta\epsilon = \frac{l_{top} - l}{l}$$

Equation I 4: Solving for change in strain on fascia side of specimen

$$\Delta\epsilon = \frac{\left(r + \frac{t}{2}\right)\alpha - r\alpha}{r\alpha}$$

$$\Delta\epsilon = \frac{r + \frac{t}{2} - r}{r}$$

$$\Delta\epsilon = \frac{t}{2r}$$

$$\Delta\sigma = \Delta\varepsilon * E_{steel}$$

Equation I 5: Convert stress from strain

Vertical change in stress between mirrors

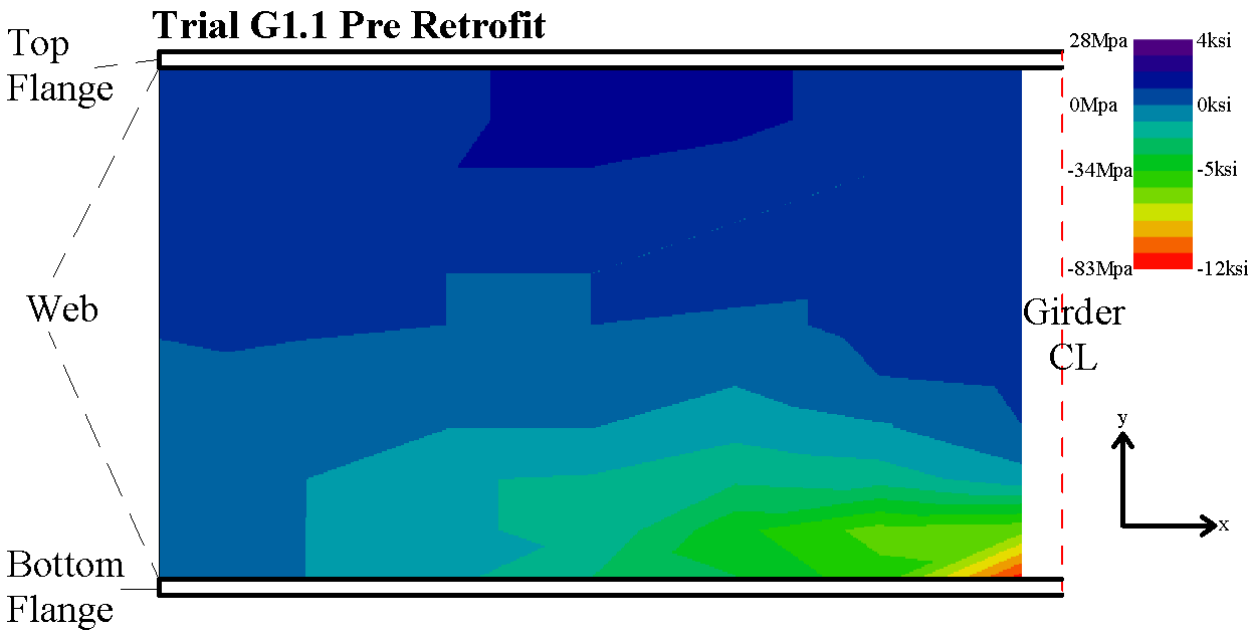

Figure I 4: Change in vertical stress contours, pre retrofit

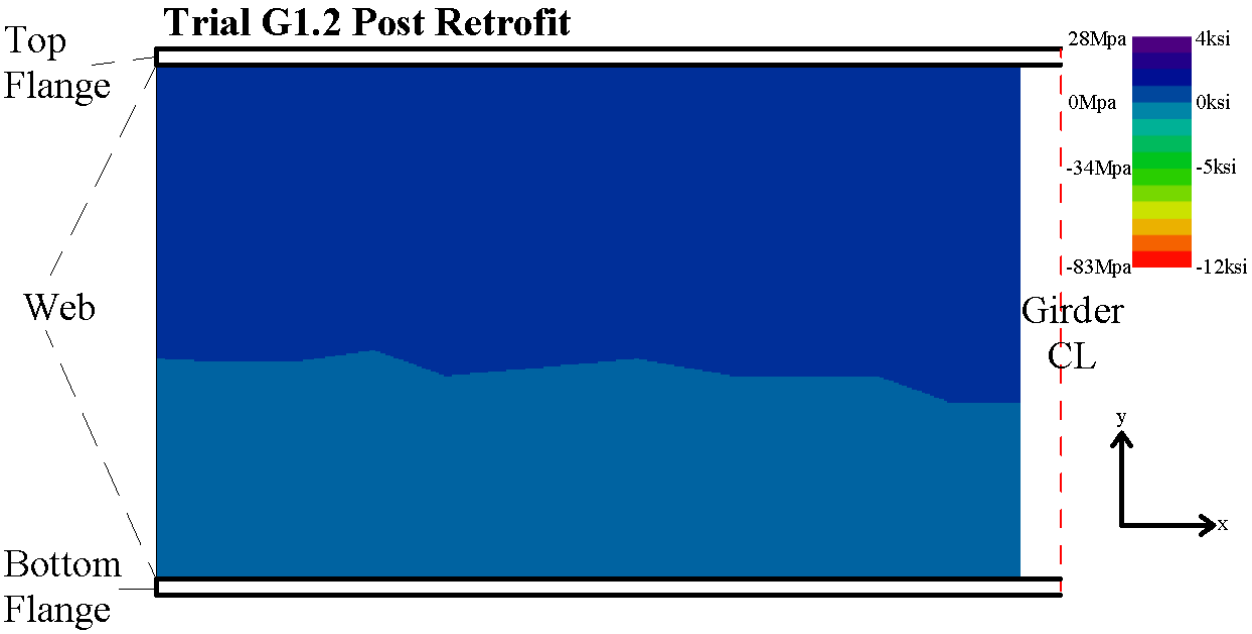

Figure I 5: Change in vertical stress contours, Post retrofit

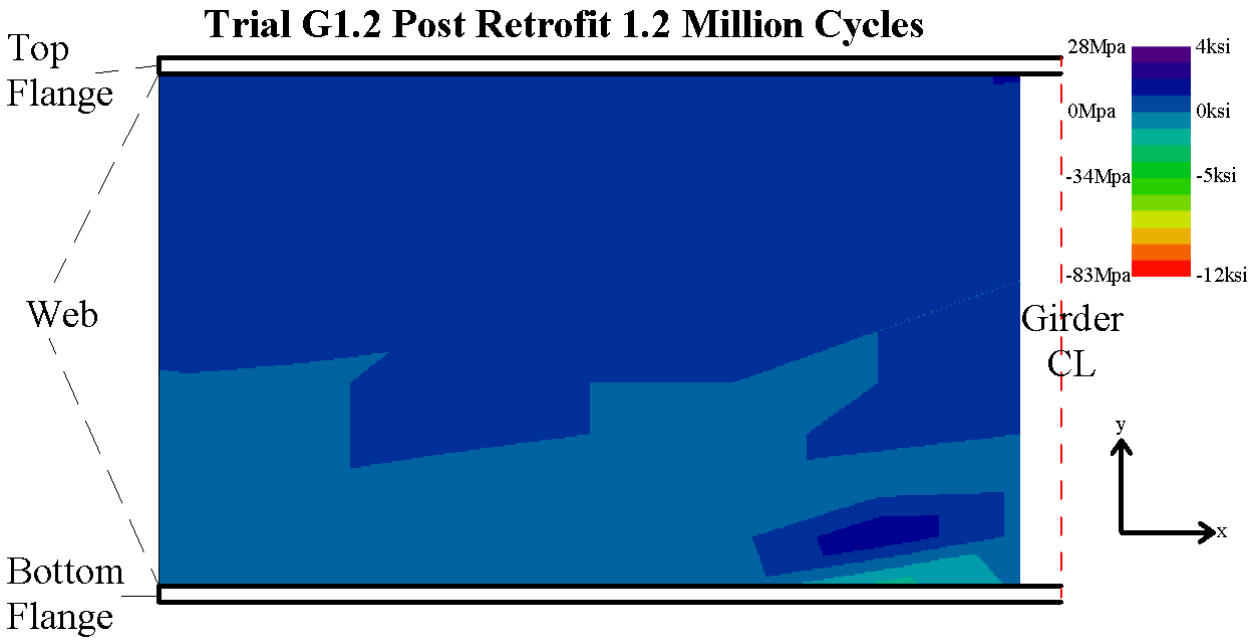

Figure I 6: Change in vertical stress contours, Post Retrofit 1.2 Million Cycles

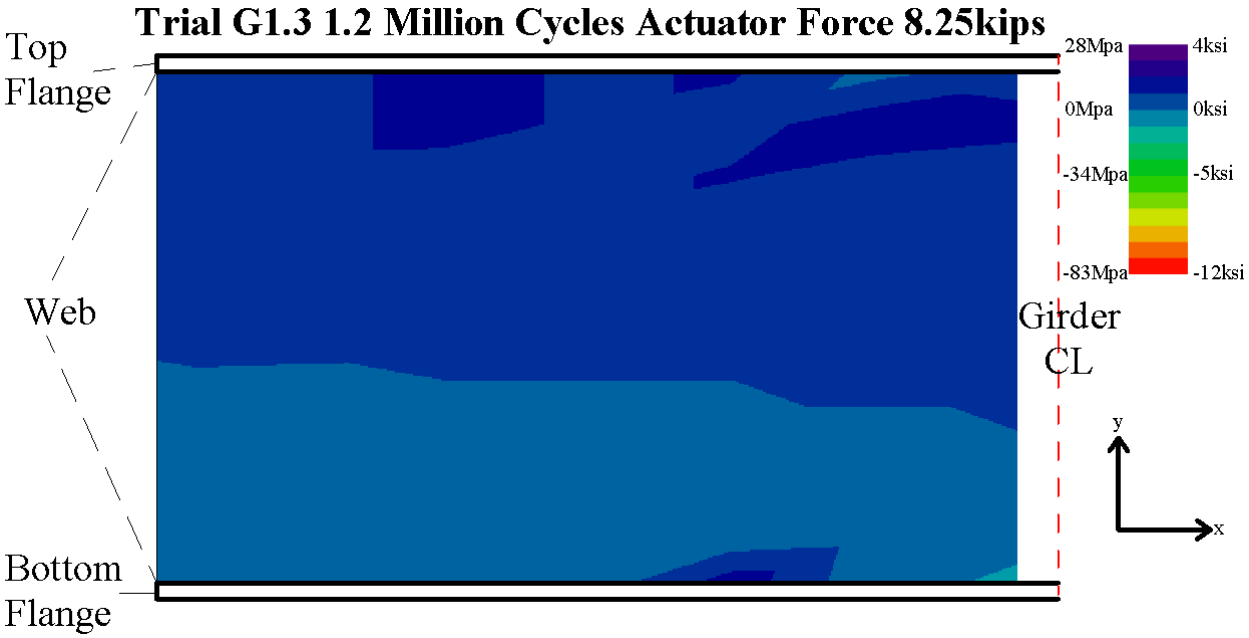

Figure I 7: Change in vertical stress contours, 1.2 million cycle's actuator force increased to 8.25 kips

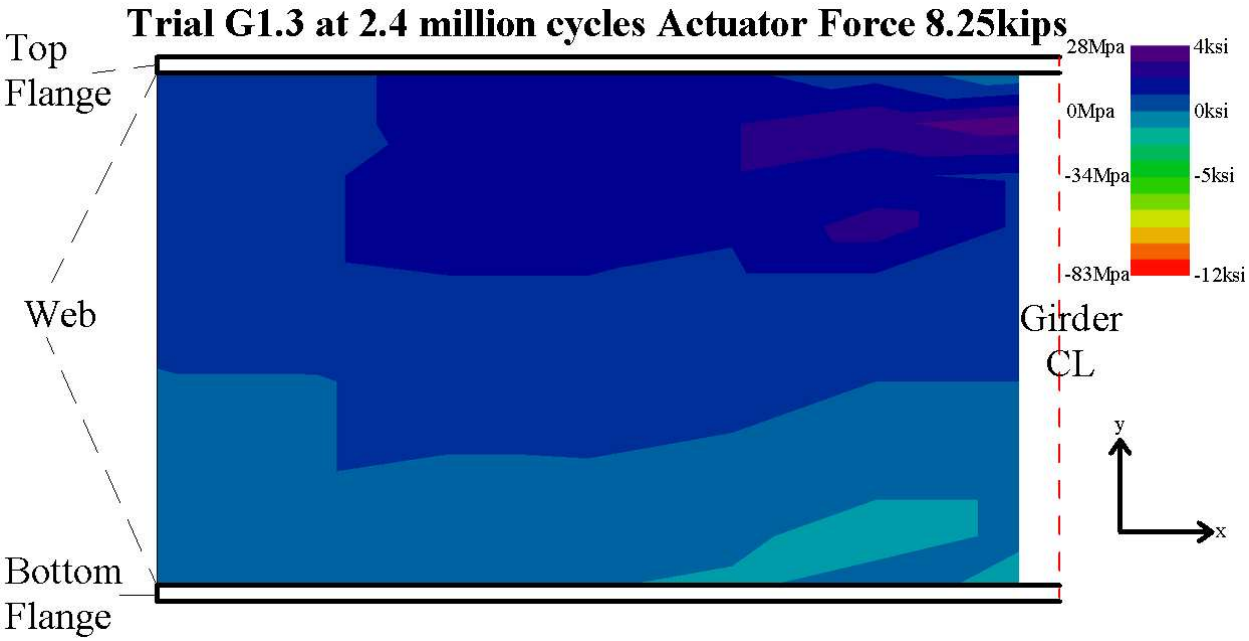

Figure I 8: Change in vertical stress contours, 2.4 million cycles actuator force 8.25 kips

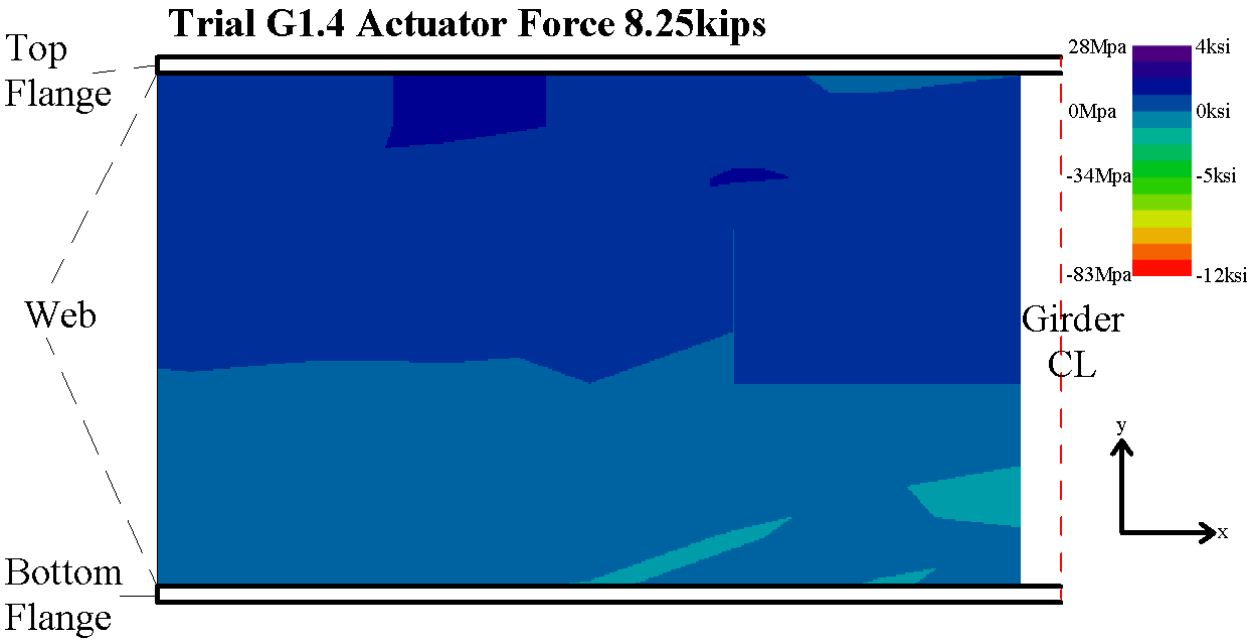

Figure I 9: Change in vertical stress contours, upper web-gap retrofitted

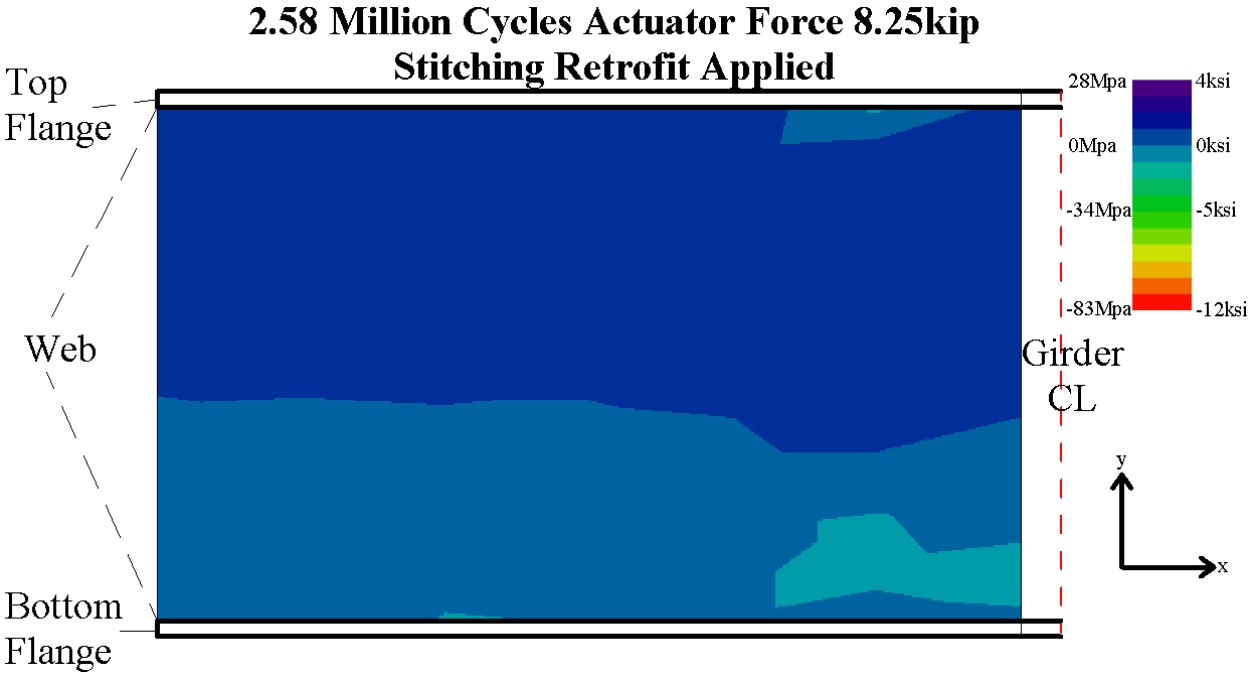

Figure I 10: Change in vertical stress contours, 2.58 million cycles stitching retrofit applied

Horizontal Change in stress between mirrors

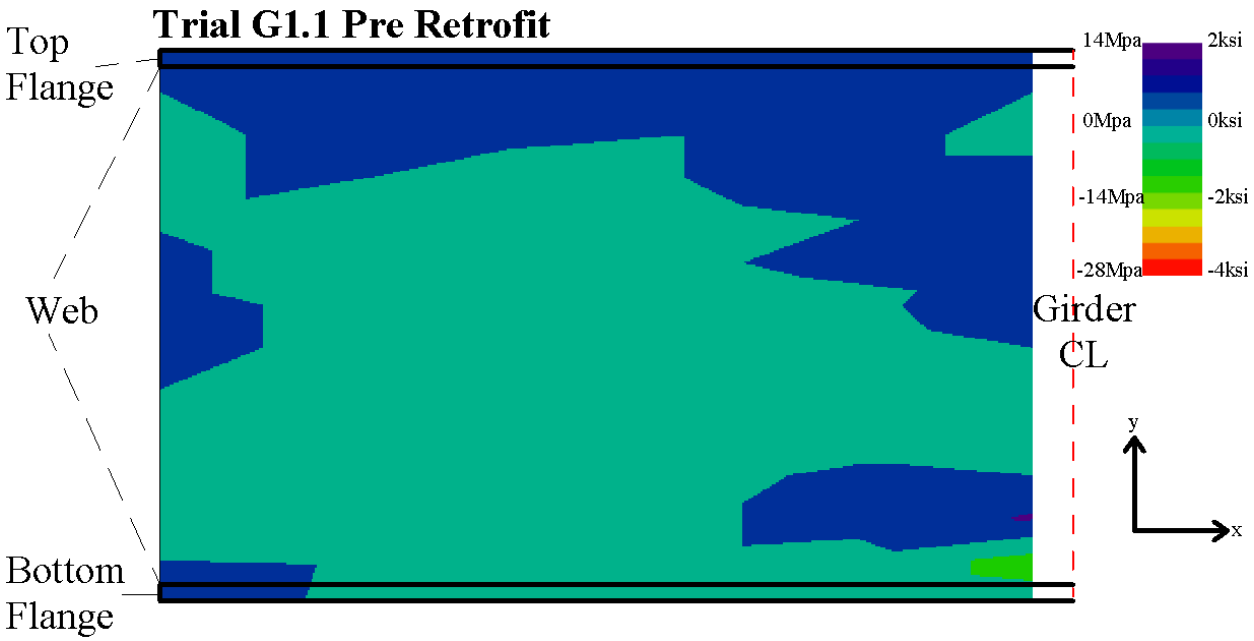

Figure I 11: Change in horizontal stress contours, pre retrofit

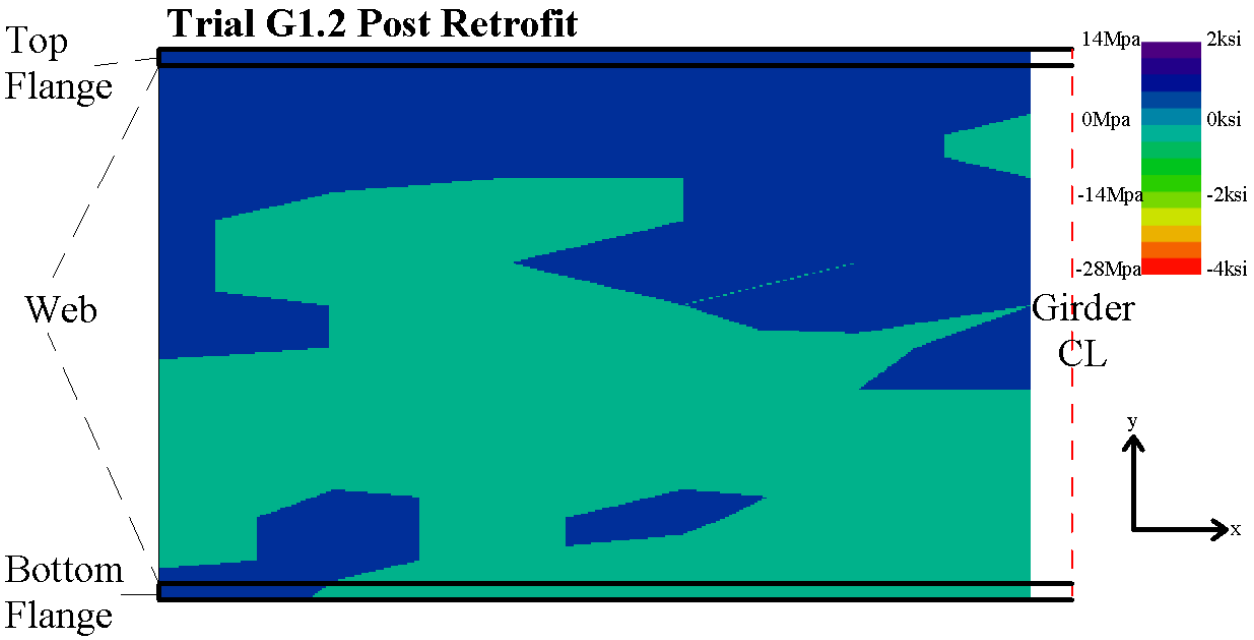

Figure I 12: Change in horizontal stress contours, post retrofit

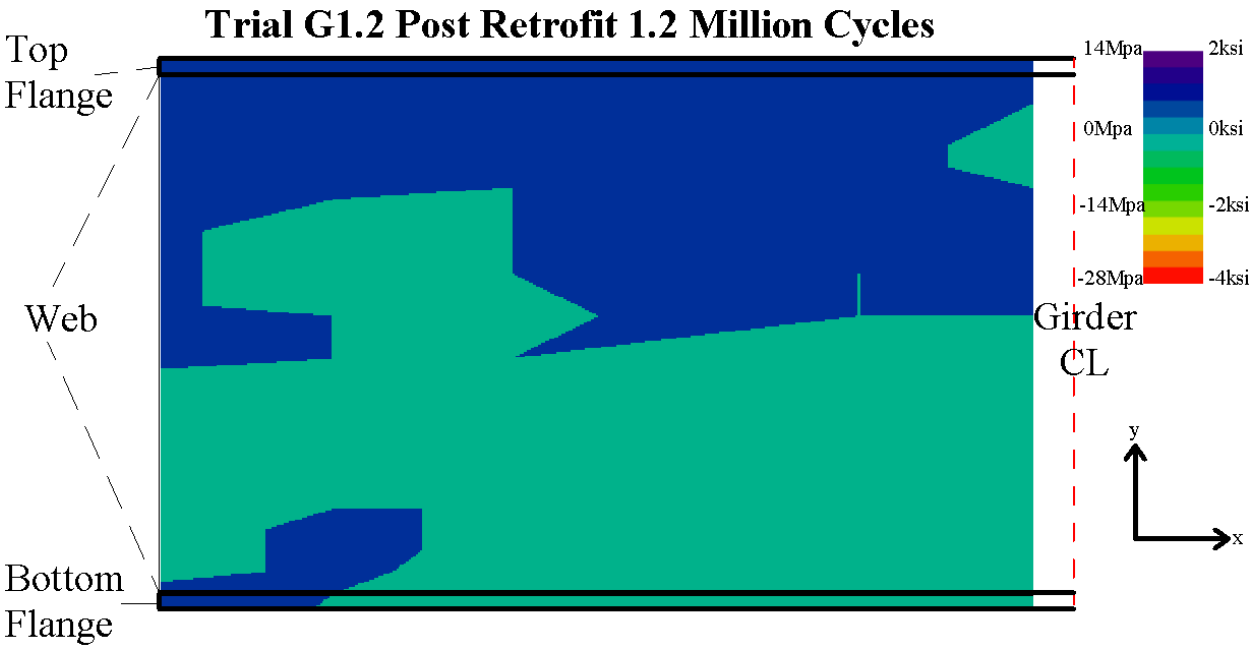

Figure I 13: Change in horizontal stress contours, post retrofit 1.2 million cycles

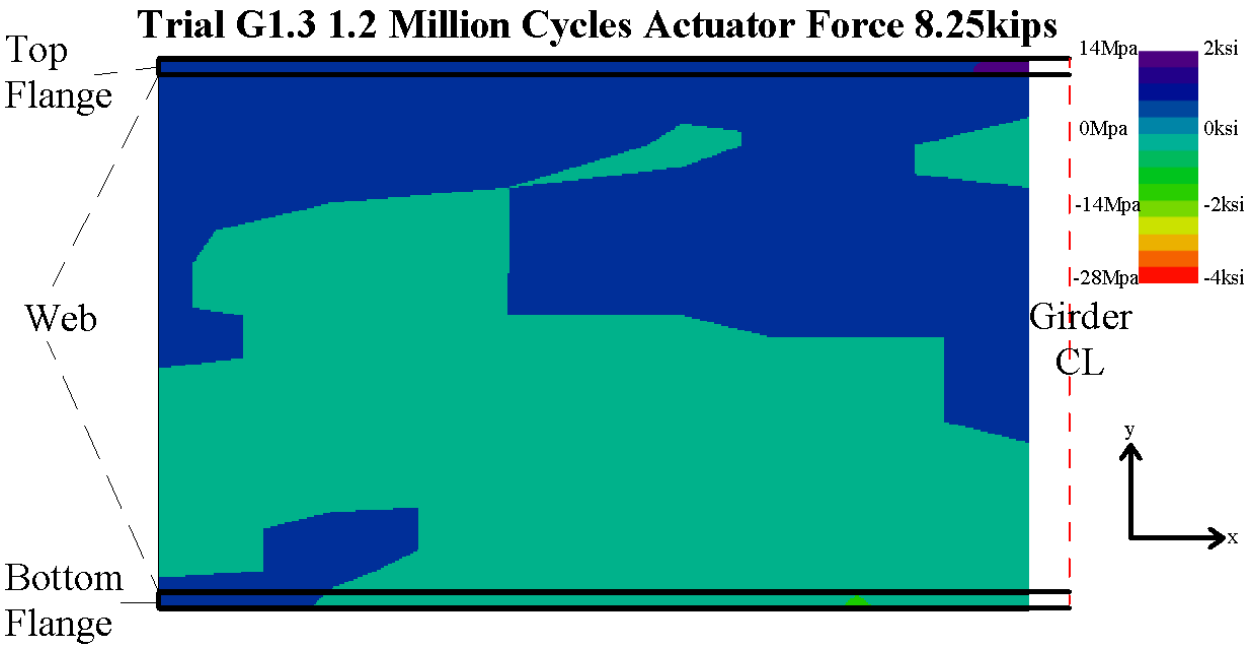

Figure I 14: Change in horizontal stress contours, 1.2 million cycle's actuator force increased to 8.25 kips

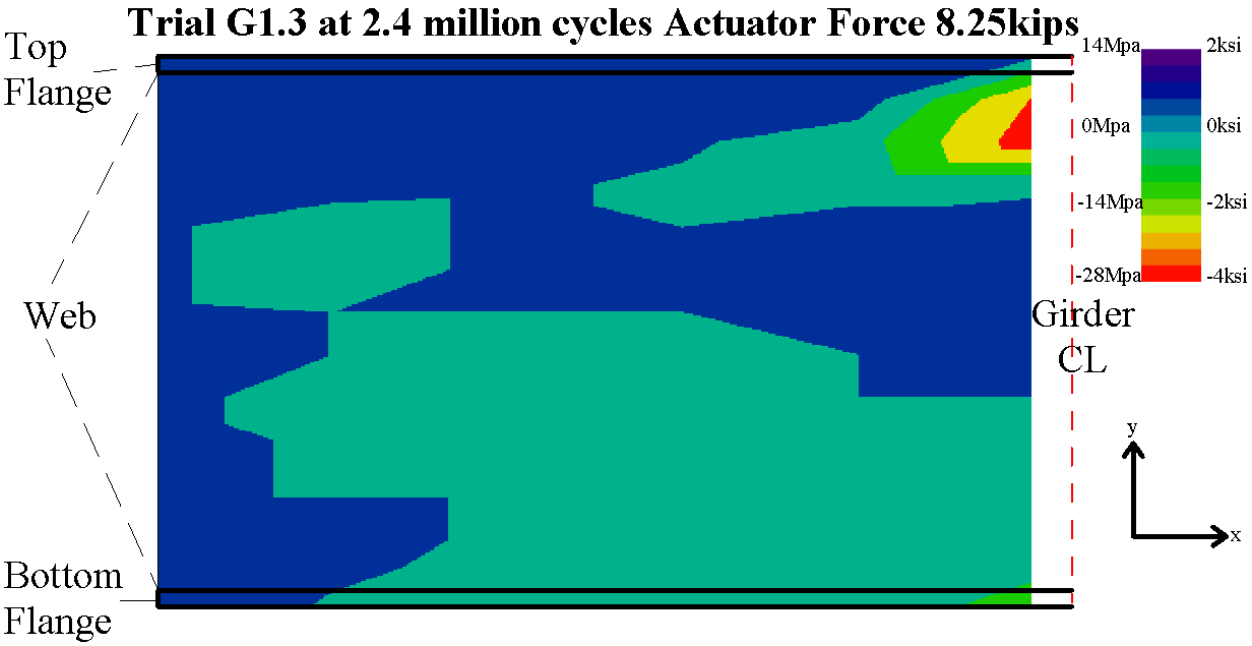

Figure I 15: Change in horizontal stress contours, 2.4 million cycles actuator force 8.25 kips

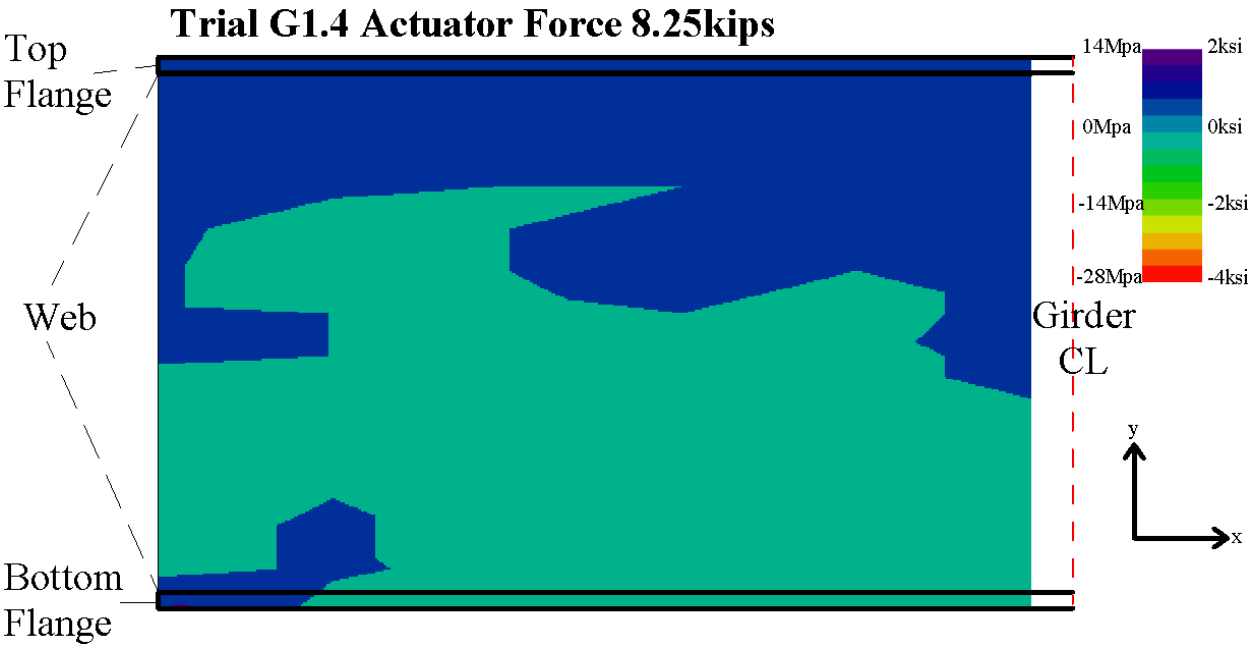

Figure I 16: Change in horizontal stress contours, upper web-gap retrofitted

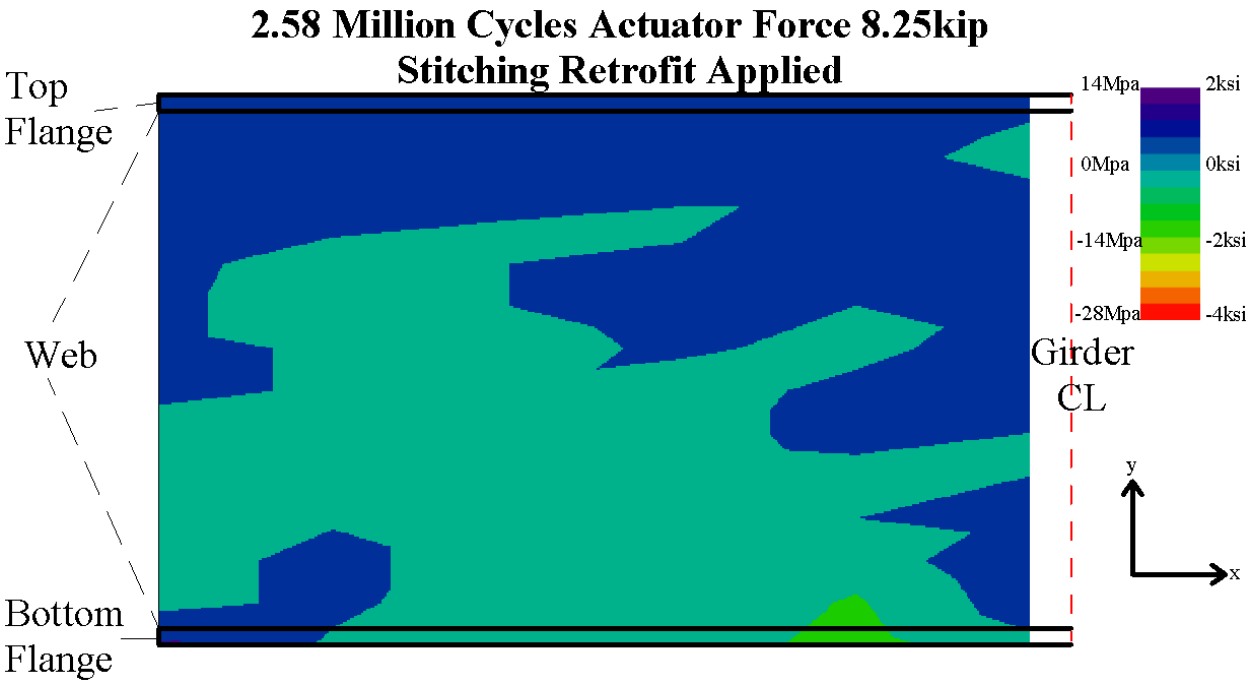

Figure I 17: Change in horizontal stress contours, 2.58 million cycles stitching retrofit applied

Appendix J: Steel Wool Tension Specimens

Three steel wool tensile specimens were fabricated in to investigate the suitability of steel wool as fibers in a composite block retrofit. The steel wool specimens were fabricated with the same procedure which was used to construct the CFRP tension specimens. With the exception of steel wool replacing the carbon fiber, in a 10% fiber volume ration compared to 15% which was used for the carbon fiber specimens. A forth steel wool specimen was attempted to be constructed with a 15% fiber volume ratio however that ratio proved to be too difficult to fabricate.

The steel wool used was RHODES AMERICAN steel wool grade three. Grade three steel wool was the coarsest available steel wool at the local Home Depot. The composite matrix was constructed out of West Systems 105 Resin and West Systems 206 Hardener. The matrix was mixed in a ratio of 5 part resin to 1 part hardener as specified by the manufacturer. The dimensions of the steel wool tensile specimens were approximately 305-mm (12-in.) x 51-mm (2-in.) x 25-mm (1-in.).

Table J 1 summarizes the results from the steel wool tension specimen tests which were conducted on Feburary 28th 2014. The specimens were tested in the Baldwin 120, the same machine which tested the CFRP tension specimens. The horizontally oriented Micro-Measurements EA-06-250BF-350/P strain gage debonded from specimen 3 halfway through the test. It is for that reason that poisons ratio wasn't calculated for specimen 3.

	Elastic Modulus (ksi)	Poisson's Ratio	F_u (ksi)
Specimen 1	404.8	0.31	2.2
Specimen 2	423.4	0.25	2.8
Specimen 3	547.5	N/A	2.0
Average	458.6	0.28	2.3

Table J 1: Steel wool tension specimens' results

When comparing the results of the steel wool and CFRP tension specimens. The CFRP had better material properties. The CFRP's average modulus of elasticity was 4750 MPa (689 ksi) compared to the steel wools which was 3165 MPa (459 ksi). The ultimate strength of the steel wool specimens were 15.9MPa (2.3 ksi) compared to the CFRP specimens which were 29.6 MPa (4.3 ksi). Even though the CFRP tension specimens had superior material properties if steel wool was utilized as the fibers in the composite block retrofit it would most likely still provide enough stiffness to be an effective retrofit. This would of course need to be verified with an experimental trial.

Conclusions from Steel Wool Tension Specimen testing

A retrofit constructed out of steel wool would be much cheaper than one conducted out of chopped carbon fibers. To compare a .45Kg (1lb) tub of CTS 6-mm (¼ in.) chopped carbon fibers costs $32.95 and a 0.20Kg (0.45lb) bag of steel wool costs $3.98 at the Home Depot which would make the steel wool cost $8.64 per 0.45Kg (1lb). Purchasing steel wool in these very small quantities still makes it over 3.8 times cheaper than

chopped carbon fibers. If these materials were purchased in bulk the price differential between the steel wool and chopped carbon fibers would most likely increase even further.

One concern which could arise when utilizing steel wool as the fibers in a composite block retrofit is the fact that steel wool is more likely to corrode. Further research would need to be conducted to determine how a block of composite with steel wool as the fibers would react in a corrosive environment.

Photographs of steel wool tension specimens fabrication and testing

Figure J 1: Compacting steel wool and epoxy into 25x51x305 mm (1x2x12 in) mold

Figure J 2: Steel wool tension specimens curing

Figure J 3: Steel wool tension specimen with strain gages attached

Figure J 4: Failure of steel wool tension specimen 1 left and 3 right

Figure J 5: Failure of steel wool tension specimen 2 occurred at lower grip

Appendix K: Aramid (Kevlar) Yarn Testing and Material Properties

The Aramid (Kevlar) Yarn used was purchased from CTS sales. The Aramid (Kevlar) Yarn used was 1510 Aramid Yarn which has 1000 filaments per strand. The yarn has the following material properties which were obtained directly online from CST sales.

- Specifications
  - Specific Density: 0.052 lb./in.^{3}
  - Tenacity: 435 x 10^3 psi
  - Modulus: 16.3 x 10^6 psi
  - Break Elongation: 2.4%
  - Specific Tensile Strength: 8.34 x 10^6psi
  - CTE: -2.7 x $10^{-6/0}$ F
  - Decomposition Temperature: 800-900^0 F

The stitching retrofit which was applied on the 2.82-m (9.25-ft) girder subassembly was constructed by creating a large loop of Aramid Yarn, 68 strands were used to create this loop meaning there were 68,000 filaments in the stitches. The strands were coated in epoxy before they were stitched through the girder. The epoxy was West Systems 105 resin and 206 hardener and was mixed in a ratio of 5 part resin to 1 part harder as specified by the manufacturer. The average diameter of the Kevlar stitching was 9.5-mm ($\frac{3}{8}$ in) giving the total strength of the fibers in the stitching approximately 725kN (163 kips). Since the yarn was coated in epoxy it hardened which allowed it to keep its shape and prevented the fibers from loosening. However by coating the fibers in epoxy many imperfections may have been created which could have the tendency to reduce the ultimate strength of the stitching retrofit.

During testing it didn't appear that any part of the stitching retrofit failed, it was just the bolts which connected the retrofit to the cross frame which failed. In order to get an approximate strength of Aramid (Kevlar) Yarn coated in epoxy several tension specimens were constructed and tested.

Aramid (Kevlar) Yarn Tension Specimen 1

The first Aramid (Kevlar) Yarn tension specimen was constructed by creating a loop of Kevlar using 32 strands. At both ends of the loop an overhand knot was tied approximately 76mm (3-in.) from the ends. The specimens were tested in the MTS testing machine using pin grips with a pin diameter of 25-mm (1-in.). The specimens had to be casted with 25-mm (1-in.) holes on either end so they would fit in the testing machine. Figure K 1 shows the Aramid (Kevlar) Yarn hanging from a 25-mm (1-in.) diameter rod before and after it was coated in epoxy. Once the specimen was hung and coated in epoxy it was left to cure for 24 hours.

Figure K 1: Fabricating the first Kevlar Tension Specimen (left pre epoxy coating, right after epoxy coating)

The specimen was placed in the MTS testing machine and the machine was set to manual displacement control. Displacement was increased at a rate of 2.5mm/minute (0.1-in/minute). The specimen failed suddenly at a load of 4.7kN (1.05-kips) and elongated 11.4-mm (0.45-in.). The failure of the specimen occurred at the grips as shown in Figure K 2.

Figure K 2: Failure of Specimen 1 at the grips

In order to attempt to prevent grip failure another specimen was constructed with a different fabrication approach.

Aramid (Kevlar) Yarn Tension Specimen 2

The second Aramid (Kevlar) Yarn tension specimen was constructed with twice the material at the grip locations in an attempt to prevent grip failure. Two small loops approximately 152 mm (6-in.) long were constructed with 64 strands per loop. A second loop approximately 457 mm (18-in.) was constructed with 32 strands. Figure K 3 shows one of the small loops and the large loop which was used to construct tension specimen 2. The two small loops were placed through the ends of the large loop and folded back on themselves, thereby doubling the strand count at the ends. The specimen was hung from the same 25-mm (1-in.) diameter rod which was used for the first specimen, coated in epoxy and left to cure for 24 hours. Figure K 4 shows the specimen curing and the fully cured specimen.

Figure K 3: Strands of Kevlar for tension specimen 2

Figure K 4: Kevlar Tension Specimen 2 (left curing, center fully cured, right fully cured grip location)

The second specimen was placed in the MTS testing machine and the machine was set to manual displacement control. Displacement was increased at a rate of 2.5mm/minute (0.1-in/minute). **Error! Reference source not found.Error! Reference source not found.** Figure K 5 plots load verses displacement for the second Kevlar tension specimen. During testing cracking was heard, the cracking was strands of Kevlar breaking. All of the sudden drops of load correspond to when cracking of the specimen was heard. At 9.3kN (2.1kips) a loud crack was heard and load suddenly decreased to 8kN (1.8kips). The specimen failed at a load of 10.2kN (2.3 kips) and had an elongation of 68.6mm (2.7-in.). The failure occurred at the upper to center loop connection as shown in Figure K 6.

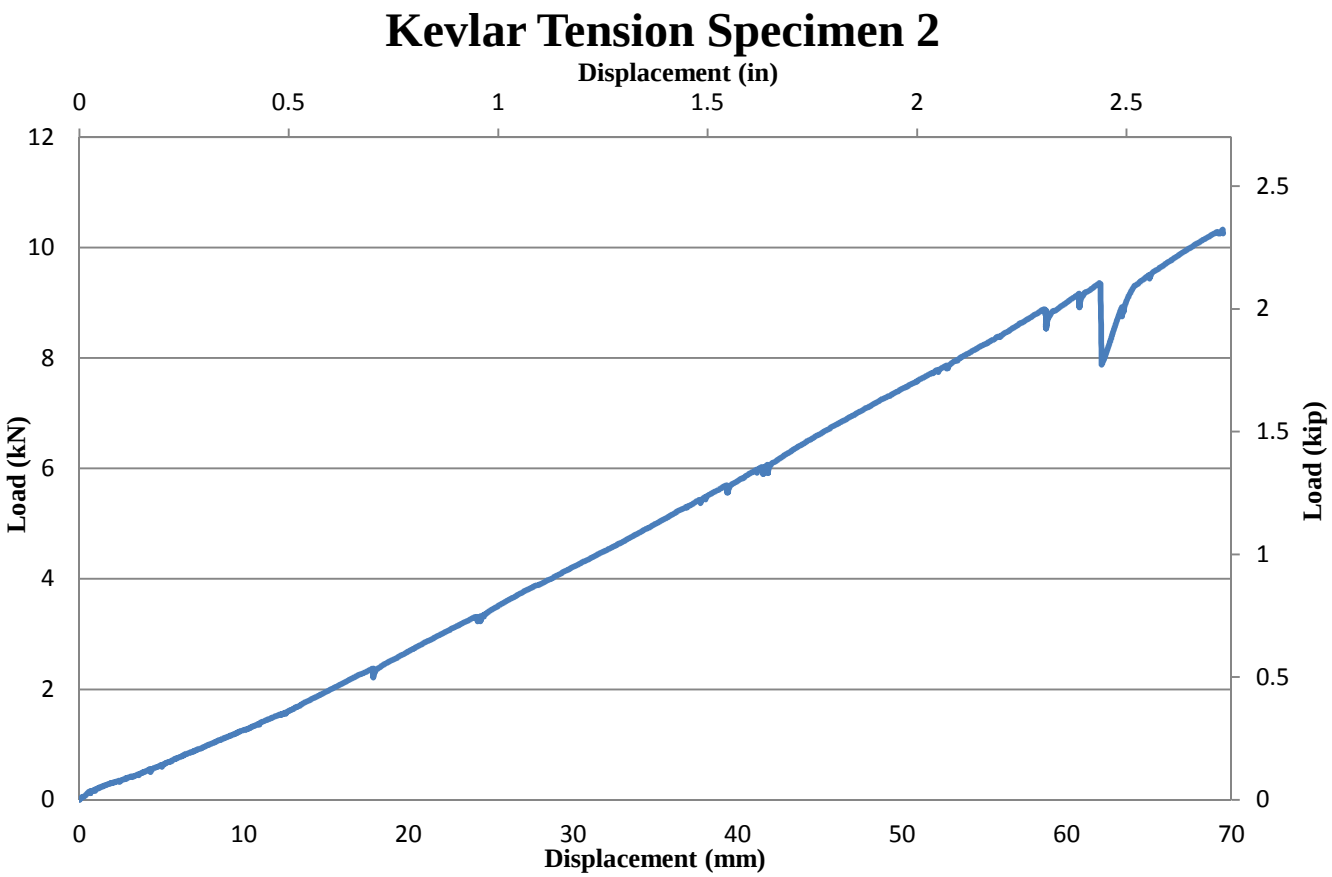

Figure K 5: Load vs. Displacement for the second Kevlar tension specimen

After the specimen was removed from the testing machine and examined a small strand of Kevlar which was approximately 2 mm (0.08-in.) in length was found broken at the lower to center loop connection. Figure K 7 shows the torn Kevlar circled in red. This was the only visible tear found in the Kevlar specimen, other than the one which caused specimen failure. It is believed that this tear is what caused the large drop of force which occurred at 9.3 kN (2.1 kips). Testing of Kevlar coated in epoxy showed that failures are most likely to occur at connection locations.

Figure K 6: Failure location of second Kevlar tension test specimen

Figure K 7: View of torn Kevlar strand

Appendix L: Corrosion Testing

If the composite block retrofit is going to be applied to a bridge, it will experience environmental conditions much harsher than those seen in a lab setting. It is important to know if the carbon fiber reinforced polymer material is resistant to corrosion, and how the material would affect structural steel in a corrosive environment. There were two different tests conducted to test the corrosive properties of composite on steel. One test involved plasma cutting the upper web gab region out of the girder subassembly with the composite block still attached and placing the entire upper web-gap region in a salt solution. The second test was conducted following ASTM B117-11 and involved the corrosive testing of 13 separate sections of L76x76x10-mm (L3x3x3/8-in) angle. The angle was cut in 76mm (3-in.) sections from the cross frame on the girder subassembly.

Composite block in salt solution

The composite block which was applied in the upper web-gap region was plasma cut from the girder subassembly once testing concluded as shown in Figure L 1. The Bonet stud is visible on the right because that portion of the composite block was removed prior to plasma cutting the upper web-gap region. Due to the high heat given off during plasma cutting the 25mm (1-in.) top flange the block debonded from the steel and a small gap formed along the composite block to steel flange interface. This gap would allow the salt solution to easily penetrate between the block and steel. To combat this epoxy was poured along all of the composite block to steel edges, successfully eliminating this gap. The epoxy used was a five parts West Systems 105 resin to one part West Systems 206 hardener mixed in a 240 ml (8-oz.) plastic cup for approximately one minute prior to poring. After the epoxy had cured for 48 hours the specimen was placed into an 85Liter (22 gallon) plastic Rubbermaid® container. 38Liters (10 gallons) of salt water solution was then poured into the plastic container as shown in Figure L 2. The specimen was left in the container for 14 days and was then removed and left to dry for 24 hours.

Heavy rust formed on the specimen in any location where there was bare steel without paint. Rust also formed along many of the composite block to steel edges. Figure L 3 shows the upper web-gap region after being removed from the salt solution for 24 hours. From visible inspection it didn't appear that any of the salt solution was able to break the bond between the epoxy and steel to cause internal corrosion. To confirm this, a cross section of the block was cut so the internal steel to CFRP connection could be examined. The cross section can be seen in Figure L 4 and was cut utilizing a 355mm (14-in.) chop saw with a metal chop saw blade. Once the cross section was cut it was visibly apparent that rust did not occur on any steel face which was covered in the CFRP.

Figure L 1: Upper web-gap region removed from girder subassembly

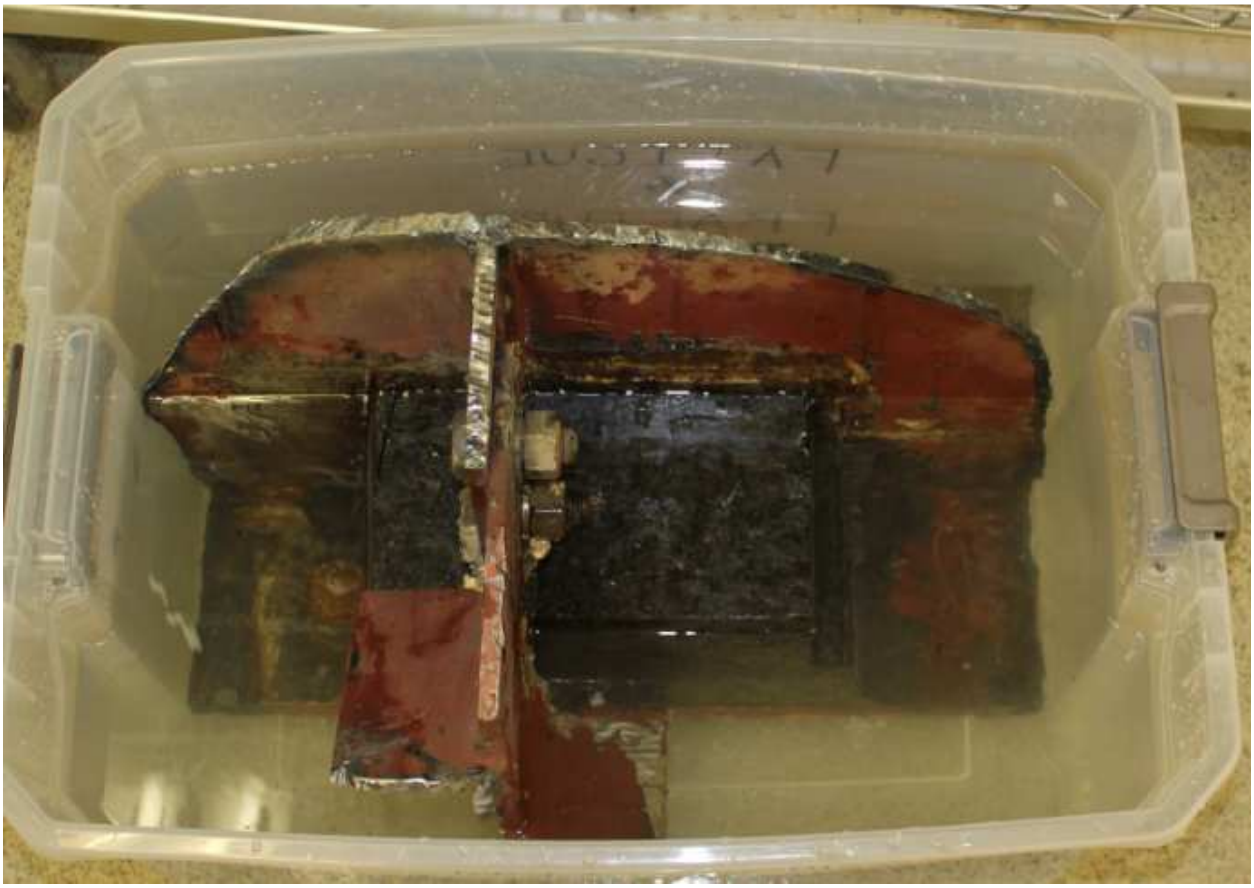

Figure L 2: Upper web-gap region in plastic container with salt solution

Figure L 3: Upper web-gap region after 14 days in salt solution

Figure L 4: Cross section of the upper web-gap region after two weeks in salt solution

ASTM B117-11 Stand Practice for Operating Salt Spray (Fog) Apparatus

The ASTM B117-11 testing was conducted in a Shingleton SCCH-Salt Fog Chamber. The 13 specimens were placed in the chamber for one week. The specimens were grouped into three main categories: (1) specimens with bolt holes and 19-mm (3/4-in) diameter A325 structural bolts fully tightened in the holes, (2) bare steel specimens with all of the paint removed, and (3) specimens with paint left on. The edges of the specimens with the paint left

on were sprayed with clear Rust-Oleum® in order to coat the bare steel which was exposed when the specimens were cut. The chamber was defogged and the specimens were examined approximately every 24 hours. Table L 1 shows the data recorded from the salt spray chamber.

Date	Collection Rate (mL/hr)		pH	SG	Temp (^{0}F)		Notes
	Near	Far			Chamber	Tower	
26-Mar	-	-	-	-	-	-	Start Test 2pm
27-Mar	2.1	-	6.8	1.035	94.9	118.2	Stop 2:18 pm, Start 2:28
28-Mar	1.7	2.0	6.6	1.032	95.0	117.8	Stop 1:58 pm, Start 2:08
29-Mar	2.8	3.0	6.8	1.035	94.5	117.5	Stop 10:27 am, Start 10:44. Nozzle Angle adjusted to correct spray rate.
30-Mar	1.5	1.8	7.2	1.035	95.4	118.0	Stop 1:40 pm, start 1:49
31-Mar	1.7	1.9	7.0	1.030	95.2	119.1	Stop 2:09 pm, start 2:21
1-Apr	1.8	1.8	6.5	1.030	95.2	118.4	Stop 2:12 pm, Start 2:22
2-Apr	1.5	1.7	6.7	1.030	95.7	117.5	Stop 2:00 pm

Table L 1: ASTM B117-11 salt spray chamber collection data.

The purpose of testing was to determine how specimens coated in CFRP would perform in a highly corrosive environment, other specimens were coated in epoxy and others were left with no coating as control. The specimens coated with CFRP utilized five parts West Systems 105 resin to one part West Systems 206 hardener and Chopped Graphite, 6.3-mm (0.25-in.) fibers with a fiber volume ratio of 15%. The resin and hardener was mixed in a 240 ml (8-oz.) plastic cup for 30 seconds then fibers were added and mixed in for another minute. The CFRP was applied directly to the surface of the specimens by hand, there was no mold used. This proved to be very challenging and had two be done in two stages, one half of the specimen was covered in the CFRP and left to cure for 24 hours. After 24 hours the specimen was flipped over and the procedure was repeated coating the other side of the specimen and allowing the specimen to cure for 24 hours. Due to the difficulty of applying the composite without a mold there were many small holes left in the cured CFRP which would allow the salt spray to directly reach the steel surface. If this test was to be repeated individual molds should be constructed for each specimen, this would allow a much more uniform application of the CFRP over the entire surface of the specimen.

The specimens, which were coated in epoxy, went through a similar procedure as the specimens coated in CFRP. The epoxy used was five parts West Systems 105 resin to one part West Systems 206 hardener. The resin and hardener were mixed in a 240ml (8-oz.) plastic cup for approximately 30 seconds and was then pored over the surface of the specimens. The application of the epoxy was also done in a two stage process, one half of the specimen was covered in epoxy and left to cure for 24 hours. After 24 hours the specimen was flipped over and the procedure was repeated coating the other side of the specimen. The epoxy was much easier to apply to the specimens when compared to the CFRP however if this experiment was to be repeated individual molds should be constructed for each specimen allowing for a more uniform application of the epoxy. The specimens with the

paint removed were much easier to apply the epoxy to. By grinding the paint down and leaving abrasions in the metal the epoxy had a much stronger bond than the specimens with the paint not removed.

Corrosion Specimens with Bolts

There were three specimens with bolts, all of these specimens had the paint left on them. One specimen was placed in the chamber as the control with no composite applied the other two specimens had the CFRP composite applied to their surface. Figure L 5 shows the specimens after they were cut off of the cross frame and before the bolts were applied. Figure L 6 shows the specimens after the bolts were applied and fully tightened; two of these specimens had the CFRP applied in the two step application process. The corrosion specimens were placed in the salt spray chamber for one week. Figure L 7 shows the specimens with bolts in the salt spray chamber after 24 hours of testing.

Figure L 5: Corrosion specimens with bolts before bolts are applied

Figure L 6: Corrosion specimens with bolts, control on left other two have CFRP applied to surface

Figure L 7: Corrosion specimens with bolts, photo taken after 24 hours in salt spray chamber

After a full week of testing the specimens with bolts were removed from the salt spray chamber. The control specimen had rust all over its surface. The other two specimens had visible rust forming on the surface of the CFRP. It is interesting to note that before the specimens were placed in the salt spray chamber there were many burrs in the CFRP which would easily prick the hands of someone handling the specimens even with leather gloves on. But after one week in the salt spray chamber the CFRP specimens could be handled with bare hands since the burs were removed by the salt spray.

Figure L 8: Corrosion specimens with bolts, photo taken after specimens were removed from salt spray chamber

The bolts and the CFRP were removed from the specimens, and there was heavy corrosion noted all over the surface of the control specimen including under the bolt. The specimens with the CFRP had much less visible rust however rust was still able form in locations where the CFRP was unable to fully bond with the surface, this was most prevalent around the edges of the specimen.

Figure L 9: Corrosion specimens with bolts, CFRP removed from the left and center specimen, right specimen was the control

Figure L 10: Corrosion specimens with bolts, CFRP removed from right and center specimen, left specimen was the control

Corrosion Specimens with and without paint

There were six corrosion specimens with the paint left on. Three of these specimens had CFRP applied to their surface, one of these specimens was fully coated with CFRP, one of the specimens had CFRP applied to only one leg of the angle and the final CFRP painted specimen had CFRP applied to half of both legs of the angle. Two of the painted specimens had epoxy applied to their surfaces, one was fully coated in epoxy and the other had one leg coated in epoxy. One of the painted specimens was left as a control with no CFRP or epoxy applied to its surface. Four of the specimens had the paint removed, one specimen was fully coated in CFRP, another was fully coated in epoxy, the third had CFRP applied to one leg of the angle and the final specimen was left as the control with no CFRP or epoxy applied to its surface.

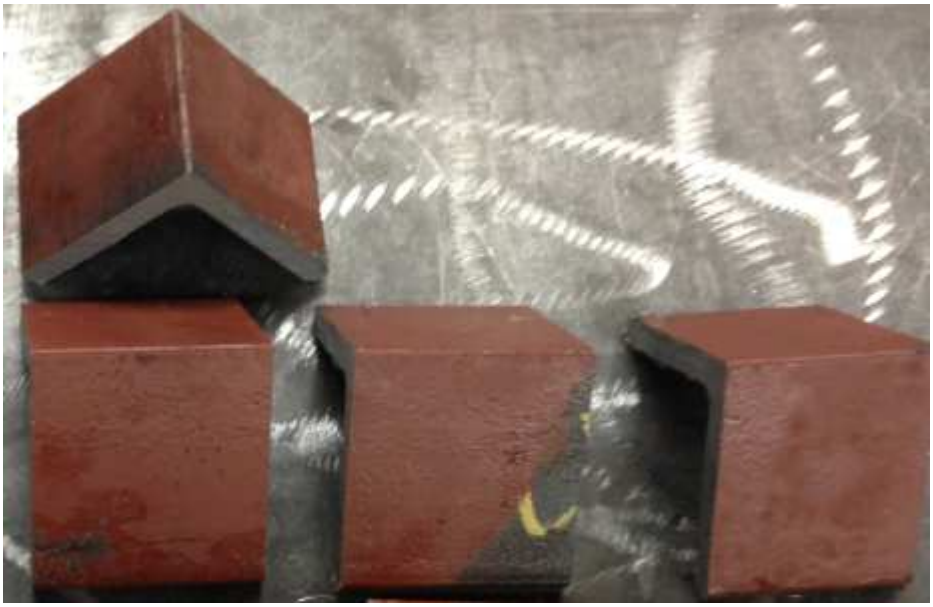

Figure L 11: Painted corrosion specimens before CFRP or epoxy is applied

Figure L 11 shows the painted corrosion specimens before any CFRP or epoxy coating is applied to their surfaces. Applying epoxy to the surface of the painted specimens proved to be very difficult because the epoxy would not flow smoothly over the surface of the specimen. Figure L 12 shows a comparison between the unpainted and painted specimens with epoxy being applied to the specimens' surface. The unpainted specimen had the epoxy smoothly and easily bond with its surface, while the painted specimen did not allow the epoxy to easily bond. The painted specimen in Figure L 12 has many locations where the epoxy pooled creating rings on the specimen without any epoxy.

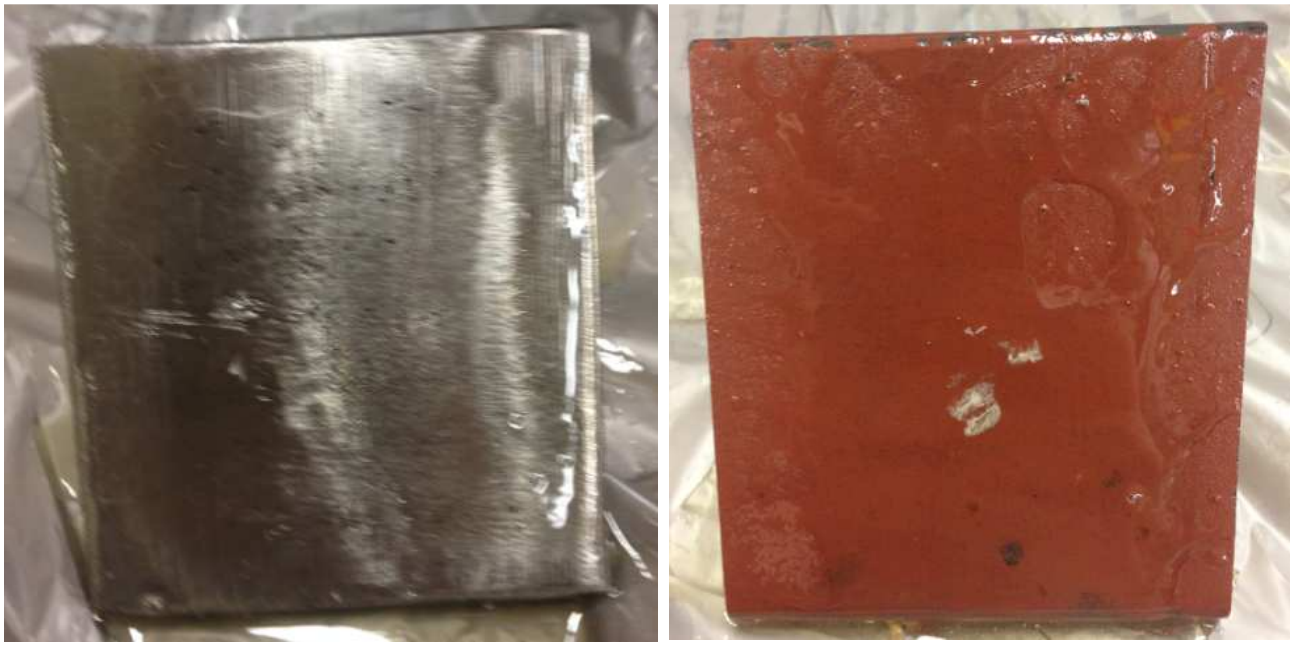

Figure L 12: Corrosion specimens with epoxy coat curing, specimen on the left has bare steel and the specimen on the right has paint

Figure L 13: Corrosion specimens being fully coated in CFRP

The specimens with CFRP applied to their surfaces are shown in Figure L 13. Because the CFRP was applied by hand it was not able to be applied in any uniform matter over the entire surface of the specimen. Around the edges of the specimen it was very difficult to get the CFRP to stay directly against the surface. There were many voids created between the edge of the specimens and the CFRP. After all of the CFRP and epoxy cured the specimens were placed in the salt spray chamber as shown in Figure L 14.

Figure L 14: Corrosion specimens in salt spray chamber

After one week in the salt spray chamber the specimens were removed. Figure L 15 shows the corrosion specimens immediately after they were removed from the salt spray chamber. The control specimen with the paint removed (upper right specimen in Figure L 15) was very heavily corroded with rust on every surface. The edges of the painted specimen (to the left of the control specimen with paint removed in Figure L 15) were also heavily corroded, showing that the clear Rust-Oleum® which was applied on the edges of the specimen wasn't

very effective at preventing corrosion. Also where the two legs of the angle connected there was paint blistering forming, most likely caused from water collecting in that corner. The two specimens (painted and paint removed) which were fully coated in epoxy can be seen in Figure L 16. These specimens had rust along the edges, in some locations this rust forced the epoxy to pop off of the specimen.

The specimens with CFRP applied to their surfaces had the CFRP removed in specific locations utilizing a band saw. The CFRP applied to the specimens was very successful at preventing corrosion in locations where the CFRP was able to bond with the surface of the specimen. The specimen with the paint grounded off which was fully covered in CFPR had corrosion present only on the edges where the CFRP was unable to bond with the specimens surface. Figure L 16 shows this specimen with a portion of the CFRP removed the gap between the CFRP and steel is visible in the figure on the right and that gap corresponds to the location where rust formed. The painted specimen with CFRP applied to its entire surface had similar results as the specimen without paint and CFRP applied to its entire surface. The edges of that specimen had rust forming due to the lack of bond between the CFRP and steel, in fact in some locations the rust along the edges of the painted specimen with CFRP was worse than the control painted specimen.

Figure L 15: Corrosion specimens after one week in salt spray chamber

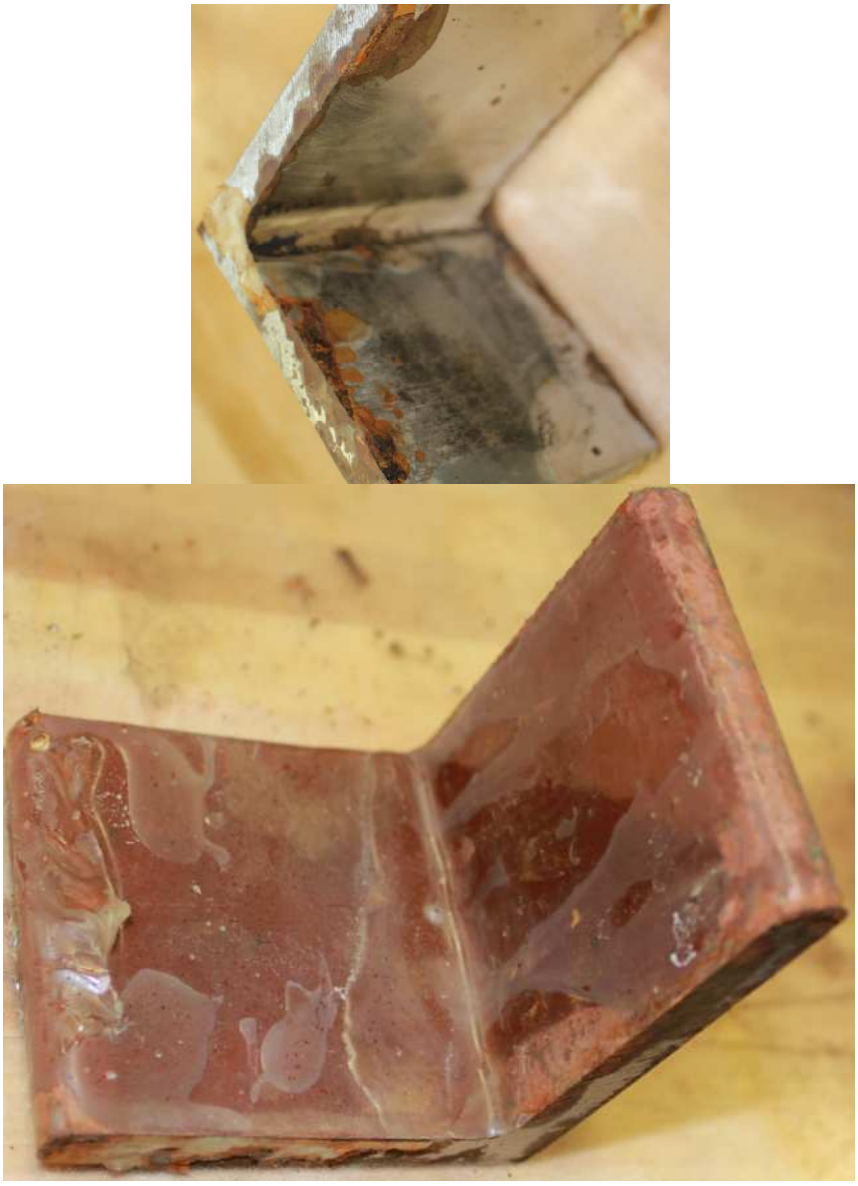

Figure L 16: Corrosion specimens with epoxy coating, left specimen with paint removed, right specimen with paint

Figure L 17: Corrosion specimen with paint removed and CFRP applied to its entire surface

The two specimens (painted and with paint removed) with CFRP applied to only one leg of the specimen can be seen in Figure L 18. Like all of the other specimens in the areas where the CFRP was applied and properly bonded with the specimen there was no corrosion present. However on the edges of the specimen there was visible rust once part of the CFRP was removed.

Figure L 18: Corrosion specimens with CFRP applied to one leg, left specimen with paint removed, right specimen with paint

Conclusions from corrosion testing

From both corrosion tests performed it is apparent that both epoxy and CFRP are highly successful at preventing corrosion if, there is a quality bond between the composite and steel. In many cases if there is not a quality bond the composite could accelerate the formation of rust due to the ability of salt to collect between the composite and steel. If CFRP is applied to a steel structure it must be applied with a mold and the CFRP needs to be placed under pressure while it is curing to prevent the formation of voids, which could create a location for salts to collect. The composite block was highly successful in preventing any corrosion to occur on the steel surface where the block was applied.

Appendix M: Procedure for installing composite block retrofit in the field

From the experimental testing performed on the composite block retrofit at the University of Kansas a procedure was developed for how the composite block retrofit would be implemented in the field. Since this retrofit requires drilling holes into the girder's top flange this procedure can only be implemented if net section fracture does not control the strength of the girder. Based off the successful results from experimental testing a total of four Bonet Studs are required to be installed in the top flange of the girder at each location where distortion induced fatigue cracking has occurred. The procedure is outlined below.

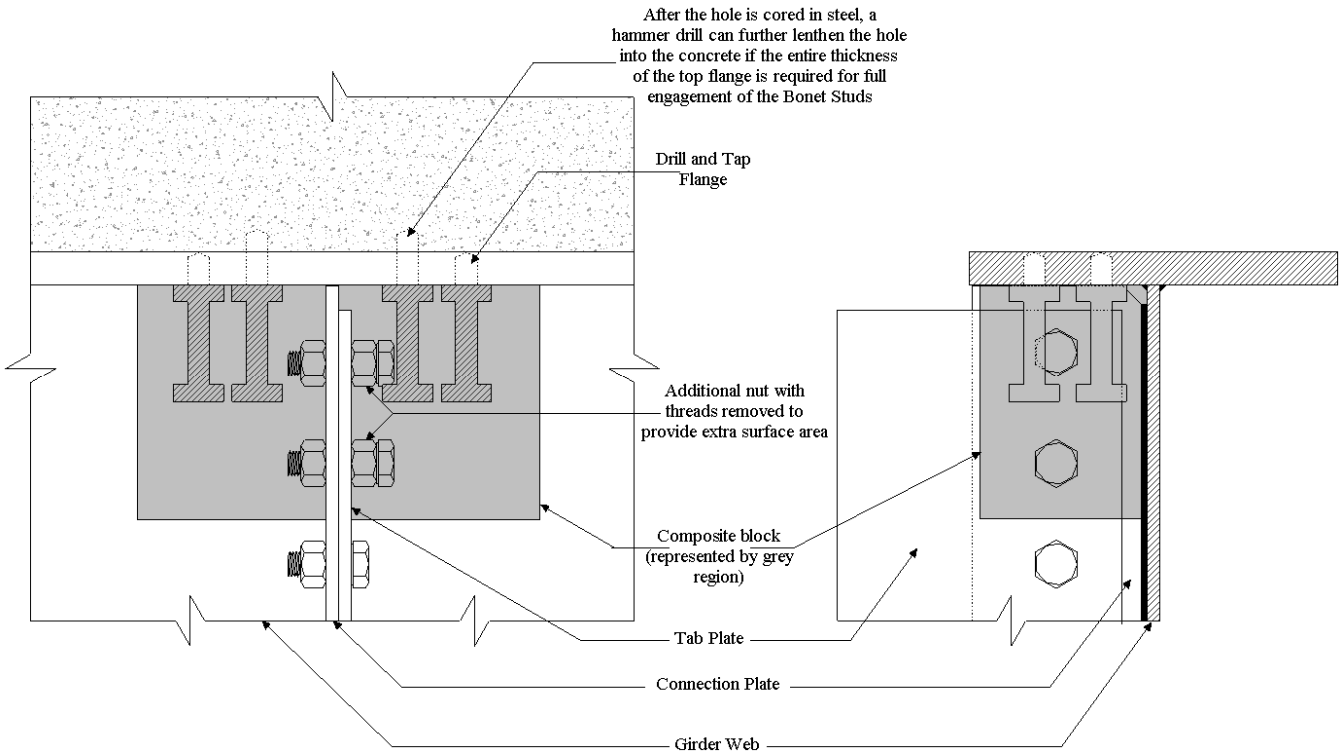

Figure M 1: Composite block retrofit procedure

Procedure

1. Identify cracked locations at connection stiffener to web connection and sandblast the areas that will be covered by the composite block to meet SSPC-SP10.*
2. Drill 17.5mm (11/16-in.) holes into the girder flange (this will require the use of a high-speed twist bits to ensure all material in the hole is removed). Follow drilling by tapping the holes with ¾-10 UNC bottoming tap.
3. Remove the two bolts closest to the top flange which connects the tab plate to the connection stiffener. Replace these bolts with bolts 25mm (1-in.) longer and place a nut with the threads removed between the bolt head and steel interface to provide extra surface area for the composite block retrofit to bond into.
4. Install Bonet Studs into tapped holes on the girder flange after first applying Locktite compound (or equivalent) to prevent the Bonet Studs from loosening from the girder.

5. Install flexible mold on both sides of the web gap region; insure Bonet Studs and the two longer bolts on the connection stiffener are covered by the mold. Magnetize the mold and ensure all sides are sealed.
6. Hang a plastic drip tray below the region where the composite block retrofit will be installed in case any epoxy drips during the installation process.
7. Pump composite into the opening of the mold until epoxy begins to leak out of the edges.
8. Let the composite cure (cure time will depend on type of epoxy used and temperature at the bridge site) then remove the plastic drip try and the mold.
9. Apply proper surface coatings to bare steel.*

* It may be possible to eliminate the need to sandblast the areas covered by the composite block. Further experimental testing would be required to verify this claim.

References

AASHTO, (2010). “AASHTO LRFD Bridge Design Specifications (2010).” American Association of State Highway and Transportation Officials.

ABAQUS (2010) Simulia, Version 6.10. http:www.simulia.com.

AISC (2011) “Steel Construction Manual, Fourteenth Edition.” *American Institute of Steel Construction, Inc.* Chicago, IL.

Altay, A. K., Arabbo, D. S., Corwin, E. B., Dexter, R. J. and French. C.E. (2003) Effects of Increasing Truck Weight on Steel and Prestressed Bridges. Report MN/RC 2003-16. Minnesota Department of Transportation. St. Paul, MN.

ASTM B117 (2011). “Standard Practice for Operating Salt Spray (Fog) Apparatus.”

ASTM D3039 (2008). “Standard Test Method for Tensile Properties of Polymer Matrix Composite Materials.”

ASTM D5961 (2013). “Standard Test Method for Bearing Response of Polymer Matrix Composite Laminates.”

Birman, V. and Byrd, L. (2006). ”Functionally Graded Stitched Laminates: Illustration on the Example of a Double Cantilever Beam.”J. Aerosp. Eng. 19, SPECIAL ISSUE: Festschrift Prof. A. K. Noor, 217–226.

Cadei J M C, Stratford T J, Hollaway L C and Duckett W G (2004), Strengthening Metallic Structures Using Externally Bonded Fibre-reinforced Polymers, C595. London: CIRIA.

Chen, L., Sankar, B. V., and Ifju, P. G. 2003. “Mixed mode fracture toughness tests for stitched composite laminates.” *AIAA Pap.*, 2003, 1874.

Cheuk P T, Tong L, Wang C H, Barker A and Chalkley P (2002), “Fatigue crack growth in adhesively bonded composite-metal double-lap joints,” Composite Structures, 57(1-4): 109-15

Colombi P and Fava G, “Rehabilitation of metallic civil infrastructure using fiber-reinforced polymer (FRP) composites: Fatigue life of steel components strengthened with fiber-reinforced polymer (FRP) composites” Woodhead Publishing Limited, Cambridge, UK, 239-265

Connor, R. and Fisher, J. ”Identifying Effective and Ineffective Retrofits for Distortion Fatigue Cracking in Steel Bridges Using Field Instrumentation.” Journal of Bridge Engineering, Vol. 11, No. 6, 745–752. (2006).

Curley A J, Hadavinia H, Kinlock A J and Taylor A C (2000), “Predicting the service-life of adhesively-bonded joints,” International Journal of Fracture, 103(1):41-69.

Deng J, Lee M M K and Moy S S J (2004), “Stress analysis of steel beams reinforced with a bonded CFRP plate,” Composite Structures, 65(2): 205-15.

Dexter, H. B., and Funk, J. G. 1986. “Impact resistance and interlaminar fracture toughness of through-the-thickness reinforced graphite/epoxy.” *Proc., 27th AIAA/ASME/ASCE/ASHS/ASC Structural Dynamics and Materials Conf.*, AIAA Paper 86-1020, 700–709.

Dexter, R and Ocel, J. (2013). “Manual for Repair and Retrofit of Fatigue Cracks in Steel Bridges.” FHWA., Washington, D.C., 39-61.

Fisher, J.W. and Keating, P.B. (1989). “Distortion-Induced Fatigue Cracking of Bridge Details with Web-gaps.” Journal of Constructional Steel Research, 12(3-4), 215-228.

Gangarao, H and Vijay, P (2010), “Feasibilty Review of FRP Materials for Structural Applications”, Engineering Research & Development Center- US Army Corps of Engineers, Vicksburg, MS.

Gui, L., and Li, Z. 2001. “Delamination buckling of stitched laminates.” *Compos. Sci. Technol*., 61, 629–636.

Hollaway L C and Cadei J (2002), “Progress in the technique of upgrading metallic structures with advanced polymer composites”, Progress in Structureal engineering and Materials, 4(2), 131-148.

Jajich, D. and Schultz, A. (2003). ”Measurement and Analysis of Distortion-Induced Fatigue in Multigirder Steel Bridges.” J. Bridge Eng., 8(2), 84–91.

Jegley, D. C., Bush, H. G., and Lovejoy, A. E. 2001. “Structural response and failure of a full-scale stitched graphite-epoxy wing.” *AIAA Pap*., 2001, 1334.

Jones S C and Civjan S A (2003), “Application of fibre reinforced polymer overlays to extend steel fatigue life”, Journal of Composites for Construction, 16(2), 138-149.

Karbhari, V.M. “Rehabilitation of metallic civil infrastructure using fiber-reinforced polymer (FRP) composites: a materials and systems overview at the adhesive bond level” Woodhead Publishing Limited, Cambridge, UK, 3-10

Kavanaugh, C. (2014). “Composite bridges on a path to wider use.” Plastics News., Crain Communications Inc.

Keating, P., Wilson, S., and Kohutek, T. 1996. “Evaluation of repair procedures for web-gap fatigue damage”, Research Report 1360-1. Texas Transportation Institute – Texas A&M University.

Lau, K., Ling, H., and Zhou, L. 2004. “Low velocity impact on shapememory alloy stitched composite plates.” *Smart Mater. Struct*., 13, 364–370.

Liu H B, Al-Mahaidi R and Zhao X L (2009), “Experimental study of fatigue crack growth behavior in adhesively reinforced steel structures”, Composites Structures, 90(1), 12-20.

McMaster-Carr, http://www.mcmaster.com/

Shaat A, schnerch, D, Fam, A and Rizkalla S (2004), “Retrofit of steel structures using fiber reinforced polymers (FRP):state-of-the-art”, Transportation Research Board (TRB) 83rd Annual Meeting, Washington, DC 11-15 January.

Taljsten B, Hansen C S and Schmidt J W (200(), “Strengthening of old metallic structures in fatigue with prestressed and non-prestressed CFRP laminates”, Construction and Building Materials, 23(4), 1665-1667 (P).

Tavakkolizadeh M and Saadatmanesh H (2003), “Fatigue strength of steel girders strengthened with carbon fiber reinforced polymer patch,” Journal of structural engineering, 129(2): 186-96.

Teng J G, Yu T and Fernando D (2012) “Strengthening of steel structures with fiber-reinforced polymer composites”, Journal of Constructional Steel Research, 78, 131-143.

The Composite Store, http://www.cstsales.com/

Weingroff, R. F (1996). “Federal-Aid Highway Act of 1956: Creating the Interstate System.” *U.S. Department of Transportation Federal Highway Administration*, <http://www.fhwa.dot.gov/publications/publicroads/96summer/p96su10.cfm> (March. 3, 2014)

Wu C, Zhao X L, Al-Mahaidi R, Emdad M and Duan W H (2012), “Fatigue tests of craked steel plates strengthened with UHM CFRP plates”, Advances in Structural Engineering – An International Journal, 15(10), 1801-1816,

Yavuz, A. K., Papoulia, K. D., Phoenix, S. L., and Hui, C. Y. 2005. “Stability analysis of stitched composite plate system with delamination under hydro-thermal pressure.” *AiAA Pap.,* 2005, 2106

Yeh, H. Y., Lee, J. J., and Yang, D. Y. T. 2004. “Study of stitched and unstitched composite panels under shear loadings.” *J. Aircr.*, 41, 386–392.

Zhao, X. L. and Zhang, L. (2007), “State of the art review on FRP strengthened steel structures”, Engineering Structures, 29(8), 1808-1823.

Koob, M. J., Frey, P. D., and Hanson, J. M. Evaluation of web cracking at floor beam to stiffener connections of the Poplar Street Approaches, FAI Route 70, East St. Louis, St. Claire County, Illinois. Wiss, Janney, Elstner Associates, for the Illinois Department of Transportation. Northbrook, IL. (1985).

Vishay Precision Group (2010), “Strain Gage Selection: Criteria, Procedures, Recommendations”, Micro-Measurements, 54.